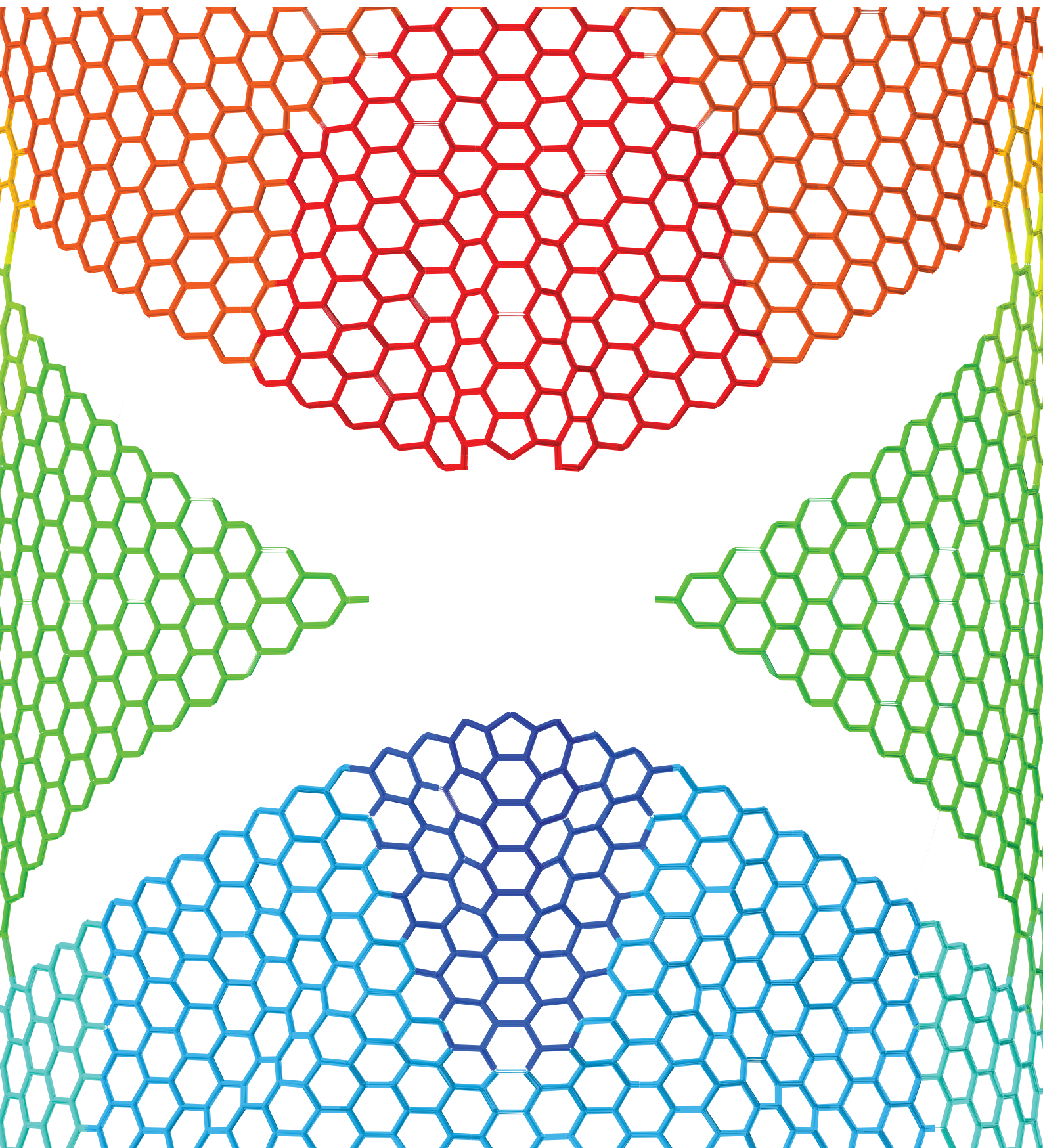
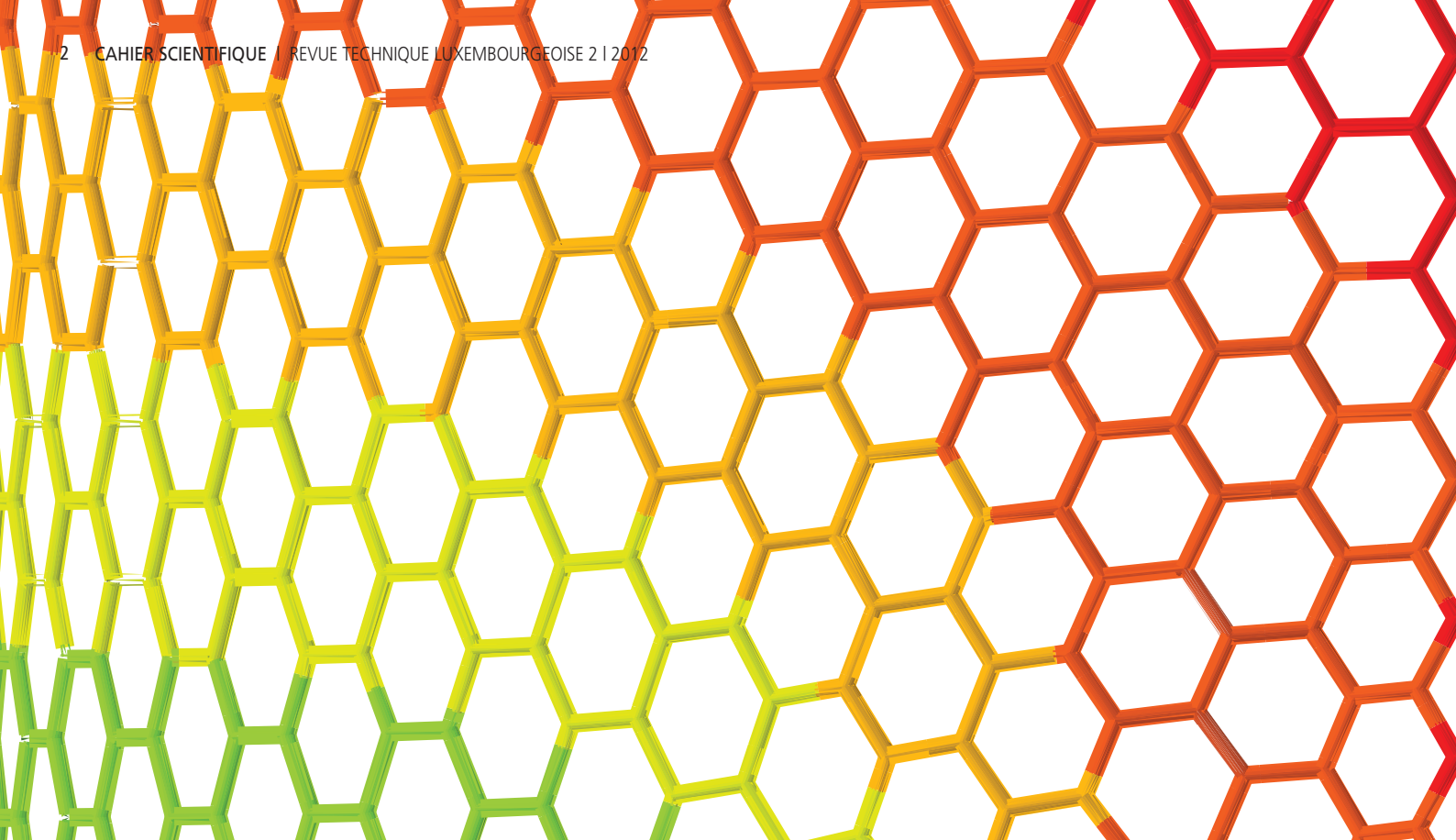


CAHIER SCIENTIFIQUE REVUE TECHNIQUE LUXEMBOURGEOISE

CAHIER SCIENTIFIQUE BIANNUEL DE LA REVUE TECHNIQUE LUXEMBOURGEOISE 2 | 2012





L'A.L.I.A.I. dans l'origine remonte à 1897, et qui regroupe plusieurs organismes apparentés, édite quatre fois par an la Revue Technique, sa publication principale, dédiée à des articles se rapportant aux sujets traités par les professionnels qu'elle regroupe.

Pour l'ALIAI la Revue Technique Luxembourgeoise et son site Internet sont des moyens de communication essentiels donnant à ses membres le contact immédiat avec l'organisation à laquelle ils sont affiliés.

Ces instruments offrent aux entreprises de présenter leur travail devant un public ciblé. La Revue Technique Luxembourgeoise possède un passé prestigieux qui lui confère une légitimité auprès des affiliés de l'ALIAI.

La Revue Technique Luxembourgeoise et le site Internet offrent aux Partenaires de la Revue Technique de l'Association des Ingénieurs, Architectes et Industriels la possibilité de

faire connaître leurs produits ou d'informer de cette manière sur la structure de leur entreprise et de toucher un public ciblé de lecteurs intéressés.

Le cahier scientifique, a pour mission de promouvoir le développement de la recherche et de la culture scientifique, en contribuant à la diffusion et à la valorisation des connaissances et des méthodes scientifiques en vue de soutenir un dialogue entre la science et la société.

Le cahier scientifique est publié 2 fois par an par la rédaction de la Revue Technique. C'est un instrument professionnel pour scientifiques, techniciens, étudiants et intéressés professionnels dans le domaine de l'ingénierie, de la technologie, de la recherche, des énergies renouvelables et de l'industrie.

Des articles sur des recherches approfondies par nos collaborateurs des instituts, des partenaires ou industriels sont publiés dans chaque exemplaire des cahiers scientifiques.

REVUE TECHNIQUE LUXEMBOURGEOISE

www.revue-technique.lu

pour

L'Association Luxembourgeoise des Ingénieurs, Architectes et Industriels

éditée par

Rédacteur en Chef Michel Petit

Responsable Revue Technique Sonja Reichert

Graphisme Bohumil Kostohryz

t 26 73 99 s.reichert@revue-technique.lu

7, rue de Gibraltar L-1624 Luxembourg

Impression 3.500 exemplaires

imprimerie HENGEN

14, rue Robert Stumper L-1018 Luxembourg

EDITO_

cover | Carbon Nanotube © A.A.R. Wilmes

L'objectif de l'Association Jeunes Scientifiques – Jonk Fuersch (A.J.S.L.) est de susciter le goût de la recherche, de l'innovation et de la créativité - et de l'entretenir- auprès des jeunes âgés entre 11 et 21 ans. Le principe directeur de l'association est donc d'inciter les jeunes à faire un travail scientifique ou technique extra-scolaire qui témoignera à la fois de leur curiosité scientifique et de leur persévérance. A cet effet, l'association organise annuellement et ce depuis 1971, un concours national: le concours Jeunes Scientifiques Ce concours national est similaire au prix «Jugend Forscht» allemand ou encore au «C'est génial» français. Il permet aux jeunes participants de gagner des prix. C'est aussi une plate-forme d'échanges car il permet aux jeunes de présenter leur travail à leurs pairs et au grand public. Le concours c'est aussi l'opportunité de pouvoir participer à des concours internationaux et y représenter le Grand-Duché. Le concours national offre aussi l'occasion aux lauréats de participer au plus grand concours scientifique en Europe organisée par la Commission Européenne, l'EUCYS. Ce concours a lieu chaque année dans la capitale d'un pays membre de l'UE et il n'est pas exclu que ce concours puisse à nouveau se tenir au Grand-Duché.

Par le concours national et l'Expo-Sciences organisés tous deux par l'association Jeunes scientifiques - Jonk Fuersch, l'association compte promouvoir les opportunités qu'offrent les sciences aux jeunes et répondre ainsi à la crise des vocations scientifiques. Une partie des jeunes participant (e)s formeront non seulement la prochaine génération de scientifiques mais aussi celle des chefs et cheffes d'entreprise de demain.

Convaincue que le progrès scientifique naît de la rencontre entre les Hommes et les disciplines, l'AJSL n'écarte aucun domaine de la recherche dans son concours. Toutes les sciences – y compris les sciences humaines – sont admises. En favorisant le croisement des compétences, l'association espère éviter que le progrès des connaissances ne se heurte à des barrières artificiellement érigées entre les différentes spécialités et disciplines.

Réconcilier science et la société, tel est le dialogue que l'association se propose à engager. Il s'agit de développer les échanges entre le monde scientifique et la société civile. Pour son engagement, l'association s'est vue décerner le prix Lions en 2011.

Nos représentants se sont vu décerner la médaille d'argent dans le domaine de «Scientific Thinking» à l'occasion de l'INESPO (International Environment & Scientific Project Olympiad 2012).

En outre, nos lauréats ont remporté la médaille de bronze à la «International Science Fair 2012» de Hong Kong.

Enfin, un lauréat a obtenu la «Vestas Power Award» dans le cadre de EUCYS 2008 (European Union Contest for Young Scientists) à Copenhague.

Carlo Hansen

Président Fondation Jeunes Scientifiques Luxembourg

INDEX

- 8_ GEOTECHNISCHE ERKUNDUNG FÜR EINE NEUE STRASSENBRÜCKE ÜBER DIE EISENBAHNLINE BEI ALZINGEN
Cindy Pereira
- 8_ SENSIBILISATION SUR LE CLOUD COMPUTING EN PME
Eric Miglioranzo, R&D Engineer
- 12_ STÄRKUNG DER ENERGETISCHEN NUTZUNG VON BIOMASSE
Dr.-Ing. Katarzyna Golkowska, Dipl.-Ing. (FH) Daniel Koster
- 16_ LES COULEURS DU CIEL
André Mousset
- 19_ ENOVOS FUTURE SUMMIT 2012
Enovos
- 20_ A PILOT IMPLEMENTATION IN WORMELDANGE
Dr. Georges Schutz, David Fiorelli
- 24_ DEVELOPMENT OF AN ANTENNA CONTROL UNIT FOR TRACKING OF SATELLITES WITH GROUND STATION ANTENNAS
Tom Mathes, Engineer, Electro-Mechanical Engineering, HITEC Luxembourg S.A.
- 30_ DEVELOPMENT OF A POSITION CONTROL FOR A TWO-LINK PLANAR MANIPULATOR USING MATLAB/SIMULINK AND ARDUINO
Laurent Breyer
- 34_ GRAPHENE AND THE VIRTUAL DESIGN OF NEXT-GENERATION COMPOSITE MATERIALS
André A.R. Wilmes, Dr. Silvestre T. Pinho
- 37_ PROJETS DE RECHERCHE CONJOINTS
Prof. Dr.-Ing. S.Maas, Ass.-Prof. Dr.-Ing. F.Scholzen, Dr.-Ing. Andreas THEWES, Ass.-Prof. Dr.-Ing. Danièle Waldmann
- 38_ EXPERIMENTAL ANALYSIS, MODELLING AND SIMULATION
Dr. Ahmed Makradi , Lyazid Bouhala, Dr. Salim Belouettar
- 46_ DÉVELOPPEMENT D'UN SYSTÈME POUR L'ANALYSE BIOMÉCANIQUE DU PIED
Guido Becker, Marc Schmiz

_comité de lecture Ingénieur dipl. Pierre Dornseiffer
Représentant membre ALI

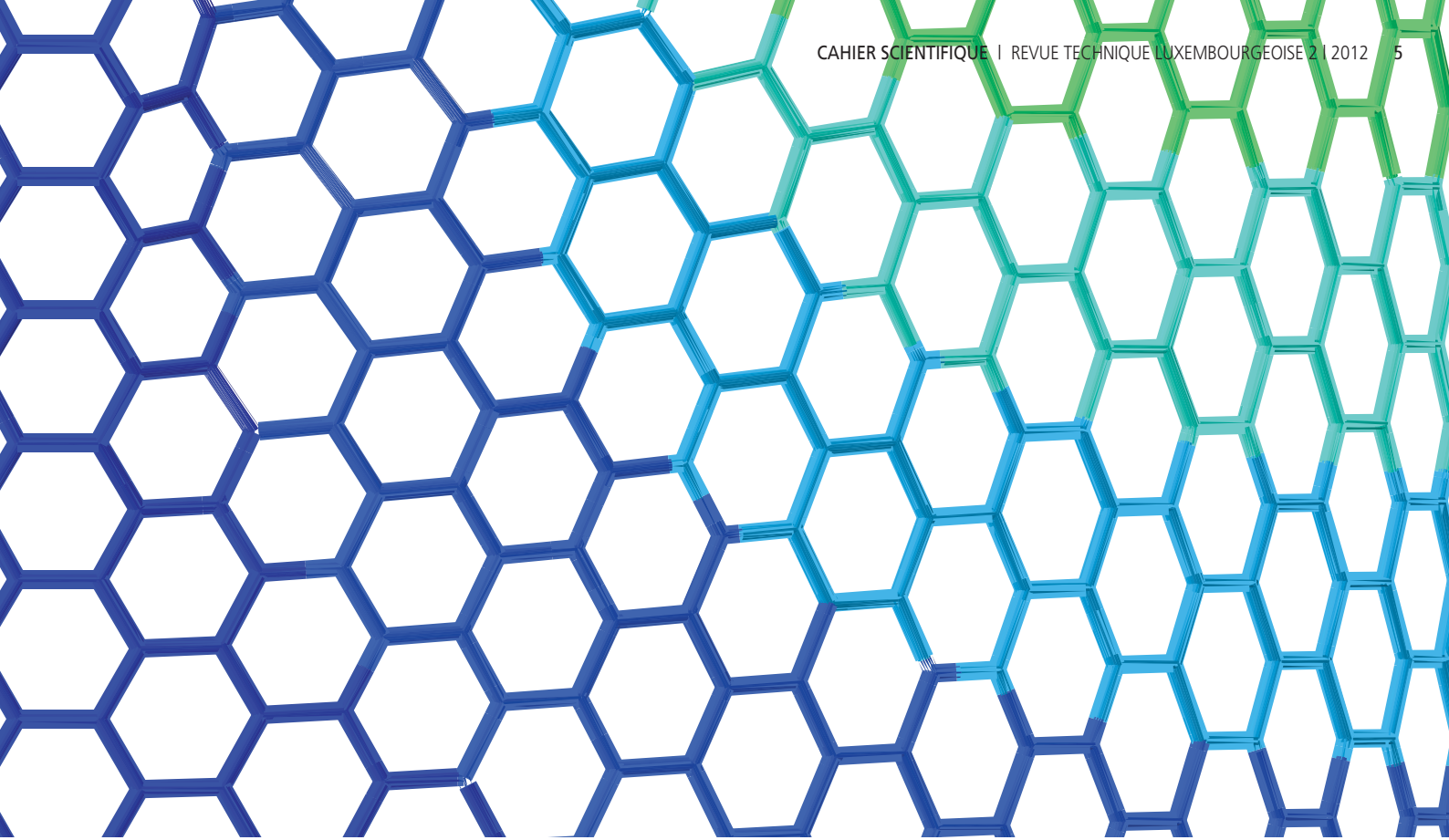
Ing. Dipl. Marc Feider
Administrateur et chef de service Bâtiments / Ouvrages
Schroeder & Associés

Prof. Dr. Ing. Jean-Régis Hadji-Minaglou
Université du Luxembourg, Unité de recherche: Ingénierie
Faculté des Sciences, de la Technologie et de la Communication

Informaticien dipl. Patrick Hitzelberger
Centre de Recherche Public - Gabriel Lippmann Département ISC

Prof. Dr. Ing. Michel Marso
Professeur en Technologie de Télécommunications
Université du Luxembourg, Unité de recherche: Ingénierie
Faculté des Sciences, de la Technologie et de la Communication

Dr. Paul Schosseler, Directeur
CRTE / CRP Henri Tudor



Carbon Nanotube © A.A.R. Wilmes

revue publiée pour_



www.ali.lu



www.oai.lu



www.tema.lu

A L I A I
 ASSOCIATION LUXEMBOURGEOISE DES
 INGÉNIEURS - ARCHITECTES - INDUSTRIELS
www.aliai.lu

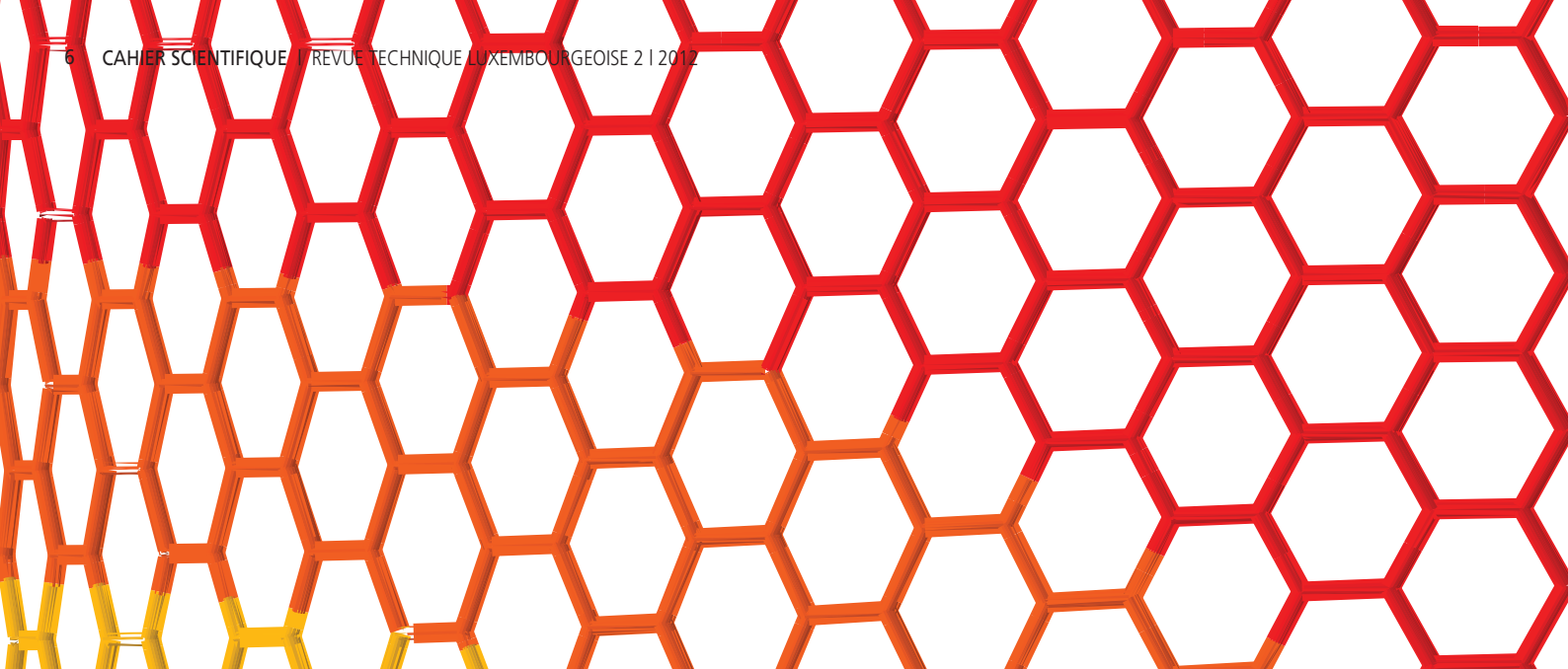


partenaires de la revue_



revue imprimée sur du papier_





C'est à l'automne 2009 que remontent les débuts de mon activité au sein de l'Association Jeunes Scientifiques Luxembourg (AJSL), lorsque j'étais en première année de médecine à l'Université du Luxembourg. Pendant un cours de physique, le coordinateur scientifique de l'association, vint nous la présenter, nous exposant en détails en quoi consistait son concours annuel. Je n'attendais qu'une telle occasion et je fus ravie de la perspective d'un projet s'inscrivant dans la durée et mené en toute indépendance dans un domaine des sciences qui m'intéressait. Une idée de projet en tête, il ne me restait plus qu'à trouver un labo au sein de l'Université, ainsi qu'un superviseur pour encadrer mes recherches. Entre-temps, Sylvia Binck, amie de longue date et étudiante de la même promotion, s'était jointe à l'entreprise ; nous eurent tôt fait d'informer de nos projets notre enseignant de laboratoire de chimie, le Dr. Brice Appenzeller, chercheur au CRP-Santé, qui voulut bien nous accueillir dans sa division de recherche.

Le projet consisterait à vérifier si la population étudiante au Luxembourg était ou non surexposée au tabagisme, par la quantification de la nicotine décelée dans des échantillons de cheveux d'étudiants volontaires. Les recherches devaient débuter fin janvier et durer trois mois. Combiner ce projet avec nos études ne fut pas toujours évident, mais j'étais toujours ravie à la pensée de reprendre nos expériences en labo après nos heures de cours. Fin avril 2010 - date à laquelle nous devons remettre le rapport de notre projet - arriva bien assez vite. Il ne nous restait plus qu'à préparer notre passage devant le jury, qui se révéla par ailleurs être une très bonne expérience.

Cependant, ni Sylvia ni moi ne nous attendions à la récompense que nous attribua le jury: il avait été décidé que nous participerions au London International Youth Science Forum (LIYSF), séjour de deux semaines sur le campus principal d'Imperial College London. J'attendais du forum qu'il me permette d'affiner ma perception du monde de la recherche scientifique et de la vocation de chercheur. Ce fut en réalité un véritable tournant dans mes études. Ces deux semaines m'offrirent en effet un condensé de découvertes s'insérant dans un environnement unique en son genre: nous eûmes le privilège, d'une part, d'assister à des conférences dispensées par d'éminents professeurs et des chercheurs originaires des différents continents et, d'autre part, de visiter des centres de recherche de renommée mondiale, qui plus est, en compagnie de jeunes et brillants scientifiques internationaux partageant tous le même profond intérêt pour les sciences. Dès le début du forum, je fus

conquise par l'engagement et la motivation des chercheurs que nous avions la chance de côtoyer et dont la détermination sincère de faire progresser le monde des sciences était communicative. J'ai espéré pouvoir à mon tour m'engager sur cette voie et, au moment de quitter Londres, je me souviens encore d'avoir formulé le souhait d'un retour futur à Imperial. J'étais alors loin de me douter que l'occasion se présenterait dès l'année suivante.

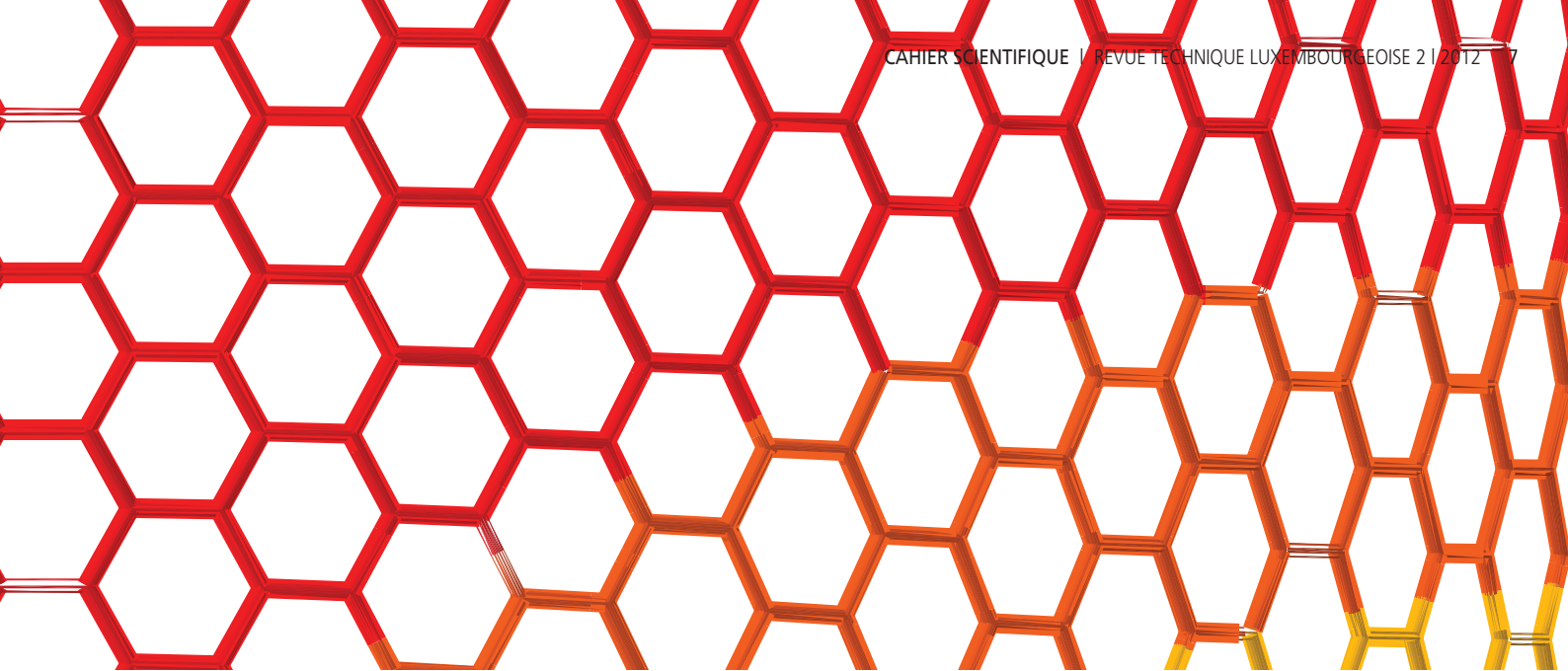
Entre-temps j'ai effectué ma deuxième année de médecine à Paris, tout en suivant parallèlement un cursus en sciences. Je me suis rapidement découvert un très vif intérêt aux domaines situés à l'interface de la clinique et des sciences fondamentales, comme, par exemple, la médecine régénérative ou encore l'imagerie médicale. C'est alors que j'ai levé l'option d'interrompre provisoirement ma formation médicale pour suivre un cursus en sciences. J'ai envisagé quelque temps de me présenter au concours d'entrée à l'École Normale Supérieure, avant de recevoir et d'accepter une offre du département de chimie d'Imperial College.

Je suis donc actuellement en deuxième année du cursus «Chemistry with Medicinal Chemistry». En d'autres termes, je me trouve de l'autre côté de la barrière par rapport à ma formation médicale initiale. J'envisage les choix qui s'offrent à l'avenir et je suis assez séduite par la perspective d'une implication directe dans la recherche. Je mise beaucoup sur un nouveau stage en laboratoire pour m'orienter au cours des prochaines années.

Actuellement, je préfère me ménager plusieurs possibilités et me laisser guider par mes centres d'intérêt. L'occasion d'une nouvelle aventure internationale s'est ainsi présentée l'été dernier, lorsque j'ai eu la chance d'être associée au Global Village Programme for Future Leaders of Business and Industry, grâce au précieux soutien de l'AJSL et du Cercle Munster. Un nouveau séjour à l'étranger, à l'Université de Lehigh, PA, USA, qui m'a permis de me plonger dans le monde des affaires en me donnant notamment l'occasion de travailler sur un projet de consultation de six semaines. Je n'aurais jamais entrepris cette expédition sans avoir participé auparavant au forum scientifique de Londres, qui demeure à mes yeux une expérience d'une valeur inestimable.

Pour l'instant je suis sûre d'une chose: je resterai dans le monde des sciences, prodigieux univers de découvertes infinies. Et comme l'a si bien dit Lee Iacocca: «With the right skills and education, we can lead the way».

Claire Roseren



Carbon Nanotube © A.A.R. Wilmes

L'année 2012 s'achevant nous entamons la nouvelle année avec une ambition renouvelée et des objectifs professionnels renforcés. La Revue Technique qui s'est instaurée comme l'organe de presse principal pour les sujets techniques des domaines de l'ingénierie, de l'industrie et de l'architecture veut conforter en 2013 son action par une qualité éditoriale approfondie.

L'action menée serait impossible à maintenir sans le soutien indéfectible des partenaires dont la constance à nos côtés reste inaltérée. Que les partenaires soient remerciés et que l'action menée soit fructueuse pour notre entreprise commune aussi en 2013. Les annonceurs nous sont précieux par le soutien qu'ils manifestent de façon répétée et continue. Notre gratitude leur soit certaine

Même à l'heure du bilan pour cette année intéressante notre regard reste orienté vers l'avenir. Depuis la signature des premiers partenariats la Revue Technique n'a cessé d'instaurer les mutations nécessaires à sa modernisation au service de la qualité du contenu. Par l'engagement de l'équipe éditoriale

et celle des partenaires la Revue Technique est devenue un pourvoyeur d'informations professionnelles performant sur support imprimé ou digital. Le site internet de la Revue Technique est facilement accessible et constamment mis à jour.

Grâce à l'intérêt croissant des lecteurs, nous continuons à augmenter notre édition. La qualité des publications est optimisée sans relâche et l'équilibre entre ingénierie, architecture et technologie est maintenu. Les thèmes traités vont de l'ingénierie appliquée à la technologie, la recherche, les énergies renouvelables, l'architecture, l'urbanisme et le design. Aussi pour l'année à venir ces thèmes seront abordés en nos diverses publications, conférences et expositions.

Nous vous souhaitons, ainsi qu'à vos familles une bonne année 2013, tous nos meilleurs vœux de santé, de bonheur et de prospérité.

Michel Petit, rédacteur en chef

Sonja Reichert, coordinatrice d'édition

MERCI POUR VOTRE SOUTIEN_



Die zu erneuernde Straßenbrücke (OA756, siehe Abbildung 1) wurde im Jahre 1918 erbaut. Sie liegt im Bereich der „Alzinger Knupp“ und führt die N3 über die Bahnlinie Berchem – Ötringen. Seit 1997 werden Risse im Mauerwerk dokumentiert, die unter anderem darauf zurückzuführen sind, dass die N3 verbreitert wurde und in der Folge die Verkehrslasten zugenommen haben. Durch veränderte Statik besteht seit 2003 die Gefahr, dass Steine unter Einfluss der verkehrsbedingten Vibrationen auf die Eisenbahnlinie und ggf. auf einen Zug stürzen könnten.

OA756, N3 über Eisenbahnlinie Berchem - Ötringen

GEOTECHNISCHE ERKUNDUNG FÜR EINE NEUE STRASSENBRÜCKE ÜBER DIE EISENBAHNLINIE BEI ALZINGEN_

Cindy Pereira

**Lauréat du prix de la
REVUE TECHNIQUE LUXEMBOURGEOISE 2012**

Die zu erneuernde Straßenbrücke (OA756, siehe Abbildung 1) wurde im Jahre 1918 erbaut. Sie liegt im Bereich der „Alzinger Knupp“ und führt die N3 über die Bahnlinie Berchem – Ötringen. Seit 1997 werden Risse im Mauerwerk dokumentiert, die unter anderem darauf zurückzuführen sind, dass die N3 verbreitert wurde und in der Folge die Verkehrslasten zugenommen haben. Durch veränderte Statik besteht seit 2003 die Gefahr, dass Steine unter Einfluss der verkehrsbedingten Vibrationen auf die Eisenbahnlinie und ggf. auf einen Zug stürzen könnten.



1_ Die Brücke OA756 besteht aus Beton mit einer Mauerwerksverkleidung. Im Vordergrund ist ein Ausfluss der Tunneldrainage zu sehen.

Da die ursprüngliche Tunnelabdichtung beschädigt wurde, dringt infiltrierendes Grundwasser durch Risse in den Tunnel und führt dort zu Kalkablagerungen (Versinterung, siehe Abbildung 2). Diese Risse können auf differentiale Setzungen der Brücke hinweisen. Auch der progressiv verwitterte Untergrund trägt möglicherweise zum Schadbild bei.

Anstatt die Brücke zu sanieren entschied man sich für einen Neubau der Brücke, der zugleich den zweispurigen Ausbau der Eisenbahnstrecke vorbereitet. Die besondere Verkehrslage - Südumfahrung der Stadt Luxemburg durch die Eisenbahn und täglich hohes Verkehrsaufkommen auf der N3- muss in der Planung und Ausführung berücksichtigt werden: eine Vollsperrung ist unter den gegebenen Um-

ständen während der Bauarbeiten weder für den Bahnverkehr noch für die Straße möglich.



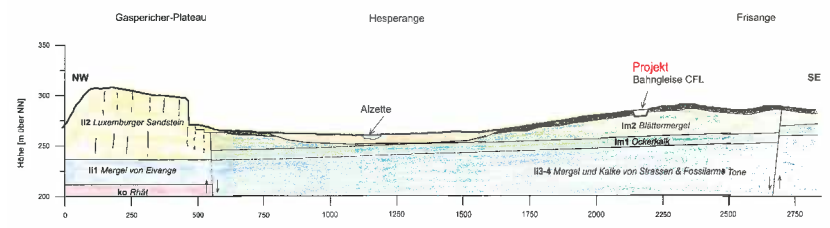
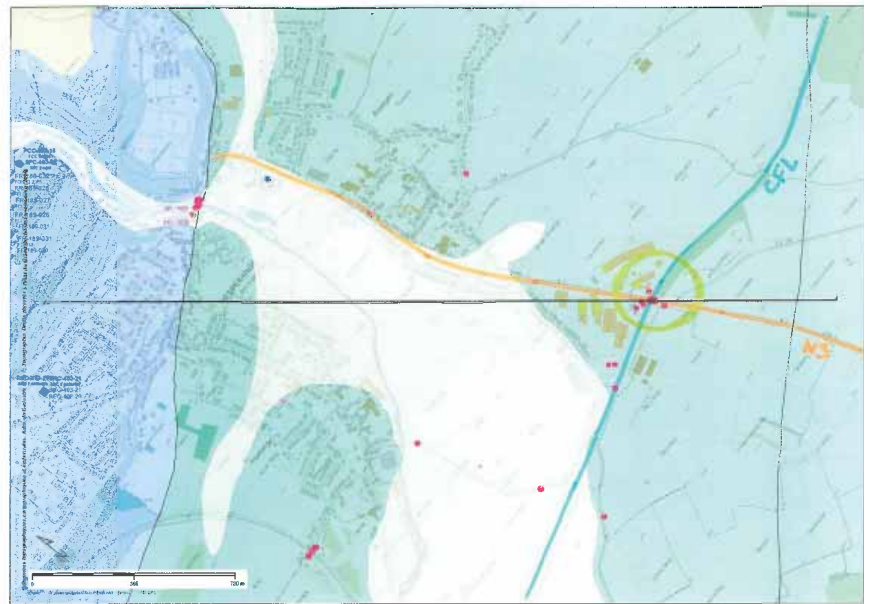
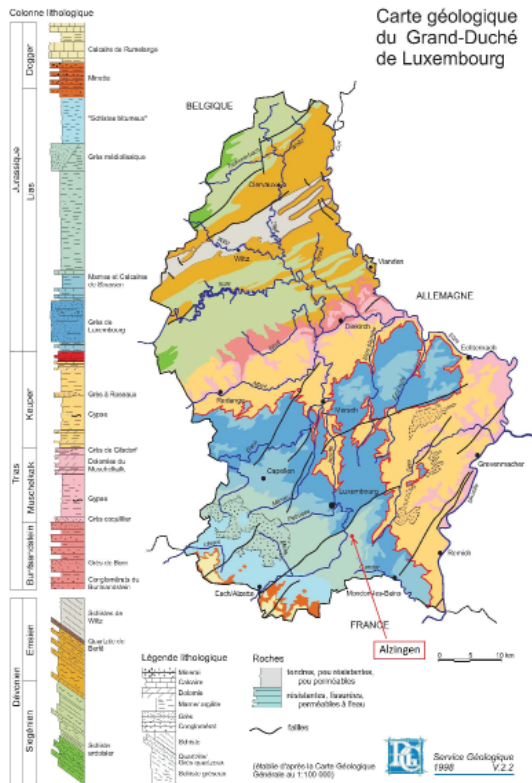
2_ Vertikale Risse mit Kalkablagerungen im Betonbauwerk

Geologie

Das Projektgebiet liegt auf tonig-mergeligen Gesteinen des mittleren Lias (Abbildung 3). Die Einheit der Blättermergel (lm2) ist ein halbfestes Gestein und wird durch eine ausgeprägte Schichtung gekennzeichnet. Es wird als wenig wasserdurchlässig, weich und wenig verwitterungsresistent eingestuft. Die im Zuge der Erkundung durchgeführten Kernbohrungen lieferten detaillierte Erkenntnisse über den geometrischen Aufbau des Untergrundes: sie zeigten die Gesteinstypen, Schichtenfolge, Neigung und Mächtigkeit der Schichten und der im Rahmen des Brückenbaus getätigten anthropogenen Auffüllungen.

Der Auszug aus der geologischen Detailkarte (Abbildung 4, Originalmaßstab 1:25.000) zeigt das Projektumfeld. Er zeigt die flächenhafte Verteilung der anstehenden Gesteine (lm2, Blättermergel und li2, Luxemburger Sandstein), sowie das auf dem geologischen Untergrund liegende Schwemmland der Alzette (a). Anhand der geologischen sowie einer topographischen Karte wurde ein Längsprofil erstellt (Abbildung 4, unten):

Im NW, nördlich Hesperingen, steht der Luxemburger Sandstein an und bildet dort einen Steilhang mit Felswänden. Der südliche Teil von Hesperingen und Alzingen liegt auf der



3_ Lage des Projektgebietes auf Gesteinen des Lias, süd-westlich der Verwerfung von Hesperingen, Auszug aus der geologischen Generalkarte und des stratigraphisch-lithologischen Gesteinsprofils © SGL 1998

4_ Auszug aus der geologischen Detailkarte (Carte géologique du Luxembourg, Blatt No. 11 Grevenmacher © SGL 1973) und geologisches Längsprofil. Lage des Projektgebietes, der Nationalstraße N3 Hesperingen-Frisingen, der CFL Eisenbahnstrecke Berchem-Ötringen sowie den zu Vergleichszwecken benutzten Projekten (SGP-208-31 und SGP-206-83, Bohrdatenbank SGL).

Einheit der Blättermergel. Im Tal der Alzette und ihrer Zuflüsse „Doulemerbaach“, „Itzigerbaach“ und „Aaleweierbaach“ liegen alluviale Talablagerungen, deren Mächtigkeiten auf mehrere Meter geschätzt werden. Der geologische Untergrund wird flächendeckend von Verwitterungsmantel bzw. Hangschutt überdeckt, deren Mächtigkeiten ebenfalls auf mehrere Meter geschätzt werden.

Eine große Verwerfung, die schon auf Abbildung 3 als schwarze Linie nördlich des Projektgebietes zu erkennen ist, begrenzt den Luxemburger Sandstein nach Süden bzw. Südwesten. Der Versatz der Verwerfung wird auf fast 100 m geschätzt. Etwa 300 m südlich des Projektes durchschneidet eine zweite Verwerfung den Untergrund. Auch hier ist der zentrale Block abgesackt, während der südliche Block gehoben wurde. Der Versatz der Verwerfung ist klein und wird auf etwa 10 Meter geschätzt. Im Bereich von Verwerfungen ist das Gestein zerrüttet und die Wasserführung viel intensiver als in nicht gestörten Bereichen. Man darf auch annehmen, dass die geotechnischen Eigenschaften der Gesteine im Bereich von Verwerfungen und ihrer Zerrüttungsbereiche weniger gut sind.

Auf der Karte der Abbildung 4 sind 2 Bohrprojekte (SGP-208-31 und SGP-206-83) dargestellt. Sie liegen an der Eisenbahnlinie und auf der Einheit der Blättermergel (Im2). Die hier in der Vergangenheit erfassten geotechnischen Eigenschaften des Gesteines wurden statistisch ausgewertet.

Erkundung

Die Planung der Erkundung erfolgte nach Eurocode 7, geotechnische Klasse 3. Die Erkundung wurde an die vorgeschlagenen Baumaßnahmen angepasst. Um detaillierte Informationen über den geologischen Untergrund zu erhalten und zur Gewinnung von Probenmaterial wurden Erkundungsbohrungen bis zu einer Tiefe von 20 m durchgeführt. Die aus den Bohrungen gewonnenen Erkundungsergebnisse gaben Auskunft über die Gesteinstypen, Schichtenfolge,

Klüftungverhältnisse, Neigung und Mächtigkeit der Schichten sowie über die Eigenschaften der einzelnen Gesteinschichten oder Auffüllungen.

Es wurden zwei Kernbohrungen mit einem Durchmesser von 100 mm abgeteuft sowie vier Pressiometerbohrungen mit einem Durchmesser von 60 mm, um den Gründungsbereich der Pfähle und Anker zu erfassen. Außerdem wurde neben einer Kernbohrung eine zweite Bohrung zwecks in-situ Scherversuche abgeteuft.

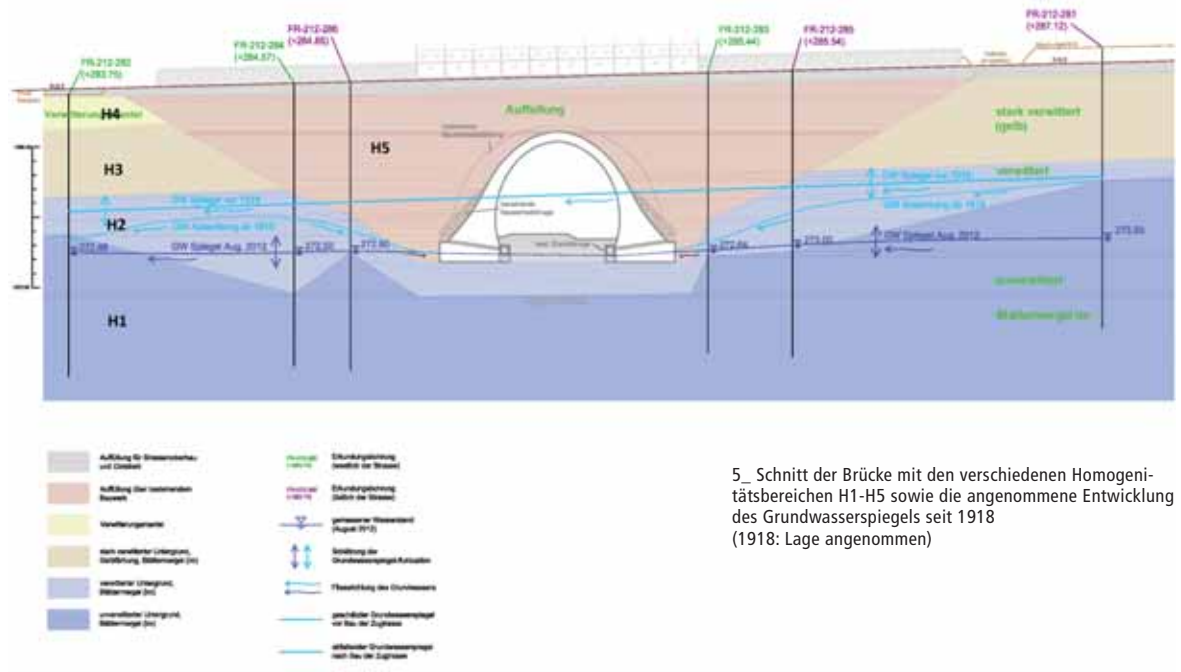
Anhand der Bohrkernbeschreibungen und der durchgeführten Bohrlochmessungen wurden im Untergrund fünf verschiedene Homogenitätsbereiche definiert (siehe Abbildung 5, H1-H5).

—H1: unverwitterter geologischer Untergrund, bestehend aus blau-grauen, geschichteten Mergeln der Blättermergeleinheit. Die Mergel sind lokal geklüftet, die Klüftflächen sind frei von Ablagerungen. Die Einheit liegt unter dem Grundwasserspiegel und ist somit permanent im gesättigten Bereich und ist keiner oberflächlichen Verwitterung ausgesetzt.

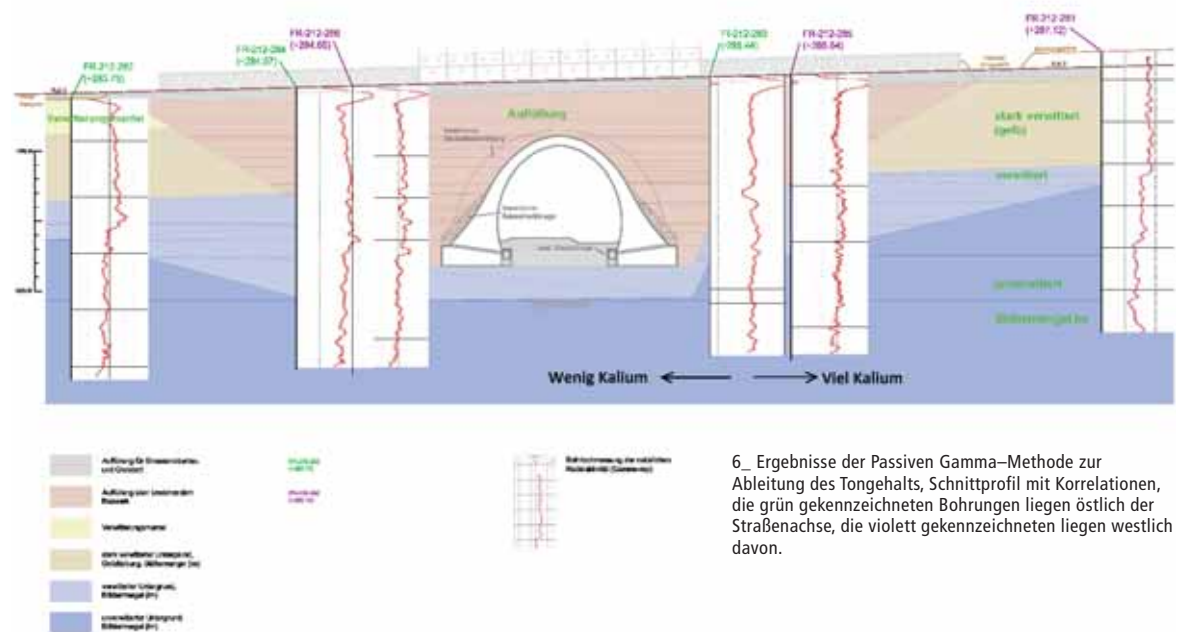
—H2: leicht verwitterter Untergrund bestehend aus blau-grauen Mergeln, welche lokal durch Verwitterung gelblich verfärbt sind. An Klüftflächen beobachtet man feine rostbraune Eisenablagerungen. Die Einheit liegt im Schwankungsbereich des Grundwassers und unterliegt der chemischen Verwitterung wie Oxidation eisenführender Minerale und Auflösung von Kalk.

—H3: stark verwitterter Untergrund, die Schichtung ist noch sichtbar, aber das Mergelgestein ist gelb-tingig verwittert. Es liegt über dem Grundwasserspiegel und ist seit historischer Zeit im ungesättigten Bereich und somit der oberflächlichen Verwitterung ausgesetzt.

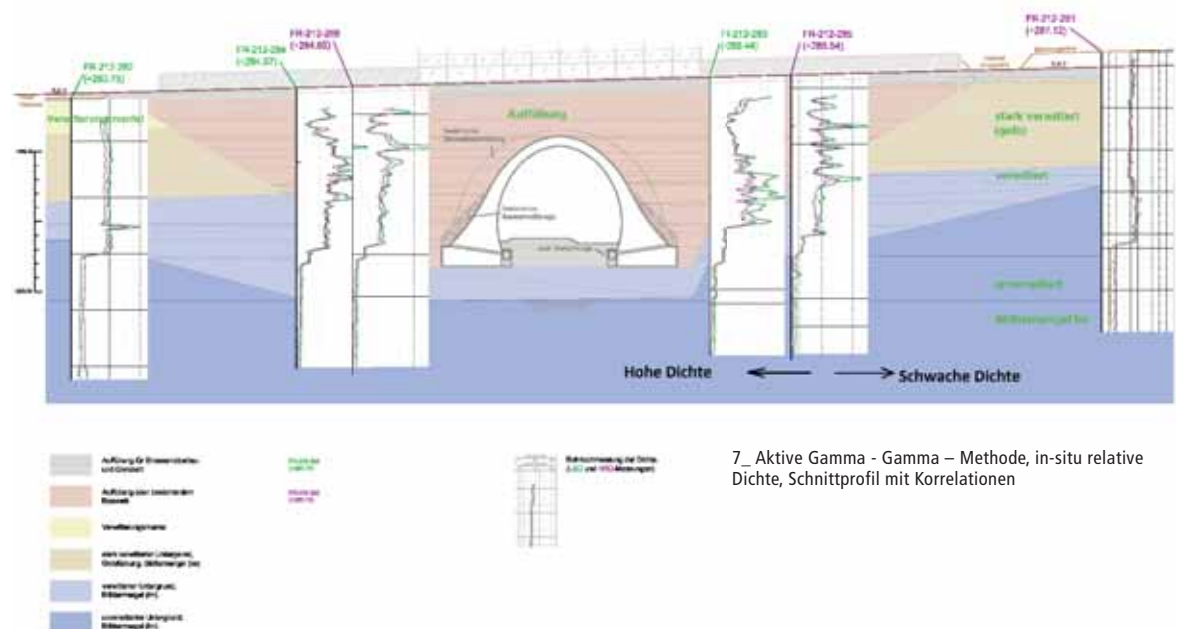
—H4: umgelagerter Verwitterungsmantel, als tonig-lehmige und wenig mächtige Deckschicht ausgebildet. Es ist



5_ Schnitt der Brücke mit den verschiedenen Homogenitätsbereichen H1-H5 sowie die angenommene Entwicklung des Grundwasserspiegels seit 1918
(1918: Lage angenommen)



6_ Ergebnisse der Passiven Gamma-Methode zur Ableitung des Tongehalts, Schnittprofil mit Korrelationen, die grün gekennzeichneten Bohrungen liegen östlich der Straßenachse, die violett gekennzeichneten liegen westlich davon.



7_ Aktive Gamma - Gamma – Methode, in-situ relative Dichte, Schnittprofil mit Korrelationen

möglich, dass ein Teil dieser Deckschicht während der Bauarbeiten abgetragen wurde.

_H5: anthropogene Auffüllungen im Bereich der umliegenden Bebauungen und im Bereich der Brücke. Diese letzteren wurden besonders anhand der Bohrlochmessungen bestimmt, sie bestehen sehr wahrscheinlich aus Aushubmaterial der Brückenbaustelle.

In-situ Versuche

In den Bohrlöchern wurden folgende in-situ Versuche durchgeführt:

_Bohrlochmessung (Diagraphie): Durch die passive Gamma-Methode wurde die natürliche Radioaktivität des Kaliums gemessen, das in Sedimentgesteinen nur in den Tonmineralien des Gesteins vorhanden ist. Dies ermöglicht Aussagen über den Tongehalt bzw. die mehr oder weniger tonige Natur der Mergel und ihrer Verwitterungsprodukte. Durch die aktive Gamma-Gamma-Methode wurde kontinuierlich die relative Dichte ermittelt.

_Pressiometerversuch: Er wurde jeden Meter durchgeführt und dient der Ermittlung des Grenzdruckes sowie des Pressiometermoduls. Diese geben Angaben über die Standfestigkeit des Baugrundes und ermöglichen die Bestimmung der Pfahltragfähigkeit.

_Phicometerversuch: Mit diesem Versuch wurde die Scherfestigkeit im Feld bestimmt. Mithilfe dieser Werte und der Wichte des Bodens kann der Erddruck ermittelt werden.

Die Diagraphien ermöglichten es, parallel zu den direkten Beobachtungen an den Bohrkernen, Korrelationen zwischen den Bohrkernen zu erstellen. Sie waren besonders bei den kleineren Bohrdurchmessern nützlich, auf denen der Bohrkerngewinn oft sehr gering war.

Die Schnittprofile zeigen den geologischen Aufbau des Untergrundes sowie verschiedene Messergebnisse der in-situ-Messungen. In den Schnittprofilen sind die Bohrungen auf die Projektachse projiziert worden. Die Bohrungen FR-212-282, -284, -283 liegen auf der östlichen Straßenseite (Richtung Ötringen), die anderen Bohrungen FR-212-286, -285 und -281 auf der westlichen Straßenseite (Richtung Berchem).

Die Veränderungen der Wasserführung im Untergrund sind auf Abbildung 5 dargestellt.

Der aktuelle Grundwasserstand befindet sich fast auf der gleichen Tiefe wie die Sohle des Bauwerks. Unter dem Einfluss der sehr gut wirkenden alten Brückendrainage wurde das Grundwasser progressiv abgesenkt, was eine progressive Verwitterung des Blättermergels induzierte. Die Brücke und der etwa 400 m lange Einschnitt unterbrechen seit 1918 den Grundwasserabfluss. Anhand der Lage der Verwitterungsschichten wird angenommen, dass der ursprüngliche Grundwasserstand etwa 3-7 m höher lag. Die Dokumentation der Grundwasserschwankungen bis nach dem Neubau wird durch den Ausbau zweier Bohrungen als Pegel gesichert.

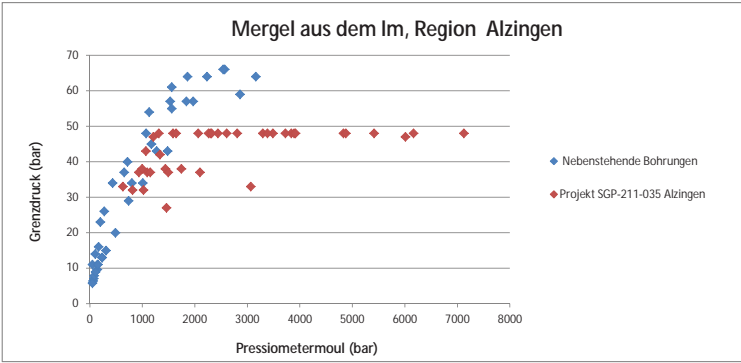
Passive Gamma-Methode

Die Ergebnisse der Diagraphien in Abbildung 6 zeigen, dass der Tongehalt bei den einzelnen Bohrungen relativ wenig variiert, in den äußeren Bohrungen zeigt sich jedoch eine deutliche Zunahme des Tongehaltes zur Oberfläche hin. Regelmäßige Änderungen wie in der südlichen (Richtung Frisingen) gelegener Bohrung FR-212-281 zeigen die Mächtigkeiten der tonigen gelb verwitterten Tonsteinschicht. Die Brückenauffüllungen sind ähnlich tonig wie das Untergrundgestein. Es wird daher angenommen, dass die Brückenauffüllung aus Aushubmaterial der Baustelle besteht. Der Straßenaufbau aus kaliumreichen Hochofenschlacken ist in den zentral gelegenen vier Pressiometerbohrungen klar zu erkennen.

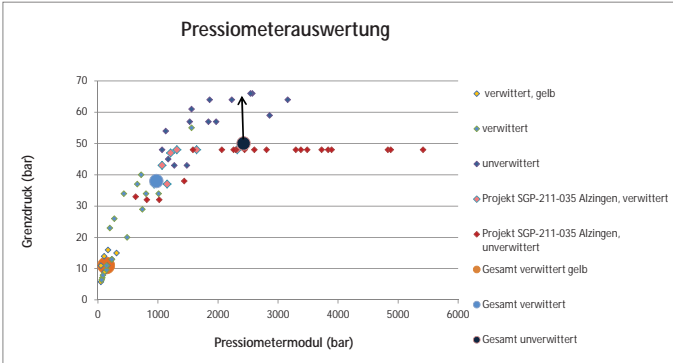
Aktive Gamma-Gamma-Methode

Die relativ erfasste Dichte des Untergrundes (Abbildung 7) ist im unteren Bereich sehr homogen. Die Messung wird anhand von Geigerzählern und Einschlägen (cps, „coups par seconde“) dokumentiert. Je weniger Einschläge, desto dichter ist das Gestein. Die Messung ergibt aber nur relative Aussagen über die Dichte. Durch den Vergleich mit Laboraten wird die vor Ort vorhandene Dichte erfasst.

Oberhalb des Grundwasserspiegels sind die Einschlagzahlen höher, da von der Luft im Bohrloch weniger Strahlen absorbiert werden als im Wasser. Im ungestörten Gelände, repräsentiert durch die links und rechts vom Projekt gelegenen Kernbohrungen, sind die Variationen auch in den höheren Schichten klein. Die Brückenauffüllung ist dagegen durch geringe Dichten und große lokale Variationen



8_ Vergleich der in diesem Projekt ermittelten Pressiometerdaten mit denen aus anderen Daten (Projekt SGP-208-31 und SGP-206-83)



9_ Darstellung der Daten der drei Proejkte(SGP-211-035, SGP-208-31 und SGP-206-83) und vorgeschlagene Werte für die einzelnen geotechnischen Homogenitätsbereiche

gekennzeichnet. Das Auffüllmaterial ist weniger verdichtet. Eine Ausnahme kann in der nördlich gelegenen Bohrung FR-212-286 beobachteten werden. Es ist möglich, dass die Verdichtung hier besser ist, weil an dieser Stelle während der Auffüllzeit ein Bauweg lag.

Pressiometerversuch

Die Pressiometerdaten sind in Abbildung 8 dargestellt. Sie helfen, die Fragestellung der Einbindung der Pfähle und deren Verankerung im unverwitterten bzw. im wenig-verwitterten Untergrund zu beantworten. Um die verschiedenen Homogenitätsbereiche zu beschreiben, wurde auf Vergleichsdaten aus Bohrungen in gleicher geologischer Situation zurückgegriffen. Prinzipiell steigen die Werte mit der Tiefe und dem abnehmendem Verwitterungsgrad des Gesteines. Für das Pressiometermodul wiesen die unverwitterten Mergel (H1) einen Mittelwert von 2427 bar auf, die grau verwitterten Mergel (H2) einen Mittelwert von 973 bar und die gelb verwitterten Mergel (H3) einen Mittelwert von 137 bar. Für den Grenzdruck lagen die Mittelwerte bei 50 bar (unverwitterter Mergel, H1), 38 bar (grau verwitterter Mergel, H2) und 11 bar (gelb verwitterter Mergel, H3).

Abbildung 8 differenziert zwischen den Ergebnissen aus diesem und den zu Vergleichszwecken herangezogenen Projekten, die ebenfalls in der Einheit der Blättermergel (Im) liegen. Die Abbildung zeigt einen regelmäßigen Verlauf des Grenzdruckes in Bezug auf das Pressiometermodul. Die Daten des vorliegenden Projektes liegen bei hohen Werten des Pressiometermoduls als Linie bei maximal 48 bar (4,8 MPa) unter der regelmäßigen Kurve, da hier der Grenzdruck normkonform und versuchsbedingt nur maximal 48 bar betrug. Die regelmäßige Kurve enthält ältere Daten, bei denen absolute Werte (Kriechdruck) für die Auswertungen benutzt wurden. Bei der kritischen Analyse fällt auf, dass die in der Abbildung 8 umkreisten Daten im Vergleich mit den anderen Daten, aus den Projekten SGP-208-31 und SGP-206-83, zu geringe Werte aufweisen. Diese sind aufgrund methodischer Probleme wahrscheinlich als falsch einzustufen.

Die Abbildung 9 zeigt die Pressiometerdaten und die Mittelwerte, welche für die verschiedenen geologischen und auch geotechnischen Homogenitätsbereichen vorgeschlagen

werden. Der Mittelwert des Grenzdrucks für den unverwitterten Untergrund ist als Minimalwert anzusehen. Nach der Modellkurve könnte dieser höher eingesetzt werden.

Phicometerversuch

Der Phicometerversuch wurde nur in diesem speziell für diesen Versuch abgeteuftem Bohrloch FR-212-288 durchgeführt. Die folgende Tabelle stellt die Scherfestigkeit dar, die in unterschiedlichen Tiefen ermittelt wurde:

Aufschluss	Tiefe [m]	Bodenart	ϕ [°]	c_1 [kN/m²]	ϕ' [°]	c'_1 [kN/m²]
FR-212-288	5	Mergel, gelbbraun	23	23	25	7,7
FR-212-288	6	Mergel, graubraun	18	84	25	28,0
FR-212-288	7	Mergel, graubraun	19	85	25	28,3

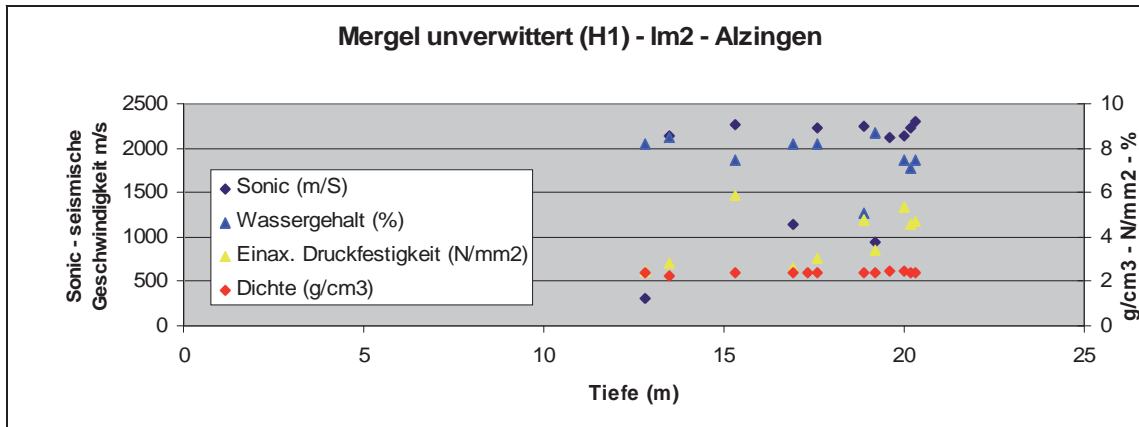
Laborversuche

Zusätzlich wurde im Labor zur Bestimmung der geotechnischen Eigenschaften des Materials der Wassergehalt, die Dichte, die seismische Geschwindigkeit sowie die Scherfestigkeit und die Druckfestigkeit an unterschiedlichen Bodenproben analysiert. Wasserproben wurden aus den Pegeln entnommen und analysiert, um die Aggressivität des Wassers gegenüber Beton festzustellen.

Der Wassergehalt ist eine einfache Größe, aus der gute Aussagen über den Zustand eines Materials abgeleitet werden können. Gleichzeitig ist er ein guter Indikator für die Homogenität des Materials. Toniges und mergeliges Gestein reagiert schnell auf Wasserzunahme oder Wasserentzug. Mit zyklischen Versuchen im Feuchtraum und Trockenschrank wurde die Verwitterbarkeit des Mergels getestet – es zeigt sich, dass die Wasseraufnahmefähigkeit des Mergels rasch zunimmt.

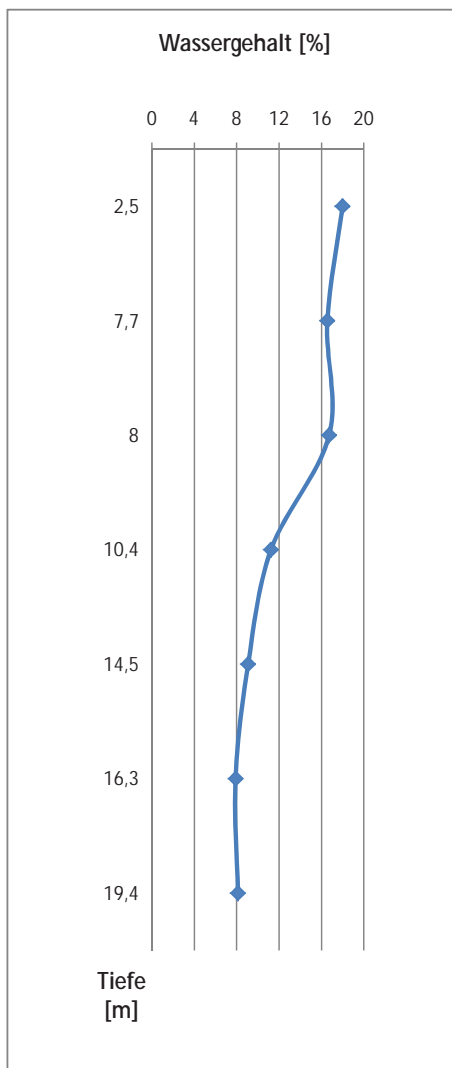
Die Messreihe in Abbildung 10 zeigt eindrucksvoll die Zunahme des Wassergehaltes mit dem Verwitterungsgrad. Der Wassergehalt sinkt bei einer Tiefe von etwa 8 m bis 10 m von 16 Gew.-% auf 8 Gew.-%.

Anhand der Werte der Wasseranalyse wird die Expositions-kategorie des Betons ermittelt. Da insbesondere aber auch der hohe Chloridgehalt bis 300 mg/l (Sommermessung)



11_ Laborversuche an 10 Mergelproben der Pressiometerbohrungen (Kerndurchmesser 60mm) aus dem unverwitterten geologischen Untergrund.

nicht vernachlässigt werden darf, müssen besondere Vorichtsmaßnahmen genommen werden. Außerdem muss der Schwankungsbereich des Grundwassers betrachtet werden.



10_ Darstellung des Wassergehaltes

Zehn einaxiale Druckversuche wurden auf den Bohrkernen der Erkundung durchgeführt. Die Werte der Druckfestigkeit variierten zwischen 2,46 und 5,87 N/mm². Der Mittelwert lag bei 4 N/mm². Parallel zu dem einaxialen Druckversuch wurden seismische Messungen sowie die Dichte und der Wassergehalt gemessen. Die Dichte-Werte sind relativ homogen und variieren um die etwa 2.54 g/cm³. 7 der Proben weisen Geschwindigkeit von mehr als 2100 N/mm² auf, bei drei der Proben variiert die Geschwindigkeit zwischen 1100 und 300 m/s; man kann annehmen dass diese Proben latente Klüftung aufweisen. Der Wassergehalt ist relativ homogen und kennzeichnet den unverwitterten Untergrund. Ein einzelner Wert von etwa 5% ist wahrscheinlich als Messfehler anzusehen.

Die oben genannten Werte kennzeichnen, so wie die Pressiometerwerte und Bohrlochmessungen, einen homogenen Untergrund, die Mittelwerte werden zur Berechnung der Länge der Pfähle und Anker herangezogen.

Zusammenfassung

Die geotechnische Erkundung mit Bohrungen, in-situ Versuchen und Laboruntersuchungen hat Erkenntnisse über den geometrischen Aufbau des geologischen Untergrundes, seine geotechnischen Eigenschaften und seine Wasserführung gebracht. Die anhand verschiedener und komplementärer Techniken ermittelten Daten erlauben dem Geotechniker sowie dem Baustatiker, die Gründung des Bauwerks zu planen und zu berechnen.

Die Planung des neuen Bauwerks muss an den geologisch-geotechnischen Aufbau des Untergrundes angepasst werden. Besonderes Augenmerk ist auf die Lage der Anker und ihrer Verpresskörper zu richten. Die Verpresskörper müssen in einem homogenen Bereich liegen, hierfür ist insbesondere die Abbildung 5 mit der Darstellung der Homogenitätsbereiche hilfreich.

Außerdem muss auf die Wasserführung geachtet werden. Es wird vorgeschlagen, die Höhenlage an das bestehende Abflusssystem anzupassen. Tieferliegende Drainagen werden neue zusätzliche Absenkungen des Grundwassers im Gebirge verursachen, dies hätte als Konsequenz, dass die Verwitterung tiefer reichen wird und sich damit die Materialeigenschaften weiter verändern.

Derzeitige energie- und klimapolitische Ziele der EU definiert in der Strategie „Europa 2020“ sollen das intelligente, nachhaltige und integrative Wachstum Europas fördern. Die Stärkung der Nutzung von erneuerbaren Energien mit dem Schwerpunkt Biomasse wird aktuell in allen Europäischen Ländern zu einer Prioritätsaufgabe. In diesem Kontext soll das ARBOR Projekt dazu beitragen die regionalen Pilotprojekte zu entwickeln, sowie die überregionale Implementierungsstrategie für eine nachhaltige Biomassenutzung zu schaffen. Dieser Artikel stellt das ARBOR Projekt vor und präsentiert das Arbeitspaket, an dem die Wissenschaftler vom Kompetenzzentrum technischer Umweltschutz (CRTE) des öffentlichen Forschungszentrums Henri Tudor arbeiten.



ARBOR Projekt

STÄRKUNG DER ENERGETISCHEN NUTZUNG VON BIOMASSE

Dr.-Ing. Katarzyna Golkowska, Dipl.-Ing. (FH) Daniel Koster

Energieziele für 2020

Der Europäische Rat hat 2007 drei energie- und klimaschutzpolitische Ziele für 2020 verabschiedet: Senkung der Treibhausgasemissionen um 20%, Ausbau des Anteils erneuerbaren Energien auf 20% und Verbesserung der Energieeffizienz um 20% [1]. Im Rahmen der gemeinsamen Europäischen Energiepolitik, haben alle EU-Länder eigene Energieziele für 2020 formuliert. Für Luxemburg, im Vergleich zum Basisjahr 2005, werden folgende Zielwerte bis 2020 angestrebt [2]:

- 1_ Erhöhung des Anteils der erneuerbaren Energie am Bruttoenergieverbrauch von 0.9% auf 11%;
- 2_ Erhöhung des Anteils der Energie aus lokalen erneuerbaren Quellen am Bruttoenergieverbrauch von 1% auf 4%;
- 3_ Anstieg in der Biomassenutzung für erneuerbare Elektrizitätserzeugung von 46 GWh auf 334 GWh;
- 4_ Anstieg in der Biomassenutzung für erneuerbaren Transport von 12 GWh auf 2509 GWh;
- 5_ Anstieg in der Biomassenutzung für erneuerbare Wärme- und Kältegewinnung von 223 GWh auf 964 GWh.

Ein Großteil der luxemburgischen Energieziele, was die Strom- und Wärmeproduktion angeht, soll durch verstärkte Nutzung von lokal verfügbarer Biomasse erreicht werden. Zu den geplanten bzw. schon teilweise implementierten Maßnahmen gehören u.a. verstärkte Mobilisierung der Holz-Potentiale aus (Privat-)Waldflächen (effiziente Bewirtschaftung sowie die Verbesserung der Ausbau der Waldinfrastrukturen), Verbesserung der Sammlung von organischem Abfall und der Nutzung von Alt- und Restholz, weitere Unterstützung von Biogasanlagen mit den Strom- und Biogaseinspeisetarifen, sowie die Unterstützung von kleinen dezentralen Kraftwerken, die Energie auf der Basis von Biomasse erzeugen [1].

Was ist ARBOR?

Die Produktion und Nutzung von Energie aus erneuerbaren Quellen gehört auch zu den strategischen Aspekten der Regionalentwicklung für Nord-West-Europa (NWE) [3]. ARBOR ist ein Projekt co-finanziert im Rahmen von INTERREG IVB für NWE, das zum Ziel hat, die energetische Nutzung

von Biomasse, mit dem Hinblick auf das Erreichen der europäischen Ziele für 2020, zu fördern. Insgesamt sind 13 Partner aus 6 europäischen Ländern (Belgien, Deutschland, Großbritannien, Irland, Luxemburg und den Niederlanden) an dem Projekt beteiligt. Die ARBOR-Projektpartner stammen sowohl aus der Forschung als auch aus der Wirtschaft bzw. Regional- und Kommunalverwaltung.

ARBOR Fokus: Energie aus Biomasse und Reststoffen

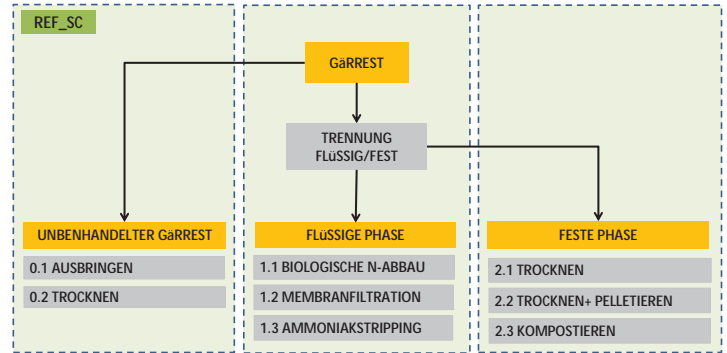
Im Rahmen des ARBOR Projektes wird die komplette Nutzungskette der Biomasse untersucht, vom Anbau der Biomasse oder der Sammlung der Reststoffe bis hin zur energetischen Verwertung (s. Abb. 1.). Dabei liegt der Fokus auf der Nutzung von biogenen Reststoffen (z.B. landwirtschaftlichen Abfällen, Grasschnitt, etc.) und mehrjährigen Energiepflanzen (Schilfgrass, Miscanthus, etc.). Es werden allerdings auch weitergehende Themen wie Agroforstsysteme und die Verbringung von Gärresten untersucht. Vor allem bei der Energiepflanzen thematik werden Konzepte entwickelt und implementiert, die als solche einen möglichst geringen zusätzlichen Eingriff in Natur bedeuten und auch nicht in Konkurrenz zur landwirtschaftlichen Nahrungs- bzw. Futtermittelproduktion stehen. Beispielsweise ist hier die schonende Nutzung von Pufferstreifen entlang von Feldern, Straßen und Gewässern bzw. industriellen Flächen zu nennen. Die analysierten Aspekte sind auch für Luxemburg von großer Bedeutung, besonders im Hinblick auf Steigerung der Energieproduktion auf der Basis erneuerbarer Energien.

CRP Henri Tudor/CRTE im ARBOR Projekt

Die Aufgabe von CRP Henri Tudor/CRTE ist, die im Rahmen von ARBOR entwickelten Pilotkonzepte mit einer Ökobilanzierung zu begleiten und die mikro- und makroökonomischen Aspekte der jeweiligen Pilotkonzepte auszuwerten. Letztlich wird eine Aussage über die Umweltauswirkungen eines Konzeptes, dessen Kosten und Nutzen und den erzeugten regionalen Mehrwert getroffen (z.B. Arbeitsplätze, Kompetenzen, regionale Kapitalbindung, etc.). Dies ist ein wichtiger Hinweis für die politischen und industriellen Entscheidungsträger.



1_ Schematische Darstellung der kompletten Nutzungskette der Biomasse untersucht im Rahmen von ARBOR-Projekt



2_ Die Behandlungsszenarien betrachtet bei der ökologischen und ökonomischen Analyse von verschiedenen Gärrestaufbereitungsmethoden

Erster Arbeitsschwerpunkt: Gärrestaufbereitung

Als erster Projektschwerpunkt wird am CRTE die Behandlung von Gärrest analysiert. Als Nebenprodukt der anaeroben Vergärung von Biomasse (z.B. Gülle, Energiepflanzen, Reststoffe, Bio-Abfälle) in Biogasanlagen fällt der Gärrest in manchen NWE Regionen (z.B. in belgischen Flandern) in großen Mengen an und darf wegen Gesetzgebung (Wasser-, Boden- und Luftemissionsschutz) nicht komplett auf die Felder ausgebracht werden. Doch auch der Export bzw. die Weiterbehandlung sind mit großem finanziellen Aufwand und zusätzlichen Umweltwirkungen verbunden. Die Ökobilanz unterstützt von einer ökonomischen Analyse wird zeigen, welche Behandlungsszenarien am günstigsten für die Umwelt und die Anlagenbetreiber ausfallen. Die betrachteten Aufbereitungsszenarien sind in der Abb. 2 dargestellt. Als Referenzszenario (d.h. die derzeit im Untersuchungsraum Flandern (B) am häufigsten angewandte Methode) wurde das Ausbringen von unbehandeltem Gärrest auf die regionalen landwirtschaftlichen Flächen gewählt. Ergänzend dazu werden auch das Trocknen des integralen Gärrestes und deren Export in andere Regionen analysiert. Diese Szenarien werden anschließend mit folgenden Aufbereitungstechnologien verglichen: die Faserseparation und die biologische Behandlung/Membranfiltration/Ammoniakstripping der Flüssigphase, sowie das Trocknen bzw. Kompostieren der faserigen Fraktion. Das getrocknete Produkt wird entweder über Pelletierung oder ohne weitere Behandlung als Kompost verwertet. Alle Szenarien beinhalten die ganzheitliche Bewertung der Prozesse. Sowohl die erzeugten Haupt- als auch die anfallenden Nebenprodukte und ihre Verwertung inkl. Transport werden analysiert. Bis auf den Prozess des Ammoniakstrippings werden alle Behandlungsmethoden mit den Primärdaten der in Flandern existierenden Gärrest- bzw. Gülleaufbereitungsanlagen bilanziert.

Thematisches Diskussionsforum für nationale Interessengruppen

Innerhalb der Projektlaufzeit, bis Mitte 2015, stehen außer Gärrestaufbereitungstechnologien eine breite Palette von Themen für die Analyse zur Auswahl. Dazu gehören u.a.

- _Anbau von Kurzumtriebsholz auf industriellen bzw. Altlastflächen
- _Nutzung von landwirtschaftlichen Zwischenfrüchten
- _Nutzung von holzhaltigem Grünschnitt aus der Landschaftspflege
- _Verwertung von Biomasse von Pufferstreifen

Bei den oben erwähnten Themen handelt es sich nicht nur um theoretische Konzepte, sondern um die in den Projektregionen in der Praxis realisierten Pilotprojekte, die sowohl die Biomasseerzeugung als auch ihre energetische Verwertung, sei es über Verbrennung oder anaerobe Vergärung in einem Biogasreaktor, beinhalten.

Um den Arbeitsfortschritt bzw. die Ergebnisse für verschiedene Konzepte in Luxemburg zu kommunizieren, werden von CRP Henri Tudor/CRTE im Rahmen des ARBOR Projekts Diskussionsforen für die nationalen Interessensgruppen organisiert. Diese werden auf irregulärer Basis stattfinden und unterschiedliche Schwerpunkte haben. Dabei erhoffen wir uns Rückmeldungen der luxemburgischen Interessensgruppen und Entscheidungsträgern, da sie den regionalen Bedarf, die bestehenden Potenziale, die rechtliche Basis sowie die lokalen Implementierungsprobleme am besten einschätzen können.

Ausblick

Ein wichtiges Ziel von ARBOR ist es, einen überregionalen Knowhow-Transfer im Bereich energetischer Konvertierung von Biomasse zu schaffen. Das im ARBOR Projekt gewonnene Wissen soll im europäischen Raum, somit auch im Luxemburg, den Behörden, Kommunen und Firmen helfen, die besten regionalen Lösungen für Einsatz von Biomasse als Energieträger zu finden. Auf diese Art und Weise können die in den Pilotprojekten gewonnenen Erfahrungen zur Beschleunigung der Entwicklung von biomassebezogenen Konzepten in anderen Regionen beitragen.

www.tudor.lu/en/projects/abor
www.nweurope.eu

Referenzen

- 1_ Europäische Kommission, (2010): Energie 2020. Eine Strategie für wettbewerbsfähige, nachhaltige und sichere Energie. Mitteilung der Kommission an das Europäische Parlament, den Rat, den Europäischen Wirtschafts- und Sozialausschuss und den Ausschuss der Regionen. Brüssel, 10.11.2010.
- 2_ NREAP, (2010): Luxemburger Aktionsplan für erneuerbare Energie. Luxemburg, Juli 2010.
- 3_ INTERREG IVB North West Europe (NWE) Programme - a financial instrument of the European Union's Cohesion

De la perfection géométrique de l'arc-en-ciel aux mouvantes aurores boréales, les spectacles lumineux que nous offre la nature émerveillent. Lors d'une conférence publique organisée le 23 janvier 2012 dans le cadre de l'exposition «Haut en couleurs» au 'natur musée', André Mousset a partagé sa passion pour «les couleurs du ciel» en présentant les raisons du bleu du ciel, des couleurs du soleil levant/couchant, de l'atmosphère vue de l'espace, des nuages, des arcs-en-ciel, des halos, des couronnes, ainsi que de phénomènes lumineux plus rares tels les arcs circumzénithaux, les parhélies, les aurores polaires.

LES COULEURS DU CIEL_

André Mousset



Extrait de la conférence: Pourquoi le ciel est-il bleu? Pourquoi le soleil couchant est-il orange?

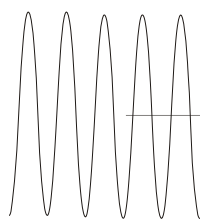
Ouvrez vos yeux et tournez-les vers la voûte céleste, en plein jour et par temps serein, sans bien sûr regarder dans la direction des rayons solaires. Vos deux rétines devraient capter de la lumière que vous nommerez «bleuâtre» après interprétation par votre cerveau des signaux électriques qui lui ont été transmis par vos deux nerfs optiques. Vous prétendrez que de la lumière plus ou moins bleue est rentrée dans vos pupilles, autrement dit, que le ciel est bleu!

D'où provient cette lumière bleue? Certainement pas du vide interstellaire, aussi immense qu'il puisse être, ni de quelques étoiles géantes, d'immenses galaxies cannibales ou d'éventuelles supernovae, émettant pourtant tous des rayonnements d'une puissance inouïe. Non, l'émetteur de la lumière bleue est infiniment faible et se trouve tout près de vous. Toute molécule d'azote et toute molécule d'oxygène de l'air qui vous entoure rayonne de la lumière légèrement bleuâtre, avec une intensité à peu près égale dans toutes les directions. Les milliards de milliards de milliards de molécules rayonnantes de votre plus proche entourage, de même que les innombrables molécules plus lointaines de

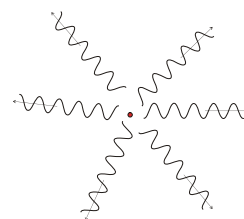
l'atmosphère terrestre, envoient un rayonnement bleu dans toutes les directions de l'espace, donc aussi dans vos yeux tournés vers le ciel.

Comment se fait-il que les molécules de l'air puissent rayonner? Se comporteraient-elles comme les antennes des stations radio, émettant leur programme sous forme d'ondes électromagnétiques? Eh bien, oui! À condition qu'on leur fournisse une énergie au moins égale à celle qui est rayonnée! Conservation de l'énergie oblige.

Lorsque les molécules de l'air atmosphérique reçoivent le rayonnement électromagnétique en provenance du Soleil, il se produit une interaction entre le rayonnement et les molécules: celles-ci en absorbent une partie pour l'éparpiller aussitôt dans toutes les directions. Le physicien dit qu'il y a eu diffusion de la lumière.



La molécule diffuse l'onde absorbée dans toutes les directions



L'onde incidente entre en interaction avec une molécule de l'air

Le rayonnement électromagnétique solaire comprend, en dehors des rayonnements ultraviolet et infrarouge, surtout la lumière visible, que nous appelons encore lumière blanche, et qui contient un assemblage judicieux d'innombrables nuances colorées qui nous sont révélées dans l'arc-en-ciel. Chaque couleur correspond à une onde électromagnétique, de longueur d'onde bien déterminée, les courtes longueurs d'ondes correspondant au violet et au bleu, les plus grandes au rouge.



Spectre visible du rayonnement solaire

Peut-être pouvez-vous concevoir que les toutes petites molécules de l'air préfèrent les plus petites longueurs d'onde pour entrer en interaction. Sinon il faudra tout simplement admettre le fait naturel que les molécules de l'air diffusent préférentiellement les ondes lumineuses de petite longueur d'onde. Ainsi le violet est diffusé dix fois plus fortement que le rouge. Nous devons l'explication théorique de la diffusion d'ondes électromagnétiques par de petites particules au physicien anglais Lord Rayleigh (1871), prix Nobel en 1904. Depuis elle est connue sous le nom de diffusion Rayleigh.

Voilà! Reprenons les pièces du puzzle. Le rayonnement en provenance d'une direction quelconque du ciel, à part de la direction du Soleil, constitue un rayonnement diffusé par les molécules d'air, dont la partie des couleurs bleuâtres (violet, bleu, vert) est renforcée par rapport aux couleurs rougeâtres (jaune, orangé, rouge). Nous percevons cet assemblage d'ondes non plus comme du blanc, mais avec la couleur justement «bleu ciel»!

La diffusion Rayleigh permet d'expliquer aussi bien la couleur bleue de l'iris humaine que la couleur bleue de la fumée de cigarette!

D'ailleurs quelle serait la couleur du ciel s'il n'y avait pas d'atmosphère? Pas de molécules d'air, pas de diffusion Rayleigh, pas de rayonnement issu d'une autre direction que celle des rayons solaires. Or l'absence de lumière perçue nous procure la sensation du noir. Nous verrions le soleil briller dans un ciel totalement obscur.



Panorama photographié de la Tête Blanche (Valais), à 8 heures du matin

Il n'échappe point à l'observateur attentif que le ciel n'est pas uniformément bleu. Près de l'horizon le bleu est beaucoup plus clair qu'au zénith. Et qu'en montagne, le bleu devient de plus en plus profond à fur et à mesure que l'altitude augmente. Et qu'un paysage situé à des dizaines de kilomètres du point d'observation tire sur le bleu.

L'atmosphère a une épaisseur d'environ 100 km, mais les 20 premiers kilomètres renferment plus de 90% des molécules d'air, ceci étant dû à la diminution de la densité de l'air avec l'altitude. Entre un paysage situé à quelque 30 km et un observateur se trouve donc une couche d'air comparable à celle qui se trouve entre un observateur regardant vers le haut et l'espace. Lorsque vous regardez le ciel bleu, les yeux ne reçoivent que la faible lumière diffusée par l'atmosphère car l'arrière-fond, l'espace noir, n'émet pas de lumière. Alors que si on contemple une chaîne de montagne lointaine, la lumière captée comprend un mélange de lumière diffusée bleuâtre et de lumière émise par la montagne. Le matin ou le soir lorsque celle-ci n'est pas trop intense, la montagne apparaît avec un excès de couleur bleue. A midi, la luminosité de l'arrière fond étant plus forte, cet excès est relativement moins important.

En altitude le bleu du ciel est plus profond, car la couche d'air entre l'observateur et l'espace renferme moins de molécules. Il y a donc moins de lumière diffusée, et, avec un arrière-fond noir, le ciel apparaît forcément plus sombre.



Volcan Sajama (6542 m) vu du Pequeño Alpamayo (5410 m), à une distance de 250 km environ, Bolivie

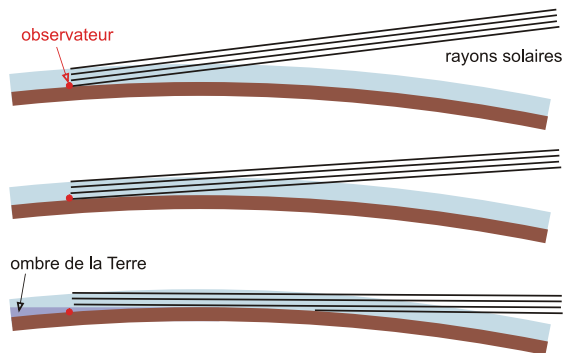
Afin de comprendre pourquoi le ciel n'est pas uniformément bleu, nous éluciderons d'abord la question pourquoi le soleil couchant est «rouge».



Soleil couchant

Lorsque le soleil se trouve à faible hauteur au-dessus de l'horizon les rayons solaires se dirigeant (pratiquement) en ligne droite vers l'oeil d'un observateur suivent un trajet beaucoup plus long à travers l'atmosphère. Sur ce parcours une proportion plus importante de bleu est diffusée dans toutes les directions. Résultat : la lumière non-diffusée atteignant l'oeil de l'observateur manque fortement de bleu. Une telle lumière est perçue orangée ou même rouge. Ce qui explique les couleurs flamboyantes de l'aurore et du soleil couchant.

La même réflexion permet de comprendre pourquoi le bleu du ciel est plus clair aux régions proches de l'horizon. En effet, notre oeil capte en dehors de la lumière bleue diffusée par les molécules proches, celle qui est diffusée par les molécules lointaines ayant perdu en cours de route l'excès de bleu à cause de la diffusion. Ce qui en reste est de la lumière orange de faible intensité, et qui atténuée la profondeur du bleu émis par les molécules proches. La couleur résultante comprend une plus forte proportion de blanc.



Lorsque le soleil se couche, le trajet des rayons solaires à travers l'atmosphère devient de plus en plus long

Le blanc dans le ciel est surtout dû aux nuages et aux poussières. En effet, les gouttelettes d'eau, les cristaux de glace et les aérosols les plus divers constituent des particules beaucoup plus grandes que les molécules de l'air. La théorie de la diffusion lumineuse par des particules de cette dimension, établie par le physicien allemand Gustav Mie (1908), veut qu'elles diffusent l'ensemble du spectre lumineux de la même façon, indépendamment de la longueur d'onde. C'est la diffusion de Mie. La lumière solaire étant blanche, la lumière diffusée doit donc l'être également.



Sur la Haute Route (Chamonix-Zermatt), le soir en refuge

De même, une atmosphère polluée par des particules solides ou liquides donne toujours naissance à un ciel de coloration moins bleue, tirant sur le blanc.

Un aspect intéressant de la diffusion de Mie est qu'elle n'a pas lieu, à l'instar de la diffusion de Rayleigh, avec une égale intensité dans toutes les directions. Elle se produit en effet principalement vers l'avant et vers l'arrière. Les porteurs de lunettes solaires savent que ce sont surtout les régions du ciel proches du soleil qui apparaissent en un blanc extrêmement intense lorsque le ciel n'est que légèrement couvert par des cirrus transparents.

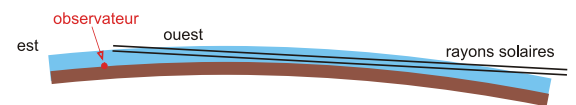
Avez-vous déjà regardé le ciel à l'est un quart d'heure après que le soleil s'est couché à l'ouest ? Dans ce cas vous avez pu apercevoir l'ombre montante de la Terre, colorée en



Arche de Vénus et ombre de la Terre

bleu foncé, surmontée d'une bande de couleur magenta appelée « arche de Vénus » ! Il s'agit de l'anti crépuscule. La coloration est due au bleu du ciel mélangée avec la lumière rouge du Soleil couchant.

Et quelle est la couleur du ciel au-dessus de vous, trois quarts d'heure après le coucher du soleil ? Le crépuscule ayant déjà bien progressé, le ciel se présente avec une teinte sombre, mais d'un bleu étonnamment prononcé. C'est « l'heure bleue » du crépuscule ! L'explication physique de ce phénomène revient à Edward Hulburt (1953) et met en jeu la couche d'ozone située entre 20 et 30 km d'altitude. En effet, cette couche de l'atmosphère est encore illuminée par les rayons solaires. L'ozone qu'elle contient absorbe certaines longueurs d'onde situées dans la partie jaune-rouge du spectre lumineux, à la manière d'un filtre bleu. La lumière rasante parvenant à traverser la couche jusqu'au zénith de l'observateur est donc bleue. Grâce à la diffusion de Rayleigh ce rayonnement bleu parvient jusqu'à l'œil de l'observateur.



Après le coucher du soleil, la couche d'ozone est encore illuminée par les rayons solaires

Terminons cet exposé pédagogiquement ! Quelle est la couleur de l'ombre dans la neige ? Besoin d'une petite indication ? D'où provient la lumière qui éclaire les parties ombragées ? Considérez que les cristaux de la neige sont assez gros pour diffuser toutes les couleurs du spectre visible dans toutes les directions, et vous aurez trouvé la réponse !



Par quelle lumière la neige ombragée du glacier Aletsch est-elle éclairée ?

Grenzüberschreitender TRENDWATCH „SMART FUTURE – SMART LIVING 2020“ in operation mit TNS zeigt überraschende Unterschiede im Ländervergleich.



EXPERTEN SEHEN ENERGIEWANDEL KRITISCH

ENOVOS FUTURE SUMMIT 2012

Die Zukunftsstudie ENOVOS TRENDWATCH „SMART FUTURE – SMART LIVING 2020“ wurde im Auftrag von ENOVOS und CREOS zusammen mit TNS Ilres, Luxemburg erstellt. Befragte aus der Energiewirtschaft, den stromintensiven Schlüsselindustrien aus einschlägigen Fachverbänden, Ministerien oder politischen Organisationen haben geurteilt, wie weit die Länder auf dem Weg zu einer zukunftsfähigen Energieversorgung bereits vorangekommen sind und wie schnell sich der Energiewandel bis 2030 vollziehen wird.

Die TNS-Studie analysiert die Penetrationsgeschwindigkeit von intelligenten Netzen und Zählern, von intelligenten Gebäudelösungen für Privat- und Zweckbauten sowie von Elektrofahrzeugen bis 2030 und darüber hinaus. Es wird erforscht, welche Treiber den Energiewandel beschleunigen oder welche Hemmnisse und standortspezifische Eigenheiten die Zukunft der Energieversorgung in den Ländern prägen.

Am 22. November wurden in der Tramschapp/Limpertsberg beim Präsentations-Event ENOVOS FUTURE SUMMIT 180 Gästen aus der Wirtschaft allererste, ausgewählte Ergebnisse des ENOVOS TRENDWATCH vorgestellt.

95% der Experten wünschen sich die Windkraft als die Energieform der Zukunft in den nächsten 20 Jahren. Beim Ausstieg aus der Kernenergie sind sich die Experten nicht in allen Ländern einig. Zwar wollen 71% der Befragten keine Kernenergie mehr in 20 Jahren nutzen. Doch 64% der französischen Experten sind der Meinung, dass der Ausstieg aus der Kernenergie „wahrscheinlich nie“ erreicht werde.

Der Ausbau erneuerbarer Energien verläuft aus Sicht der Experten nur in Deutschland nach den Vorgaben der EU. Als wichtigsten Grund für das Nichterreichen der von der Europäischen Union vorgegebenen Ziele geben 83% aller Experten an, dass die von ihrer Regierung eingeleiteten Maßnahmen zum Energiewandel nicht ausreichend seien.

Zudem halten lediglich 54% der Experten eine flächendeckende bei intelligenten Netzen bis 2030 für wahrscheinlich - bei der flächendeckenden Penetration intelligenter Zähler in privaten Haushalten sind dagegen 75% der Befragten zuversichtlich. 79% der Experten glauben, dass sich Smart Meter nur dann flächendeckend durchsetzen werden, wenn die alten Zähler kostenfrei ausgetauscht werden.

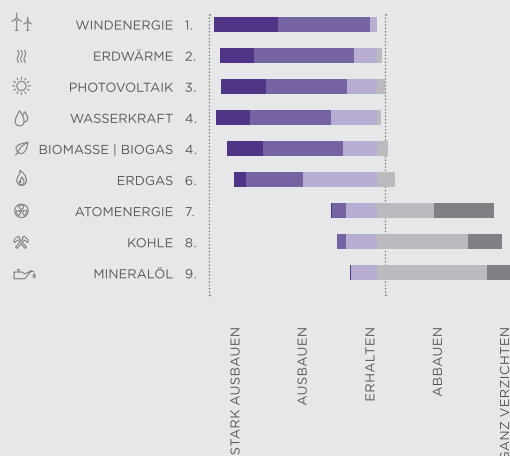
„Um den Energiewandel in diesen Bereichen umzusetzen, bedarf es erheblicher unternehmerischer Investitionen in

Netze, Speichertechnologien sowie in den Ausbau erneuerbarer Energien. Den Investitionskosten stehen deutliche Einsparungen beim Energieverbrauch und die Reduktion der Treibhausgasemissionen gegenüber. Aber: der Energiewandel sollte für den Endverbraucher bezahlbar sein und bleiben“ – so kommentiert Dr. Sabine Graumann, Senior Director und Projektleiterin des ENOVOS TRENDWATCH von TNS die Ergebnisse.

Bei der Penetration mit Elektrofahrzeugen kommt man in den Ländern nicht so recht voran. 75% der Befragten meint, dass die bis 2020 angestrebten Zulassungszahlen in ihren Ländern nicht erreicht werden. 70% der Experten aller Länder geben an, dass ein wettbewerbsfähiger Marktpreis für Elektrofahrzeuge der ausschlaggebende Treiber der Elektromobilität sei. 56% der Experten sehen in der flächendeckenden Ladeinfrastruktur und international einheitlichen Standards und Normen weitere wichtige Treiber.

ENERGIEMIX

WELCHE ENERGIEFORMEN SOLLTEN IN DEN NÄCHSTEN 20 JAHREN IHRER MEINUNG NACH AUS- ODER ABGEBAUT WERDEN?



GESAMTVERGLEICH ALLER LÄNDER: JEWEILS NUR WERTE FÜR DIE KATEGORIEN „STARK AUSBAUEN ODER AUSBAUEN“. BEI KOHLE: NUR „AUSBAUEN“

Drinking water is a precious resource. Important efforts are made to implement drinking water protection zones in Luxembourg and the communes and municipal syndicates are updating the inventories of their drinking water infrastructures through the "dossiers techniques". Rising water prices due to the introduction of the European polluter-consumer-pays principle should, however, also encourage the communes and water syndicates to review the management procedures of their drinking water networks, as important savings can be achieved through advanced control. Though larger cities in Luxembourg have high-tech supervision and data management systems, many urban water systems are operated with basic or no control. Thanks to the project MoGREPo – „Management Model of Drinking Water Networks“, CRP Henri Tudor offers an advanced control approach to optimize the management of Water Distribution Networks (WDNs) also for smaller. A first „made-to-measure“ pilot system is currently being installed in the commune of Wormeldange.

tudor
PUBLIC RESEARCH CENTRE HENRI TUDOR



MODEL PREDICTIVE CONTROL OF DRINKING WATER DISTRIBUTION NETWORK:

A PILOT IMPLEMENTATION IN WORMELDANGE_

Dr. Georges Schutz, David Fiorelli

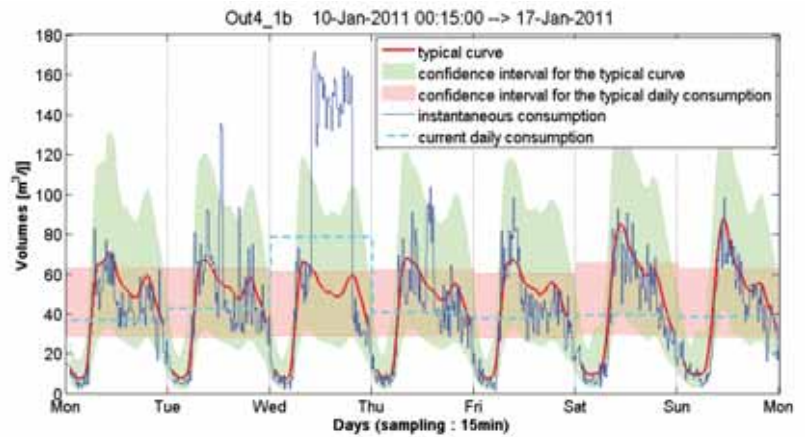
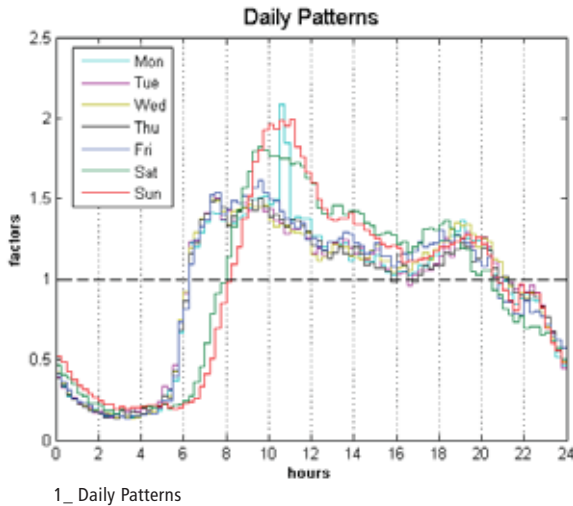


Storage tank "Bridel" (VdL)

Context and Overview

The MoGREPo project was born out of a request made by the commune of Wormeldange, which enlisted the help of Tudor to improve its water management system. With its 2,600 inhabitants and its many vineyards, the town of Wormeldange faces the problem of regulating the level of its water basins while meeting the specified daily consumption limit. This limit was introduced by the local water authority, the Syndicat Intercommunal pour la Distribution

d'Eau dans la Région de l'Est (SIDERE), through the implementation of the European Water Framework Directive [CEC 2000]. As well as the commune of Wormeldange, which is one of the first commune to react by improving the management of its WDN, several other public institutions have already expressed an interest in these research works. A water distribution network consists of storage tanks, pumps, valves, interconnected by pipes which carry water to demand nodes from the supply areas. In most cases, the



control of this system is basic. An example for this is the classical two-point control of a valve to fill a tank: the inlet valve is open at a low level and closes when the high level is reached. These low/high-level setpoints are often fixed [DVGW-W400 2004] and not dynamically adjusted towards the current WDN situation. Furthermore, the network is divided into subsystems which are operated on a local control level. This means that an actuator depends only on process measurements taken directly at the actuator site. It can be shown that, for a given network system, a global, network wide control can be more efficient [Colas 2004, Schütze 2004]. Moreover, it is difficult to integrate correctly all the different operating goals in such a limited local level control approach. Therefore, the MoGREPo project aims to support the development of advanced control strategies for greater operational efficiency and a better coordination of possible actions of all actuators over the WDN.

Methods

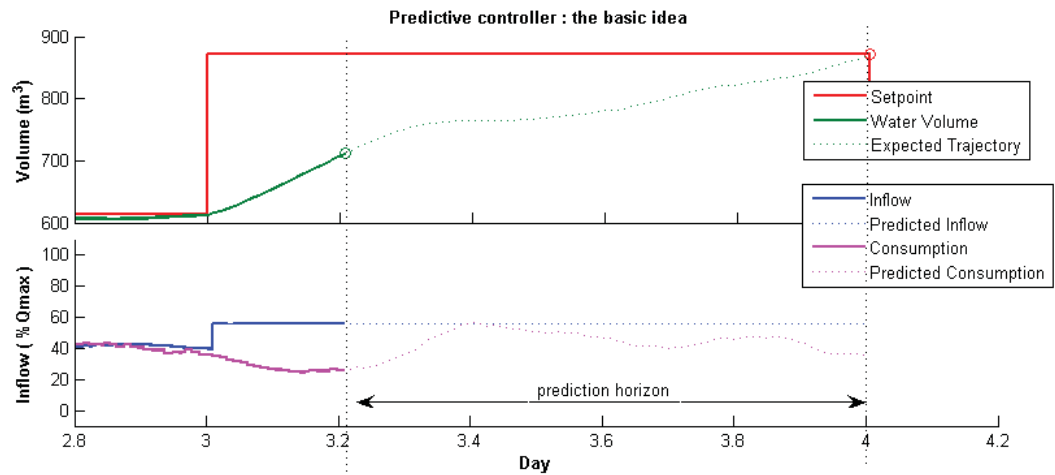
Before designing and building a global control for a WDN, the first step is to analyse data from this system and study the real time consumption as well as the variations in the water demand. A common approach is to find the typical consumption patterns for each consumption zone. Water demand is highly dominated by daily, weekly and yearly seasonal cycles and it is also weather dependant. For example, the results plotted in Figure 1 show that for the studied zone, the average daily consumption patterns for weekdays are significantly different from those of the weekend days. These typical consumption patterns can be integrated into a monitoring system to detect leaks or unusual consumptions. For this purpose, different aggregation levels like 15 minutes profiles and daily or weekly consumptions are enriched with corresponding confidence intervals around the average behaviour. Both average daily consumption and average daily pattern are illustrated in Figure 2, which represents a weekly water consumption profile for one zone in January 2011. It can be observed in this figure that on Wednesday an abnormal consumption occurs during the day where the blue solid line exceeds the green area representing the confidence interval around the average daily pattern. At least as interesting to note is that the uncer-

tainty interval is tight during the night, so night consumption becomes a good indicator for leak detection, which is confirming common knowledge in the WDN domain.

The real time control approach proposed in the MoGREPo project deals with **model predictive control** (MPC) [Rawlings & Mayne 2009] applied to the management of WDNs. This on-line optimisation-based strategy is computed iteratively by solving a set of mathematical equations, which describe the operative goals, in a given time horizon and uses a representative model for the network dynamics, as well as a demand forecast. Mathematical optimisation of the WDN is defined in a way as to be able to account for all the requirements put forward by the authorities (both the commune, the regional drinking water provider as well as the national water agency), without ignoring the operating and physical constraints of the network. The operational performance goals may include the following, according to the specified needs and requirements: reduction of supply and pumping costs, improvement of water quality and pressure regulation for leak prevention [Duzinkiewicz 2005, Ocampo-Martinez 2009, Skworcow 2009]. All the required goals Φ_i are summed to one objective function J through the use of weighting coefficients w_i to assign a relative significance to each goal. This function is therefore composed of multiple and often antagonistic goals and the solution of the optimisation problem is the solution that achieves all the goals, or offers the best trade off, while respecting the constraints $c_i(x)$ associated with the system.

$$\begin{aligned} \text{minimize } J &= \sum_{n=t}^{t+H_p} w_1 \Phi_1(n) + w_2 \Phi_2(n) + w_3 \Phi_3(n) + \dots \\ \text{subject to } c_e(x) &= 0; \quad c_i(x) \geq 0 \quad i \in E; \quad i \in I \end{aligned}$$

As the term predictive indicates, the idea of MPC is to somehow foresee the future and use this prediction to make a decision. Indeed, classical process control methods don't take into account a kind of prediction part or only over an infinite small time horizon (role of the derivative term in the standard proportional-integral-derivative (PID) controller for example). In this aspect, MPC is more akin to human reasoning which plans its decisions as a function to its process evolution forecasts. An analogy is often drawn



3_PredictiveControl Basic Idea

between MPC strategy and playing chess game: foresee the next moves (model, prediction), plan the best attack ahead of time (optimisation), play one move and repeat this thinking process at the next step by adapting to the new situation (receding horizon principle). For our purpose, we use a prediction horizon (H_p) of one day or up to the end of the day. Over this period, the consumption is assumed to follow a typical pattern with a daily volume estimated based on the consumptions measured the days before (see Figure 3).

Outcome

During the MoGREPo project the MPC approach has been tested on a simulator developed for the pilot plant of Wormeldange composed of 5 storage tanks. Based on realistic consumption scenarios, this control strategy has been analysed and compared against a standard PID control for each local station and an uncontrolled situation where the tanks are always completely filled [Fiorelli 2011]. For the pilot study the required objectives were:

- _Avoid exceeding the volume of the daily reserved capacity.
- _Minimise the residence time of the water in each tank.
- _Maintain constant flow rates into the reservoirs.
- _Ensure natural (zero energy) ventilation of the tanks, by using water level fluctuations.

As costly penalty fees have to be paid if the first objective is not achieved, it acts as the most important, overriding operating goal. With an appropriate definition of the optimisation problem and a suitable choice of the weighting coefficients impacted on each goal, the following advantages of the MPC approach can be highlighted:

- _Complete elimination of days when the daily reserved capacity is exceeded even while reducing this limit. For example, based on the consumption of 2010, a reduction of the reserved capacity by 17.5% could be achieved without any exceedance using the MPC approach, while, in the uncontrolled state, there would have been 32 days where the reserved capacity would have been exceeded by up to 25% (10% in average), and there would have been one day with 13% exceedance for the PID control. Note: the penalty the commune will pay if it is exceeding the daily limit is currently fixed according to the exceeded volume and is independent of the number of days a higher capacity is required.
- _Reduce the residence time of water in each tank to about 1 day compare to its uncontrolled state.

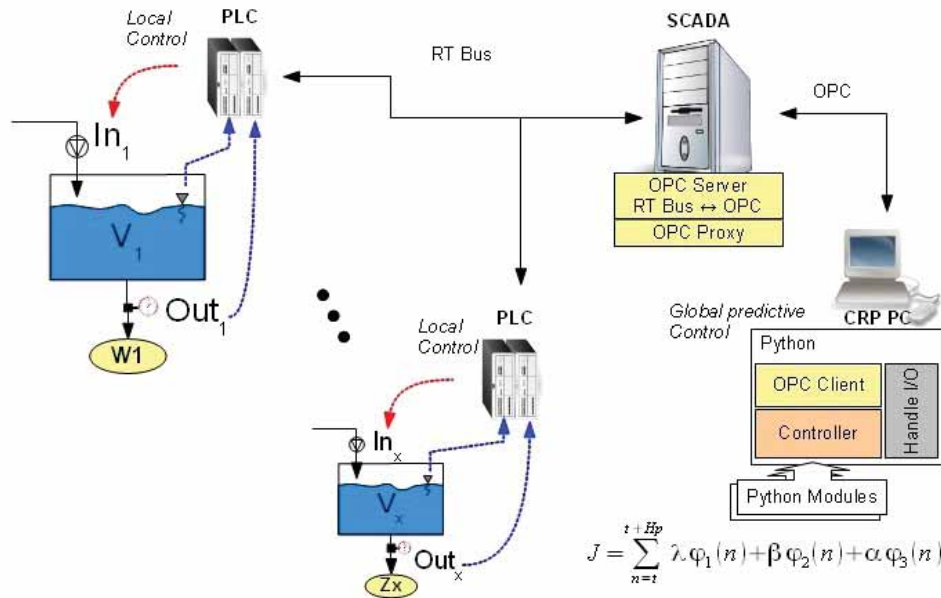
- _Reducing the variations of the tank inflow rates by 20 up to 40% while preserving a daily ventilation of around 5% of the water volume.

The considered WDN in Wormeldange is a gravity-fed network that allows transport of the water without the need for pumping. It is widely known that pumping costs represent the most significant part of the total expenditure of the operational management of WDNs. Developed for the pilot-plant of Wormeldange, the researchers of Tudor are working on the generalisation of the control system to meet the needs of others communes or syndicates already in contact with Tudor. By adding other objectives into the optimisation problem the MPC strategy is expected to achieve an even higher level of benefits for WDN, especially when it comes to finding the optimal operational schedules for pumps.

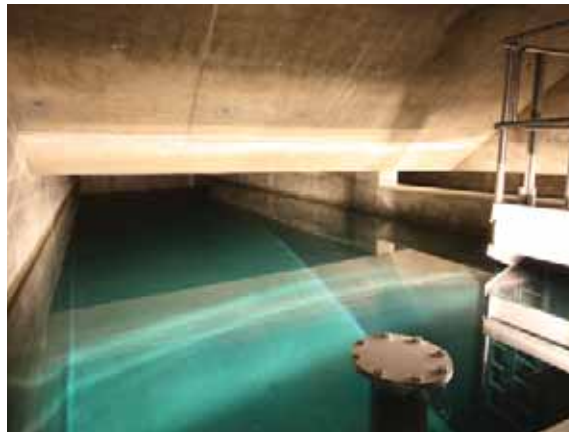
The above global control approach is conceptually a high level controller using all available network information to compute the future actions that are forwarded to the distributed low level controllers which, in turn, control the actuators. The tanks have to be connected via a real time communication network to a supervisory control and data acquisition (SCADA) system. To consider unconnected tanks in the global approach, they stay, from the system viewpoint, in an "autonomous" state. This means that these basins can be taken into account in the optimisation without the ability to control them. Currently the needed hardware and software structure is being installed in Wormeldange together with industrial partners. The communication protocol used by the MPC is based on OPC (OLE for Process Control) and a client-server architecture (see Figure 4). The new control system developed by Tudor has currently been implemented on one of the town's five drinking water basins and, by the end of 2012, the extension of the control system to the three major tanks is planned.

Perspectives

In a parallel project, the research team of Tudor is implementing a similar type of control, based on prediction and optimisation, for the management of the new sewer network currently build around the lake of the "Haute-Sûre" in collaboration with the Syndicat Intercommunal de Dépollution des Eaux résiduaires du Nord (SIDEN) [Schutz 2012]. Further applications of this type of control in other domains, such as energy distribution (smart grids), are also



4_ImplementationConcept_MoGREPo



Storage tank "Puddel" (Wormeldange)

considered and partners are sought to initiate such projects. Moreover, the gained competencies in MPC can also be applied to others industrial control problems.

The CRP Henri Tudor is assisting the communes and syndicates to make these highly advanced type control systems more accessible to operators of water distribution networks or sewer systems. We provide methodologies and tools which allow real time control of urban water networks to be considered as an option to minimise adverse impacts on the environment as well as to minimise costs. Finally, we hope to convince consulting engineering firms and other equipment suppliers that this type of technology can be an interesting avenue for them to build future product lines upon which to explore the advanced possibilities of network management. Such strategies could achieve serious reductions in the expenditure relating to the construction costs of new WDNs and this kind of control approaches could, as part of an overall scheme, lead to cost reductions that could subsequently be passed on to all of us the end consumers.

The CRP Henri Tudor wishes to acknowledge co-financing of the MoGREPo project by the Ministère de l'Intérieur et à la Grande Région (MIGR).

www.tudor.lu
www.wormeldange.lu

References

- CEC – Council of the European Communities. 2000. Directive of Establishing a framework for Community action in the field of water policy. EC Directive No. 2000/60/EEC of 23 October 2000. Official Journal of the European Communities, L 327, 1–72. <http://eur-lex.europa.eu/LexUriServ/LexUriServ.do?uri=CELEX:32000L0060:EN:NOT>.
- Colas, H., Pleau, M., Lamarre, J., Pelletier, G. and Lavallée, P. 2004. Practical Perspective on Real-Time Control. *Water Quality Resource Journal of Canada*, 39(4), 466-478.
- Duzinkiewicz, K., Brdys, M.A., Chang, T. 2005 Hierarchical predictive control of integrated quality and quantity in drinking water distribution systems. *Urban Water Journal*, 2, 125-137.
- DVGW-W 400. 2004. Technische Regeln Wasserverteilstanagen (TRWV). Arbeitsblatt des Deutschen Verein des Gas- und Wasserfaches e.V.
- Fiorelli, D., Schutz, G. and Meyers, J., 2011. Application of an optimal predictive controller for a small drinking water network in Luxembourg. In *Computing and Control for the Water Industry (CCWI 2011)*.
- Ocampo-Martinez, C., Puig, V., Cembrano, G., Creus, R. and Minoves, M. 2009. Improving water management efficiency by using optimisation-based control strategies: the Barcelona case study. *Water science and technology: water supply*, 9, 565-575.
- Rawlings, J.B. and Mayne, D.Q. 2009 *Model Predictive Control: Theory and Design*, Nob Hill Publishing, Madison, WI.
- Schutz, G., Fiorelli, D., Seiffert, S., Regneri, M. and Klepiszewski K., 2012. Modelling and optimal control of a sewer network. In *9th International conference on Urban Drainage Modelling (UDM)*.
- Schütze, M., Campisano, A., Colas, H., Schilling, W. and Vanrolleghem, P. 2004. Real Time Control of Urban wastewater Systems-where do we stand today? *Journal of Hydrology*, 299, 335-348.
- Skworcow, P., AbdelMeguid, H., Ulanicki, B., Bounds, P. and Patel, R. 2009. Combined energy and pressure management in water distribution systems. *World Environmental & Water Resources Congress*, Kansas City, USA.

In summer 2012, HITEC Luxembourg successfully completed the development of a Program Track, Step-Track and Monopulse capable Antenna Control Unit (ACU). The purpose of an ACU is to calculate the correct pointing angles of a ground station antenna towards a satellite. This article first introduces the basic concepts needed to understand the working of a ground station antenna, then focuses on the problem of target tracking in various situations and finally explains how these tasks are performed by the ACU sub-system.



DEVELOPMENT OF AN ANTENNA CONTROL UNIT FOR TRACKING OF SATELLITES WITH GROUND STATION ANTENNAS_

Tom Mathes, Engineer, Electro-Mechanical Engineering, HITEC Luxembourg S.A.

Introduction

The ACU is one of the central elements of a ground station antenna: it resides at the intersection of radiofrequency (RF), astrodynamics, servo control and mechanics and is the main interface towards the ground station control center for everything related to the antenna movement. It consists of a dedicated software application running on a server inside the antenna capable of pointing the antenna towards a moving target (e.g. a satellite) given a physical model of its trajectory and of handling the automatic tracking of this target across the hemisphere of the sky by sending appropriate commands to the antenna axis control system.

Promising market opportunities, mainly due to the sales stop of an important stakeholder in the high-end ACU market and HITEC Luxembourg's product strategy based on a software-based and modular design, coupled with an existing client base which had expressed interest for the planned development, led to a positive business case for the envisaged development. Moreover, with Luxembourg's accession to the European Space Agency (ESA) in 2005, the development of an ACU system was seen as a contribution to the emerging space industry in the Grand Duchy of Luxembourg. In-house know-how and IPR (intellectual property rights) in related fields (servo and antenna control) further strengthened the planned development project. The HITEC Luxembourg ACU product line was developed under the ESA ARTES 3-4 program (see [2]) providing project support and partial funding of the activity.

Ground Station Antennas

Satellite Ground Stations. Human-made objects in space, like for example satellites, interplanetary probes or space stations must constantly be commanded and controlled from the ground via RF signals. Their health is monitored, they are tracked to determine their orbital position, and their attitude is determined from sensor information. Payload data, such as images from an Earth observation satellite, may be downloaded. Every space-related system is therefore generally composed of a so-called space segment (e.g. the satellite) and a ground segment (the infrastructure needed to communicate with the satellite). For more information on ground segment architectures, please refer to [1], [5] or [6].

One of the ground segment elements is the antenna sub-system generally having a transmitting and a receiving section. The ground segment also includes the equipment for interfacing with the terrestrial network together with monitoring and electrical supply installations. Figure 1 provides a picture of a ground station antenna designed by HITEC Luxembourg.



1_ HITEC FM-130-Ka ground station antenna in Weilheim, Bavaria, Germany

An important characteristic of a ground station antenna is its high directivity towards the satellite position. This is necessary as signal levels are very low due to the limited signal power available on the spacecraft, the large distances and strong signal attenuations by the atmosphere. A high directivity means that the emitted and received electromagnetic power is concentrated in a small region around the point-

ing direction of the antenna, i.e. that the power density in that direction is very high. At the same time the antenna has a low directivity in other directions, in particular that of nearby satellites in order to limit interference.

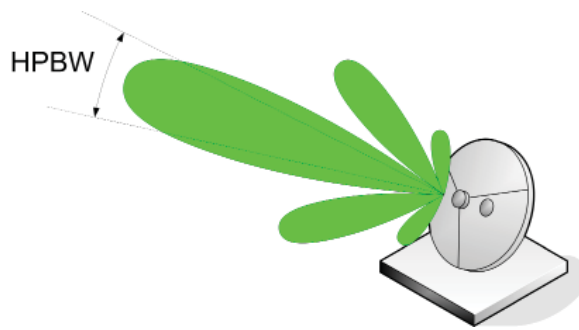
In order to continuously point the antenna in the direction of the satellite with the required accuracy without being affected by wind and other degrading effects, and to respond to orbital perturbations which, even in the case of a geostationary satellite, cause small apparent displacements of the satellite, the antenna has a tracking subsystem which compensates the relative movement of the satellite and the station. The performance of the tracking system depends of the antenna radiation characteristics and the type of satellite orbit.

Parabolic Reflector Ground Station Antennas. One of the most widespread types of ground station antennas for satellite communication is the parabolic reflector antenna, i.e. an antenna that uses a parabolic main reflector, which is a curved surface with the cross-sectional shape of a parabola, to direct the radio waves. Similarly to a flashlight, which is much more directive than a simple light bulb, a parabolic antenna has a much higher directivity than a simple omni-directional antenna. The down-side of such high directivities is that the beamwidth of parabolic antennas is very small (like the light beam of a flashlight), which complicates the pointing of the antenna in the direction of the satellite.

The angular width of the main beam radiated by high-gain antennas is measured by the half-power beam width (HPBW), which is the angular separation between the points of the antenna radiation pattern at which the power drops to one-half of its maximum value (i.e. 3dB on a logarithmic scale). For parabolic antennas, the HPBW is given by:

$$\theta_{HPBW} \sim \frac{\lambda}{d}$$

where d is the diameter of the main antenna reflector in [m], λ is the wavelength of the radio waves in [m]. The radiation pattern, together with the HPBW, is illustrated in Figure 2.



2_ Antenna radiation pattern

The directive qualities of an antenna are measured by a dimensionless parameter called gain, which is proportional to the ratio of the power received by the antenna from a source along its beam axis and the power received by a hypothetical isotropic antenna. The gain of a parabolic antenna is given by:

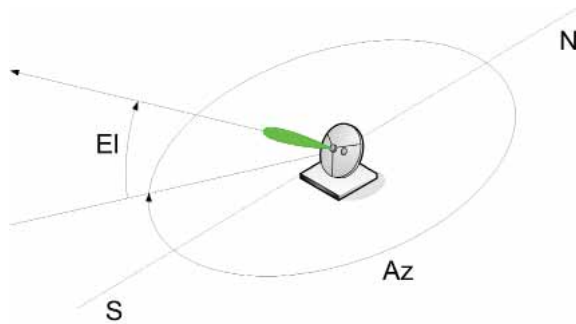
$$G \sim \left(\frac{\pi d}{\lambda} \right)^2$$

From the previous two formulas it can be deduced that the higher the signal frequency (i.e. the smaller the wavelength) and the larger the diameter of the parabolic reflector, the smaller the HPBW and the larger the gain. If one wants a larger gain, one has to accept a smaller field of view.

The following table provides a few examples from the HITEC Luxembourg antenna product range. The HPBW for these examples is in a range from around 1 deg to less than 0.1 deg. These are indicative values based on the simplified formulas above and might differ from the real values of these antennas. See [8] for product sheets of the different antennas from the table.

Type	Diameter [m]	Frequency [GHz]	HPBW [deg]	Gain [dBi]
FM-036-C	3.6	6.000	0.972	45.5
FM-130-S	13.0	2.250	0.718	48.2
LM-060-C	6.0	6.000	0.583	50.0
LM-130-C	13.0	6.000	0.269	56.7
LM-060-Ka	6.0	19.000	0.184	60.0
LM-090-Ku	9.0	14.000	0.167	60.9
FM-130-Ka	13.0	19.000	0.085	66.7

It is customary to use the elevation and azimuth angles to locate a satellite from a ground station on the surface of the Earth. The elevation angle is the angle between the local horizon at the antenna location and the satellite, measured in the plane containing the antenna, the satellite and the centre of the Earth. This angle generally varies between 0 deg and 90 deg. 0 deg means that the target is at the level of the horizon and 90 deg means that the target is exactly above the antenna. The azimuth angle is the angle measured in the horizontal plane at the antenna location between the direction of the geographic north and the intersection of the plane containing the satellite and the centre of the Earth. This angle varies between 0 and 360 deg as a function of the relative positions of the satellite and the ground station and is counted positive towards the east.



3_ Azimuth and elevation angles used for antenna pointing

Satellite Orbits. To a first approximation, satellites evolve on elliptical trajectories around the Earth. The plane of the orbit can have any orientation in space. The orbital parameters (the orbit's shape and orientation in space) are determined by the initial conditions present when the satellite is injected into orbit. According to Keplerian assumptions, the orbital parameters will remain constant with time. In the real world however, various types of perturbations (non-uniformity of the Earth's gravitational field, drag caused by the atmosphere, gravitational effects of the Moon, the Sun and the other planets, etc.) will cause the orbital parameters to slowly change with time.

Orbits can be classified according to their shape, altitude or orientation in space; the type of the satellite's orbit depends on the application the satellite is used for. For example, polar and non-polar circular orbits are used by communication services or Earth observation systems using low earth orbits (LEO) or medium earth orbits (MEO). Inclined elliptical orbits (Molnya, Tundra) are used for providing regional communications services to regions below the apogee of the orbit. Geostationary satellite systems (GEO) provide large coverage of the Earth with a single satellite; they are typically used by television satellite operators.

All non-geostationary orbits lead to large apparent motions of the satellite as seen from the ground station, making the satellite eventually appear on the horizon at a given moment, flying through the celestial hemisphere above the antenna and disappearing below the horizon at a later moment. The trajectory between appearance and disappearance of the satellite is called a pass. Passes can last from as long as several hours (MEO orbits) to only several minutes (LEO orbits). Both [4] and [7] provide a good introduction into the subjects of astrodynamics, celestial mechanics and satellite orbits.

Target Tracking

Tracking consists of maintaining the antenna beam's axis constantly aligned with the direction of the satellite in spite of the relative movement of the satellite (along its elliptical orbit) and the antenna (on the rotating Earth). Good tracking performance is of crucial importance, especially in high-

performance ground stations, where pointing needs to be extremely accurate in order to maintain a communication link with a sufficient data rate. The angular width of the beam (the HPBW defined earlier) and the type of satellite orbit affect the type of tracking. The de-pointing loss L expressed in [dB] for a small de-pointing angle θ expressed in [deg] with respect to the direction of maximum gain can be approximated by:

$$L = 12 \left(\frac{\theta}{\theta_{HPBW}} \right)^2$$

This equation shows that de-pointing has a direct consequence on the link performance. The maximum allowable link deterioration therefore determines the maximum de-pointing angle, which is the smaller the higher the frequency and the larger the dish, as seen previously. The required pointing accuracy is usually much smaller than the HPBW.

Different types of tracking methods are possible. In the following sections, 3 of the most wide-spread methods are presented. They provide a tracking accuracy and a complexity and cost increasing from the first to the last one described below.

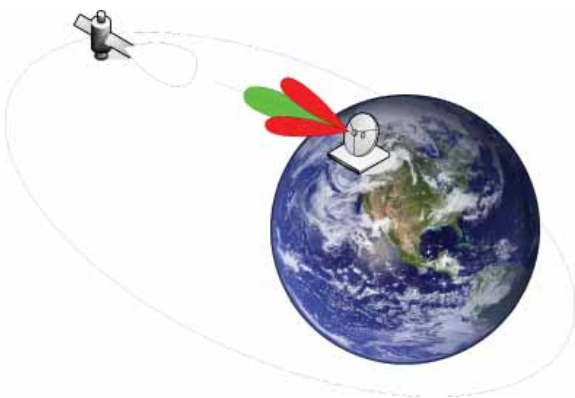
Program tracking is the simplest and most common tracking method. It consists in moving the antenna axes according to data files provided to the ACU by the flight dynamics centre. Such data files take into account the rotation of the Earth and the satellite trajectory and report the exact pointing angles required at any given moment. Alternatively the ACU can use a trajectory model contained in a so-called two lines element (TLE) file and compute the required pointing angles by itself, given that it knows the antenna's geographical position and the exact time. The pointing accuracy therefore depends on the accuracy of the estimated satellite position, of the antenna's geographical position and of the time reference on the one hand and on the antenna's capability to follow the commanded pointing angles on the other hand. In the case of large antennas (like the 6 to 13m antennas built by HITEC Luxembourg), gravity, wind and thermal distortions of the parabolic reflector may have a significant impact on the pointing precision. As a consequence, if the mentioned effects are not accounted for, the antenna may suffer a de-pointing due to these load cases affecting its mechanical structure, and the beam direction may thus differ from the one commanded by the motors. Parts of these effects can be compensated by the ACU in a functionality called error correction, described further down. Figure 4 illustrates program tracking by showing the satellite trajectory and the ground station aligned to the satellite in order to optimize the communication link. The system is in an open loop and does not foresee a real-time computation and correction of the pointing error between the actual satellite position and the ground station beam direction.



4_ Program tracking technique

Step-tracking is a more advanced tracking method than program tracking. In step-tracking the received signal level is taken into account. At regular intervals (10 to 20 minutes), the antenna makes signal level measurements by performing small changes in the pointing direction with both axes. If during these small movements, the signal level decreases or increases, the antenna knows if it is moving away or towards the direction of maximum signal level. Successive measurements allow learning a model of the satellite's trajectory. This model can then be used to position the antenna in-between measurements. As this tracking method is a closed-loop method, slow perturbation effects which are relevant in program tracking, like gravity and thermal deformations, are automatically filtered out. While program tracking can be used with all kinds of satellite trajectories, step-tracking is only suited for slow-moving satellites, like GEO orbits or slightly inclined geosynchronous orbits.

Monopulse tracking is the most advanced, complex and expensive of the three presented tracking techniques employed in ground station antennas. This approach makes use of a particular property of the antenna's RF signal reception parts which allows the antenna to have something like a second radiation pattern (also called delta or difference pattern) exhibiting a central null, as opposed to the standard pattern's (sigma or sum pattern) central maximum. This is illustrated in Figure 5, where the sum pattern's main lobe is represented in green and the difference pattern is represented in red. Ideally, the null of the difference pattern coincides with the peak of the sum pattern. As a consequence, if the ground station is perfectly aligned with the satellite, the difference pattern receives a zero signal. If the alignment is not perfect, the signal received via the difference pattern is proportional to the error for reasonably small errors. A component inside the antenna called the tracking receiver compares the signal received via the difference pattern to the signal received via the sum pattern and from this computes the de-pointing angle in real-time. Once the tracking receiver has computed the antenna alignment errors, it transfers the data to the ACU which computes the commands to be sent to the axes in order to re-align the antenna with the satellite.

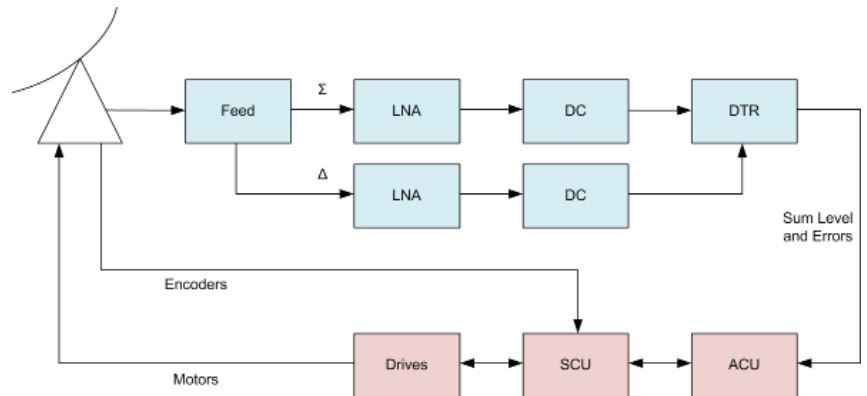


5_ Monopulse tracking technique

The HITEC Luxembourg Antenna Control Unit

Figure 6 shows a simplified block diagram of the tracking subsystem of a ground station antenna. In the case of a step-track antenna, after amplification by a low-noise amplifier (LNA) and conversion to lower frequencies by a frequency down-converter (DC), a tracking receiver (TRR) receives the incoming RF signal and transforms it into an analog voltage read by the ACU. In the case of a monopulse antenna, the TRR additionally receives the difference signal; in this case the ACU receives from the TRR also the monopulse error signals. Based on this information, the ACU computes the

pointing angles to be sent to the Servo Control Unit (SCU) which contains the control algorithms required to steer the individual antenna axes.



6_ Antenna tracking subsystem block diagram

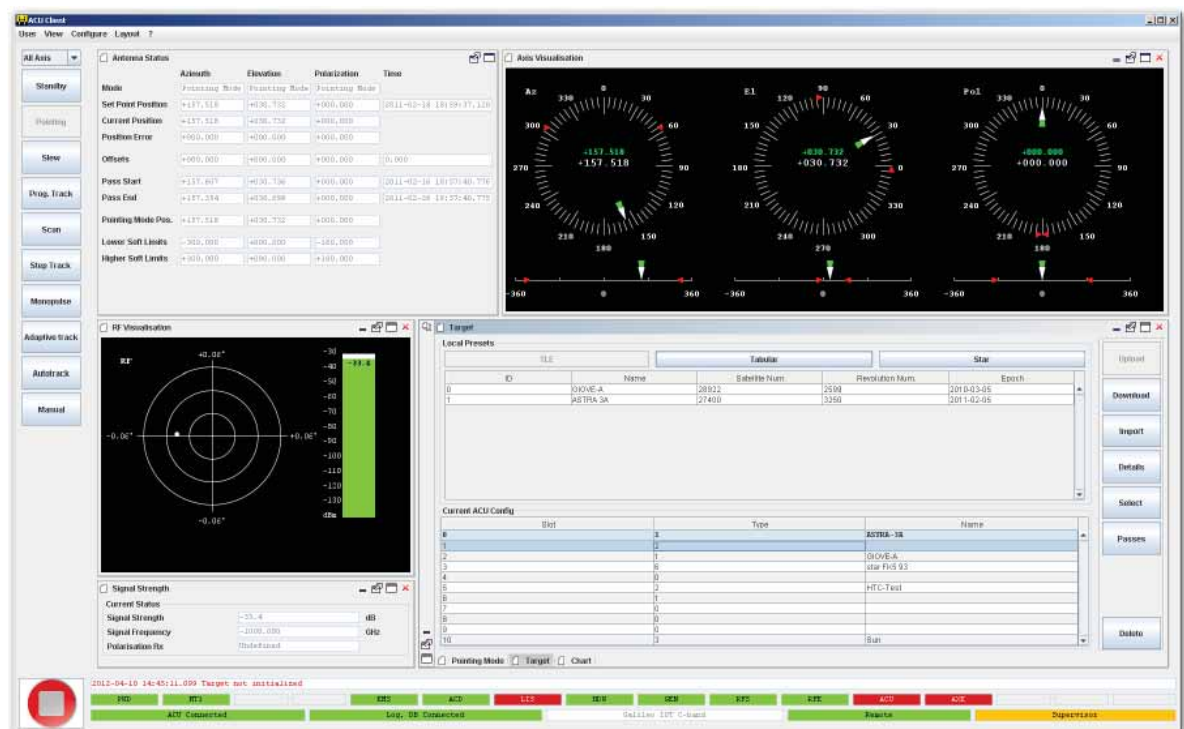
In physical terms, the HITEC Luxembourg ACU consists of a 19" industrial server PC with a dual power supply and redundant hard drive architecture. The ACU is compatible with various types of tracking receivers and can be procured as a standalone component for existing antenna systems or as a component integrated in new antenna systems fully provided by HITEC Luxembourg. See [9] for datasheets providing detailed information about the different ACU versions available from HITEC Luxembourg.

Among the various pointing/tracking modes of the ACU there are 3 so-called basic modes: the *stand-by mode*, in which the antenna is at rest with the brakes applied, the *pointing mode*, in which the antenna is pointed towards a user-defined fixed position and tries to hold this position and the *slew mode*, in which the antenna moves according to a constant pre-defined speed on the axes.

The underlying principles of the *program track mode* have been described above. A target trajectory can be provided in various formats to the ACU. Targets like satellites are often defined in terms of TLEs which consist of an orbital parameter set allowing reconstructing the orbit using an SGP4 integrator (TLE track). Furthermore, the position of the Sun (Sun track) and the stars (star track) can be computed by using dedicated astrophysical models, and the user usually simply specifies which target he wants to track. Any of these target types may also be specified in terms of a list of time-tagged pointing angles (tabular track).

Target tracking algorithms must be initialized with a good estimation of the target's position. For high-precision antennas, orbital data provided to the program track mode is sometimes not precise enough to estimate the target's current position up to a fraction of the antenna's beam width. In that case, the antenna cannot "see" the target. To solve this inconvenience, the ACU has a so-called *scan mode*. It searches for the target by performing a scan around the target's estimated position. The scan generally consists in a small-scale pre-defined trajectory like for example a spiral which is superimposed on top of the target's trajectory. During the scan, the signal level is monitored and the ACU can switch automatically to an automatic tracking mode as soon as a given minimum signal level is reached.

The ACU's *step-track mode* is typically used to track geostationary satellites. A geostationary satellite's position is not perfectly constant but drifts from its orbit due to various astrophysical effects. The integral effect of these factors is an oscillation of the satellite around the nominal GEO position. Since the ground station antennas under consideration usually have narrow beam widths, a small deviation of the satellite from its ideal position greatly reduces the strength of



7_ ACU graphical user interface

the received signal. Therefore it is necessary for the antenna to update its pointing position at regular intervals by using the step-track technique complemented by an adaptive trajectory learning algorithm allowing predicting the satellite movement in-between measurements or in case the signal is temporarily lost.

A monopulse mode capable antenna provides to the TRR a set of two signals: the sum and difference signals. These signals have the same RF frequency and are related to each other in amplitude and in phase as functions of the antenna pointing error in cross-elevation and elevation. In the TRR, the main and error signals are processed to estimate the antenna pointing error from the known amplitude and phase relationship. In the ACU, the detected errors are processed by the *monopulse mode*, and the antenna position is corrected accordingly. The position error signals from the tracking receiver are corrupted by noise due to the limited signal-to-noise ratio (SNR) of the satellite downlink signal. The monopulse algorithm smoothes the target trajectory and learns a local adaptive trajectory model allowing the algorithm to cope with an intermittently disappearing target signal.

Knowing that TLE files have only a limited period of validity and that pre-generated tables for tabular tracking can be limited in time too, the HITEC Luxembourg ACU has an adaptive track mode with which it is able to build an estimation of the orbit itself by using the pointing angle measurements obtained during tracking (with step-track or monopulse). This estimated orbit can then be used to predict the position of the target at the beginning of subsequent passes, thus rendering the acquisition of new TLE files superfluous. This task of adaptive orbit determination is performed by the adaptive track mode in the background.

An *automatic mode switching* functionality allows switching automatically between pointing or program track mode, scan mode and step-track or monopulse mode. This means that for example if the ACU is currently working in program track mode and searching the target with a superimposed scan mode pattern, it can be configured to switch automatically to monopulse as soon as the target is found. If on the other hand during monopulse tracking the signal is lost during a sufficiently long period, the ACU can automatically

switch back to program track and scan modes.

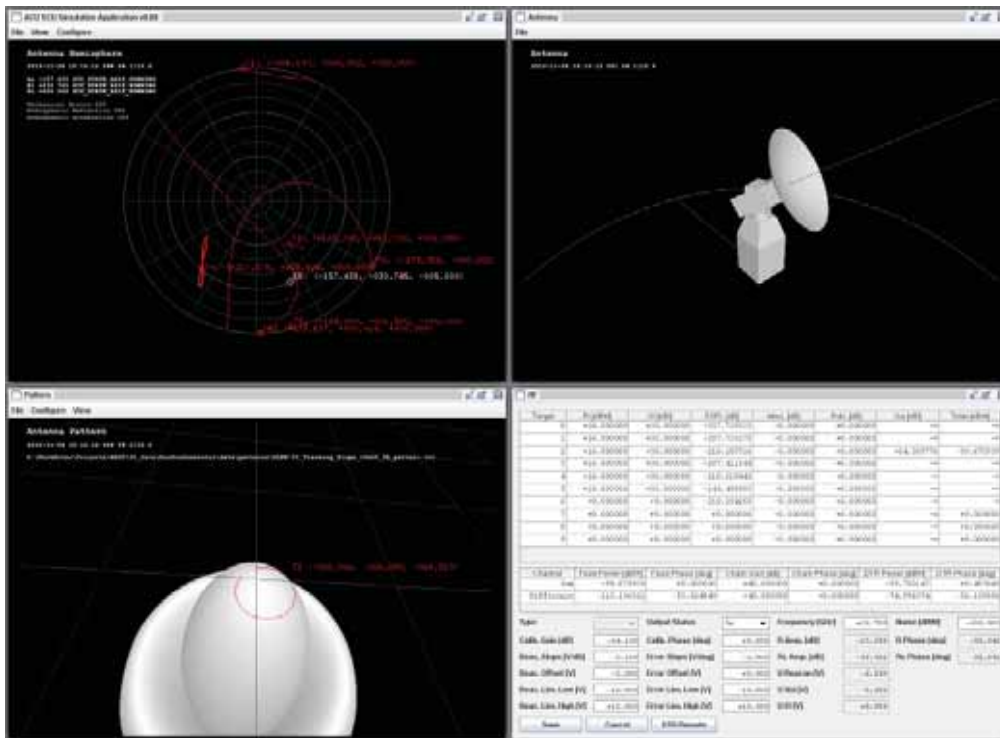
Some mechanical, geometrical and other imperfections of a real antenna make that the RF beam does not always point in the direction that is indicated by the antenna axis encoders. It is therefore required to compensate predictable errors. This is done by using pre-computed *error correction* tables which contain the pointing correction values for each point of the celestial hemisphere visible from the antenna location. The electromechanical waves being refracted by the atmosphere, especially for low elevation angles, the antenna pointing angles must be adapted to also take into account this effect. The compensating offsets are computed by different user-selectable *atmospheric refraction correction* models available in the ACU.

Figure 7 provides a screenshot of HITEC Luxembourg's ACU graphical user interface (GUI) over which all major functionalities of the ACU can be monitored and configured. Additionally it is possible to plot the data collected by a logging application. The GUI can be installed locally on the ACU server or on any remote computer in the network.

HITEC Luxembourg has also developed a simulation application which can replace the SCU, the drives, the RF part and the antenna in an in-house environment, and which can be used for testing the ACU, or for demonstration or training purposes with the HITEC Luxembourg product environment. Figure 8 provides a screenshot of the application.

The simulation software contains an antenna dynamical model, an antenna pointing error model, an atmospheric refraction module, a trajectory simulation module, an atmospheric attenuation model, a configurable antenna radiation pattern, an RF chain model, a TRR model, a user interface and a logging port. Optionally, the TRR model block of the simulator can be replaced by one of the real TRRs and an RF setup generating the TRR input signals in real-time.

The HITEC Luxembourg ACU has been extensively tested and validated during two test campaigns on real antennas: a step-track test campaign at a satellite provider's premises with a 6m Ka-band limited motion antenna and with the two different step-track TRRs and a monopulse test campaign with the 13m antenna from Figure 1. The ACU is



8_ Antenna simulation software

currently being deployed in several of HITEC Luxembourg's antenna projects.

www.hitec.lu

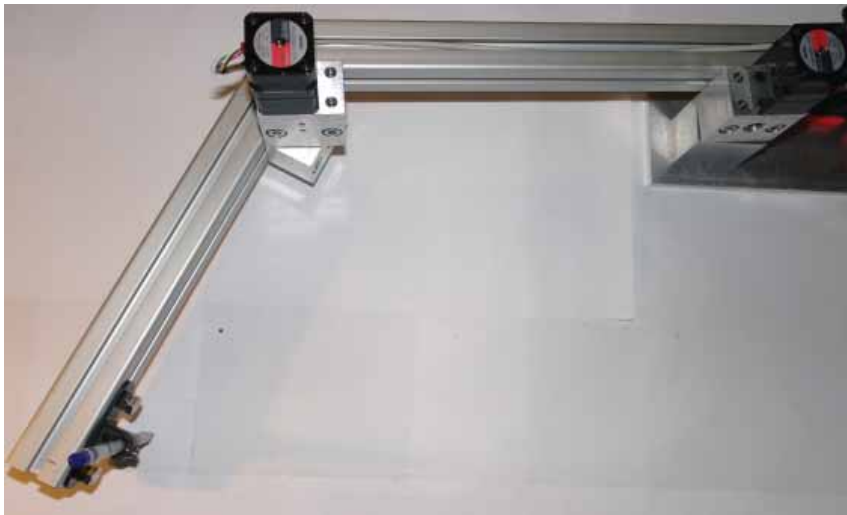
References

- 1_ Satellite Communication Systems, Systems, Techniques and Technology, Gérard Maral, Michel Bousquet, 5th edition, 2009, John Wiley & Sons Ltd.
- 2_ HACU-01, Development of an Antenna Control Unit, Final Report, v1.00, 22/05/2012, HITEC Luxembourg S.A.
- 3_ Enhanced Modeling and Design of Ground Station Antennas for Space Applications, Doctoral Thesis, Marco Formaggi, 2007, University of Pavia.
- 4_ Fundamentals of Astrodynamics and Applications, David A. Vallado, 3rd edition, 2007, Space Technology Library.
- 5_ Space Mission Analysis and Design, James R. Wertz and Wiley J. Larson (editors), 3rd edition, 1999, Space Technology Library.
- 6_ Handbuch der Raumfahrttechnik, Wilfried Ley, Klaus Wittmann, Willi Hallmann (Herausgeber), 4., aktualisierte und erweiterte Auflage, 2011, Hanser.
- 7_ Satellite Orbits, Models, Methods and Applications, Oliver Montenbruck and Eberhard Gill, 1st edition, 2000, Springer.
- 8_ HITEC Luxembourg S.A., www.hitec.lu
- 9_ HACU-1000, HACU-2000 and HACU-3000, Antenna Control Unit Data-sheets, 09/2012, HITEC Luxembourg S.A., www.hitec.lu

In the frame of this project, a position control for a two-link planar manipulator is designed with the help of the simulation environment Matlab/Simulink and implemented on an Arduino real-time controller platform. The resulting mechatronic system is simulated, tested, and evaluated to determine its resolution, accuracy, and repeatability. This paper explores the design decisions, and trade-offs made in achieving a low-cost robotic arm with reasonable performance.

DEVELOPMENT OF A POSITION CONTROL FOR A TWO-LINK PLANAR MANIPULATOR USING MATLAB/SIMULINK AND ARDUINO_

Laurent Breyer



1_ Photo of the assemble robot arm

Introduction

In many applications, computer controlled machines with two degrees of freedom (DOF), which are able to reach a certain position, or to move along a given trajectory, are used to fulfil a specific task. Some examples are a 2D plotter, a fabric cutting machine, or a computer numerical control (CNC) plasma cutter. In the conventional design, the machine has to be larger than the work surface and uses two independent rectangular axes called X and Y. For machines that run day and night this space requirement is justified, but for operating only at most a few times a year, this might be a waste of space.

In looking for a concept to reduce machine space requirements and costs, the idea of a robot arm that is moving like a human arm becomes more interesting. After the work is completed, the upper and forearm, which are also called first and second axes, can be folded away to save space. Thus it is a compact machine that is able to work on a relatively large surface. However, there are some disadvantages. First, it is more difficult to handle the high torques on the axes, which are caused from the forces between tool and workpiece. Secondly, a high angular resolution is needed on the axis in order to achieve an acceptable precision at the

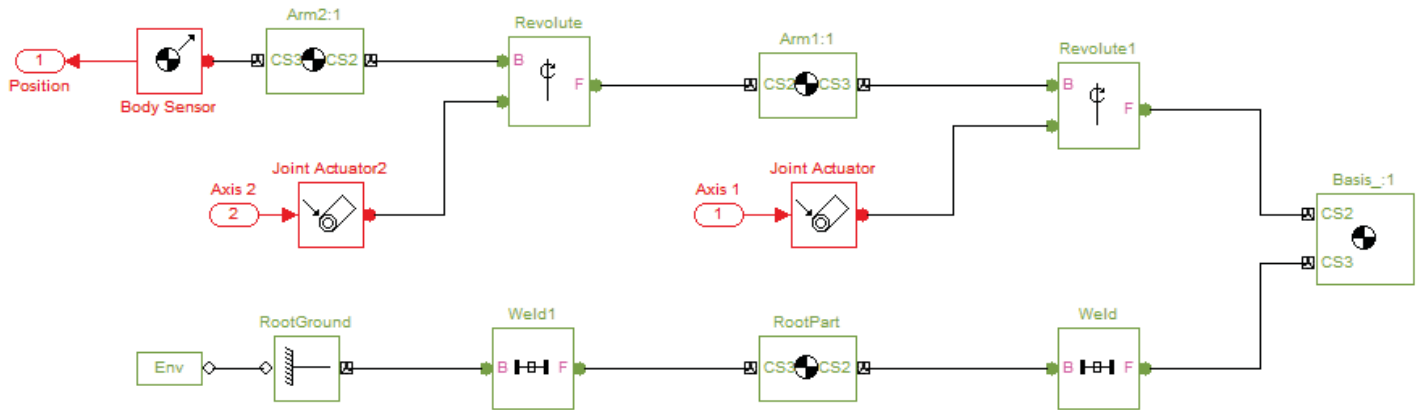
end. Thirdly, the inverse kinematics equations, which transform a desired position into an actuator or joint trajectory, are highly nonlinear and in some cases difficult to solve. But for a two DOF system the mathematical and computational effort are still affordable. A good introduction to this topic can be found in the following papers [1][2].

The two-link planar manipulator in Figure 1, built-up for this project, uses two-phase stepper motors with an integrated transmission, and a resolution of 0.1° per full step. With four micro-stepping configured on the 2M415 motor driver unit, one obtains a resolution of 0.025° per pulse. The micro-stepping technique reduces resonances, and the operation becomes smoother. The power for the drivers and motors are supplied by a conventional 12V transformer.

The core of the motion control is based on an Arduino Mega 2560 microcontroller board, using an 8-bit ATMEGA CPU, and running at 16 MHz. This inexpensive electronic platform is flexible, easy to use, and provides digital/analog connectivity as well as a serial USB communication interface [3]. The coupling, and programming with Matlab/Simulink is well documented, and a tutorial can be found in [4]. The combination of Arduino with Matlab/Simulink allows the user to develop and simulate complex algorithms in the shortest time and to run them on the control hardware without too many portability issues for validation on the real machine. The comprehensive range of toolboxes and the graphical user interface in Simulink simplify the program development work, and support the design of a logical hierarchy of subsystems. Hence, Simulink is an adequate tool for this kind of R&D project.

Design of the Mechanical Model

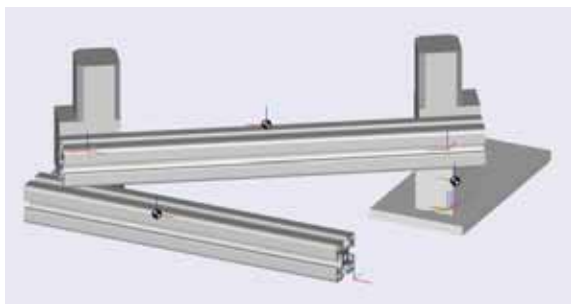
In order to simplify, and enhance the development of the controller algorithm, a physically realistic model of the two-link planar manipulator is needed. For this purpose, the previously created CAD model was exported from Autodesk/Inventor to Simulink with the SimMechanics Link Software [5]. This way, the 3D geometry, the constraints, and the joints that are already defined in the CAD model are automatically represented by the related blocks in the Simulink model. One advantage of this automated export process is that the physical parameters like masses, iner-



2_ Mechanical model of the robot arm in Simulink

tias, dimensions, and the corresponding coordinate systems are passed through without errors. Subsequently, actuator, respectively sensor elements are added to apply forces/torques respectively to measure positions/angles, or their derivatives. Moreover, with the resulting physical model, a kinematic or a dynamic analysis of the system can be carried out. For a kinematic analysis the desired movement of the axis is given, and the required forces and torques are calculated. For the dynamic analysis it is just the opposite. Hence the resulting motion of the machine is calculated from the given forces and torques.

Figure 2 shows the mechanical model of the robot arm in Simulink. Physically relevant are only the three geometries called Basis, Arm1, and Arm2 that are interconnected by revolute joints. The green blocks were created by the automated export process from the CAD environment into Simulink, and the red blocks represent the added actuator and sensor elements. In this case, input Axis 1, and 2 set the angular position for both axes, respectively, and the model calculates the resulting machine position on output 1. Note that Simulink shows the motion of the physical model during the simulation on Figure 3.



3_ Display of the robot arm movement in Simulink

Design of the Motion Control

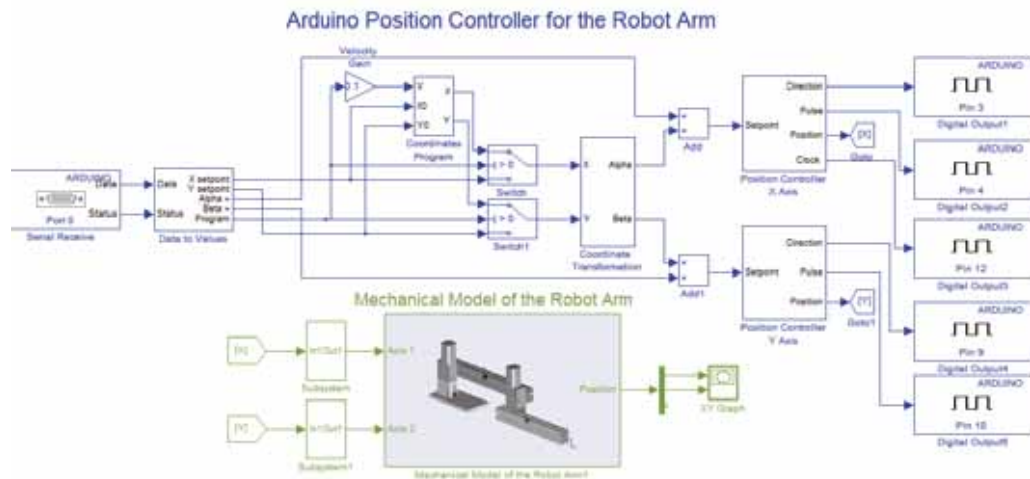
The developed position control in Simulink is represented by the blue blocks on Figure 4. The remaining green blocks correspond to the physical model of the robot, which are used to test the elaborated algorithms. By executing the "Run on Target Hardware" command, the generated C-code of the blue blocks is copied to the Arduino. Once the

code has been completely downloaded to the device, it is executed.

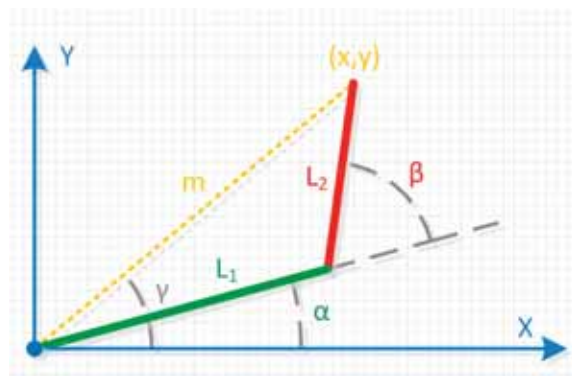
Inside the controller, the "Serial Receive" block gets all the commands, and coordinates sent over the serial interface to the device. This incoming data stream must be correctly interpreted by the "Data to Value" block in order to make the difference between the coordinates and the commands. Principally, the controller accepts the position setpoints (X,Y) in a Cartesian coordinate system, the angular setpoints for both axes (Alpha, Beta), and the start execution command for a coordinate file. This file contains up to 3000 setpoints with a time mark, which have the following structure (T_i , X_i , Y_i). Here, the value $T_{i+1}-T_i$ gives an indication on how long the machine needs to move from coordinate X_i to X_{i+1} , respectively, from Y_i to Y_{i+1} . In other words, the value $T_{i+1}-T_i$ defines the execution speed for every row of the coordinate file. The controller will linearly interpolate between the coordinates and thus move on a straight line from point (X_i , Y_i) to point (X_{i+1} , Y_{i+1}). The just-described programming code is located in the "Coordinates Program" block. The following two switches indicate if the controller is executing a coordinate file, or waiting for an input data over the serial interface.

The "Coordinate Transformation" block transforms the Cartesian coordinates (X,Y) into angular setpoints (Alpha, Beta) for the first, and second axes. If the machine moves on a straight line from point to point, the actuators in the joints have to follow a nonlinear trajectory. For this purpose, the following equations are used, which are derived from the law of cosines in Figure 5. In these equations (347 mm), and (266 mm) are the lengths of the first and second axis, respectively.

After the angular setpoint is determined, the "Position Controller" block compares it to the current axis position. If the difference between these values is larger than a half of a micro-step in use, the internal clock will start generating pulses on the output. If the difference is a positive value, the direction output is set to 1 in the opposite case it remains 0. Internally, the position controller updates for every generated pulse its current axis position. Moreover, if the moving direction of the axis is changed, the algorithm takes



4_ Design of the position control architecture in Simulink



5_ Sketch for the representation of the equations

care on the backlash effect due to the clearance between the pinions in the drive chain. In other words, the controller compensates the direction change by a fix number of pulses, until he assumes that the axis is moving again. The correct programming of this effect and the allowing of multiple direction changes inside the backlash can be a real challenge. In this paper the original backlash block available in the Simulink toolbox is used, which though does not require additional developpements.

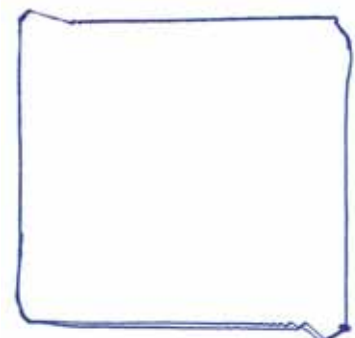
The outputs of the "Position Controller" block are connected to the digital pins. When the Arduino board is executing the generated C code, it uses the pins 3; 4; 9; 10 and 12 to communicate with its environment. In the application the pins 3, 4, are used for the first and 9, 10 for the second motor driver board, respectively. Pin number 12 is applied to measure the pulse frequency of the first axis. This is an indication for the code execution speed on the device. However, this parameter is always checked with an oscilloscope after major changes in the control structure.

One of the first tests of the two-link planar manipulator showed that the backlash on both axes was much higher than expected. Initially, a measurement of the unloaded motor and the speed reducer showed a backlash of 1° . That was relatively high compared to its resolution of 0.1° , but expected since the speed reducer is a simple triple gearing. In the assembled robot arm the first and second axis had

a backlash of 8.21° and 2.2° , respectively. A part of this increase came from the coupling element between motor and arm, but the rest was caused by a different effect.

A further analysis of the problem showed that the first axis was unable to move, even when the motor rotated, until an angle difference of 0.8° was reached. Then the machine jumped to the requested position, or even a little further due to its inertia. Here, it is stuck again, if no continuous motor movement is generated. This phenomenon is called stick-slip effect and can be overcome by reducing the difference between static and dynamic friction. To reach this goal, the stiffness of the drive can be increased, the inertia of the structure reduced, or the axis lubricated. None of these recommendations has been implemented so far.

For a comprehensive test of the machine, the controller was programmed to move two times along a rectangular square with the dimensions of $10 \times 10 \text{ cm}$. With an attached pen, the way of the machine is traced on a piece of paper. The results are shown on Figure 6. The chosen starting position was the lower right corner, hereafter the robot arm continued to move in the clockwise direction. It was observed that the backlash compensation inside the controller works reliably. Furthermore, the machine is able to move precisely on a straight line as far as both axes are moved continuously. For all the corners a sudden jump is noticed and at the starting position some oscillations are seen. This observation is explained by the stick-slip effect.



6_ A square drawn by the robotic arm



Conclusion

The article presents a low cost position controlled two-link planar manipulator, of which the design and the practical implementation are based on the simulation environment Matlab/Simulink and an affordable Arduino real time micro-controller platform that allow short development times. The prototype development brings a lot of experience, helpful for a further optimisation of the control process. One optimisation would be the use of encoders. In this way the axis position can be measured in real-time and corrected if necessary. In a second step the stiffness of the first axis should be increased to overcome the negative influences of the stick-slip effect. However, the present paper represents a proof-of-concept for the development of an inexpensive position control of a robotic arm.

- 1_ http://www.researchgate.net/publication/221074508_A_low-cost_compliant_7-DOF_robotic_manipulator
- 2_ <http://eprints.utm.my/9747/1/78047.pdf>
- 3_ <http://arduino.cc/en/Main/ArduinoBoardMega2560>
- 4_ <http://www.mathworks.nl/academia/arduino-software/arduino-simulink.html>
- 5_ <http://www.mathworks.nl/help/physmod/smlink/ug/installing-and-linking-simmechanics-link-software.html>

Prima Aussichten!

**Du interessierst Dich für Technik?
Du willst wissen, wie die Dinge
wirklich laufen? Dann solltest Du
Ingenieurwissenschaften studieren.**

**Ob Hochhaus oder Handy, ob Windkraft
oder Windkanal:
Hinter jeder Innovation stehen
Ingenieure - und wir bilden sie aus.**

Wir bieten:

- zwei Bachelor-Studiengänge
- anschließende Master-Studiengänge
- ein flexibles Studienprogramm
- eine internationale Ausbildung
- individuelle Betreuung
- Industriekontakte
- ein Umfeld mit exzellenten Jobaussichten

Interessiert? Mehr Infos per Mail an
ingenieur@uni.lu

Universität Luxemburg - my University!

www.uni.lu

Tel. +352 46 66 44 - 6617/6222

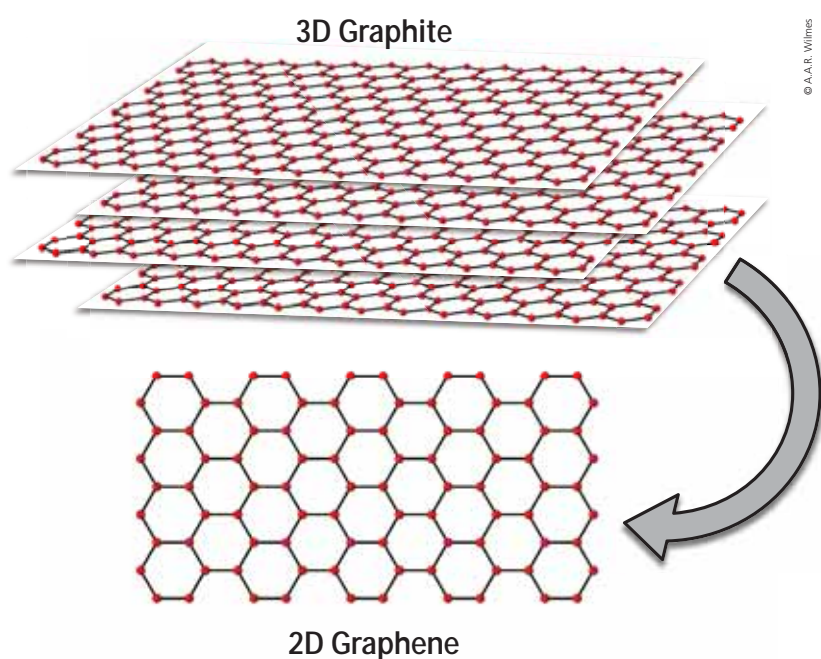
Graphene is the thinnest, strongest, stiffest, and best conducting material known to man. So, what is this wonder material? Why did it take until 2004 for it to be reported? What are the possible future applications for it? Can computer simulations design new Graphene-based materials before they are actually produced?

Imperial College
London

Fonds National de la
Recherche Luxembourg

GRAPHENE AND THE VIRTUAL DESIGN OF NEXT-GENERATION COMPOSITE MATERIALS _

André A.R. Wilmes, Dr. Silvestre T. Pinho



1_ Graphene is a single, flat layer of carbon atoms in a honeycomb lattice which can be stacked into Graphite, as found in pencil lead.

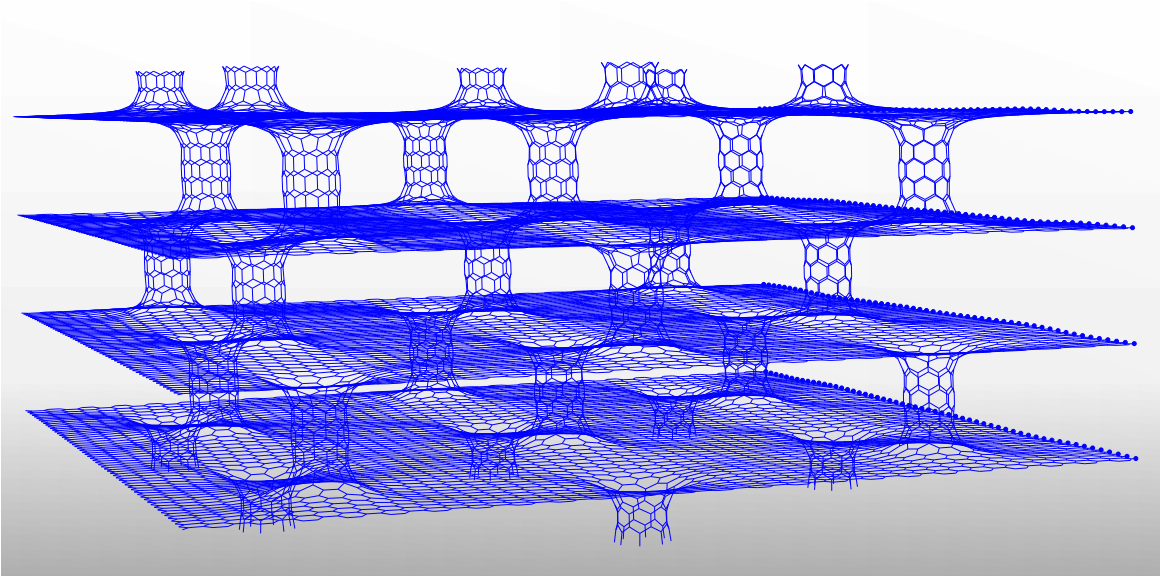
Graphene is a single, flat layer of carbon atoms arranged in a hexagonal honeycomb pattern – imagine one single layer of atoms within graphite, see figure 1. First reported in 2004 by Professors A. Geim and K. Novoselov [1], Graphene has since risen to become the new ultimate superstar material. Graphene's record-breaking properties are only a glimpse of the known superlative qualities which have not all been fully explored yet. Current measurement indicate that Graphene can undergo deformations of up to 25%, has a stiffness of about 1TPa and with a failure stress of about 130 GPa [2], it is around 200 times stronger than steel.

The applications seem to be limitless. To mention but a few, Graphene is expected to be the gateway to long-dreamed technologies such as foldable touchscreens [3] or ultra-fast computers which practically do not heat up and use but a fraction of the energy required today [4]. Graphene can also be used to create impermeable coatings to protect existing metals from corrosion, and it is a good candidate to replace copper for electrical wiring in applications where weight is crucial, such as in aircraft design. Scientific publications involving Graphene have risen to about 10'000 in 2011 with patent filings each year surging from slightly more than 200 in 2008 to almost 1'000 in 2010 [5].

Having just celebrated its 8th birthday, Graphene already led to a Nobel Prize and enjoys several hundred million euros in funding annually worldwide. Even though Graphene is not yet widely-known to the non-scientific community, a milestone for Graphene will be its first commercialisations in products. This is expected to occur within one to two years, when it will help boost the performance of lithium-ion batteries and will be a part of more flexible touchscreens.

In 2004, the first Graphene samples were about 5 μm in size, nearly ten times smaller than a human hair. New techniques for manufacturing Graphene have since emerged and in 2010, rectangular Graphene sheets measuring as much as 75 cm across the diagonal, with a surface area around 0.25 m^2 , were manufactured [3].

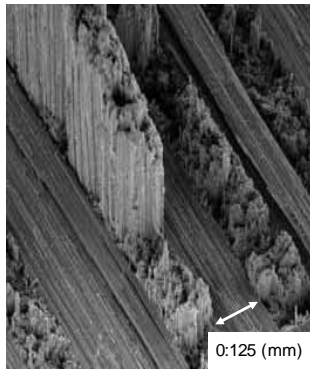
Current, advanced aerospace composite materials are built by embedding layers of carbon fibres in a polymer matrix. Because fibres are only very stiff and strong along their axis, the adjacent layers of fibres in a composite are orientated



© A.A.R. Wilmes

3_ Computational simulation of a Pillared Graphene Structure which is currently being researched as the molecular design for next-generation Graphene Composite Materials.

in different directions so that the final material is globally reinforced, see figure 2.



© Dr. S.T. Pinho

2_ Fracture surface of an advanced Carbon Fibre Reinforced Composite material with alternating, perpendicularly-aligned layers of carbon fibres.

Being a flat sheet, Graphene is strong and stiff along any direction on its plane. This removes the need for different orientations of the reinforcing layers, and hence this leads to a considerable weight reduction. Additional weight savings can be obtained because Graphene is also stiffer and stronger than carbon fibres. These next-generation Graphene Composite Materials (GCM) are the focus of the authors' current research [6-8].

Of particular interest is the development of fast and accurate computational methods for simulating the exact molecular structure of the Graphene sheets. These sheets may be embedded in next-generation Composite Materials instead of the layers of fibres shown in figure 2. The molecular structure of these reinforcing Graphene sheets can be tailored to produce different macroscopic material properties depending on the application.

Molecular Dynamics (MD) is a computational method used to study the geometry and dynamic behaviour of molecules. MD is unable to predict electronic properties, for which very expensive Quantum Mechanics (QM) methods are required, but it is ideally suited to simulate structural behaviour of large domains consisting of up to several billion atoms. For example, a 1 mm^2 Graphene sheet already contains about a thousand billion (10^{15}) atoms, while sheets of $0.2\text{-}0.3 \text{ m}^2$, contain yet ten thousand times more, some (10^{19}) atoms.

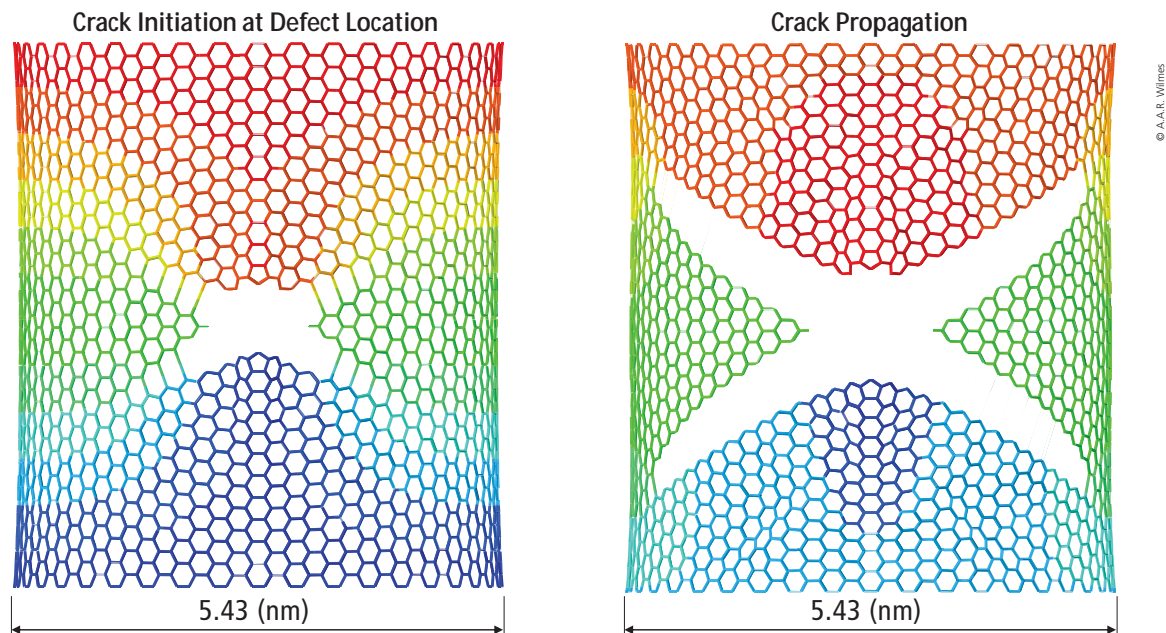
MD is a research tool and a common method for chemistry related problems, yet it is not widely employed for simulating large-scale structural behaviour. In engineering, another method, the Finite Element Method (FEM), has become dominant and is virtually used by any engineering company, from car to airplane manufacturers. FEM software feature powerful graphical interfaces where engineers can create entire simulations interactively. These programs have very computationally efficient solvers which can be run in parallel on many computers and they can perform analyses which are unavailable in MD, such as buckling or natural frequency calculations.

Both MD and FEM are based on the concept of equilibrium of forces, yet their numerical formulations operate differently. The authors' research takes advantage of computers' increasing ability to perform algebraic mathematics, i.e. analytical differentiation or integration of complicated functions, to obtain the necessary mathematical expressions for embedding MD exactly within the computationally more favourable FEM. The resulting method is termed the "Molecular Dynamics Finite Element Method" (MDFEM) [6-8].

MDFEM is computationally more favourable than MD because when doubling the number of atoms in a simulation, the computational time also doubles, while for MD this time quadruples. This linear computational scaling of MDFEM is crucial when considering simulations with millions, billions or even more atoms, which is the case when designing atomic structures beyond 1 mm^2 . The linear scaling of a method is decisive whether simulations of large molecular structures are feasible or impossible, even on supercomputers.

Current design efforts for next-generation Graphene Composite Materials (GCM) include Pillared Graphene Structures (PGS) [9,10], see figure 3. In this molecular design, adjacent Graphene sheets are connected by carbon nanotube towers, which are necessary to prevent the sheets from sliding over each other, as is the case in graphite. The envisioned PGS-based GCM could offer what has so far eluded material scientists: a low-weight, high-strength and high-stiffness but ductile composite material.

A strong and stiff material can develop cracks during service, but these cracks must grow in a predictable manner



4a, 4b_ Crack initiation and propagation in a Carbon Nanotube due to a lattice defect, as obtained with the authors' Molecular Dynamics Finite Element Method.

and must result in a gentle reduction of the material's performance, not in sudden catastrophic failure. MDFEM is able to investigate this fracture behaviour [8], as shown in figure 4, which displays the initiation and growth of a crack in a carbon nanotube due to a defect in the atomic lattice (Stone-Wales defect).

MDFEM allows for the virtual design and optimization of molecular structures prior to manufacture and can hence lead to very significant experimental cost and time savings in developing new materials. This could result in a paradigm shift in how materials are tailored for specific applications. The authors' new method for simulation molecular designs is both intuitive to use and has a favourable numerical behaviour, especially its scalability for large simulations.

André A.R. Wilmes, Dr. Silvestre T. Pinho
Department of Aeronautics Imperial College London

Acknowledgements: The present project is supported by the National Research Fund, Luxembourg (Grant No.: 1360982)

www.fnr.lu

<http://www3.imperial.ac.uk/people/silvestre.pinho/>

References:

- 1_ K. S. Novoselov, A. K. Geim, et al., Electric field effect in atomically thin carbon films, *Science*, vol. 306, no. 5696, pp. 666–669, 2004.
- 2_ C. Lee, X. Wei, et al., Measurement of the Elastic Properties and Intrinsic Strength of Monolayer Graphene, *Science* vol. 321, no. 5887, pp. 385–388, 2008.
- 3_ S. Bae, H. Kim, et al., Roll-to-roll production of 30-inch graphene films for transparent electrodes, *Nature Nanotechnology*, vol. 5, no.8, pp.574–578, 2010.
- 4_ F. Schwierz, Graphene transistors, *Nature Nanotechnology*, vol. 5, no.7, pp. 487–496, 2010.
- 5_ United Kingdom Intellectual Property Office, Graphene Report, www.ipo.gov.uk/informatic-graphene.pdf
- 6_ A.A.R. Wilmes, S.T. Pinho, Molecular Mechanics based FEM for complex graphene structures, *Proceedings: 15th European Conference on Composite Materials (ECCM15)*, Venice - Italy, 24th–28th June 2012.
- 7_ A.A.R. Wilmes, S.T. Pinho, A Molecular Dynamics derived Finite Element Method for structural simulations and failure of graphene nanocomposites, *Proceedings: 10th World Congress on Computational Mechanics (WCCM10)*, São Paulo - Brazil, 8th–13th July 2012.
- 8_ A.A.R. Wilmes, S.T. Pinho, A New Molecular Dynamics Finite Element Method with Applications to Failure of Graphene Structures, *Submitted* 2012.
- 9_ G. K. Dimitrakakis, E. Tylanakis, et al., Pillared Graphene: A New 3-D Network Nanostructure for Enhanced Hydrogen Storage, *Nano Letters*, vol. 8, no. 10, pp. 3166–3170, 2008.
- 10_ R. K. Paul, M. Ghazinejad, et al., Synthesis of a Pillared Graphene Nanostructure: A Counterpart of Three-Dimensional Carbon Architectures, *Small*, vol. 6, no. 20, pp. 2309–2313, 2010.

Delphi Automotive, leader parmi les équipementiers automobiles mondiaux, et le Centre Interdisciplinaire pour la Sécurité, la Fiabilité et la Confiance (SnT) de l'Université du Luxembourg ont signé un accord de coopération de quatre ans sur un programme de recherche conjoint impliquant des systèmes de contrôle électroniques pour les applications automobiles. Il s'agit de la première coopération entre Delphi et le SnT.



DELPHI

DELPHI SIGNE UN ACCORD DE COOPÉRATION AVEC L'UNIVERSITÉ DU LUXEMBOURG

PROJETS DE RECHERCHE CONJOINTS

Le programme, intitulé «Vérification automatisée et économique du codage de gestion moteur», comprend initialement deux projets de recherche. L'un concerne les tests de logiciels (basé sur le modèle test du codage du calculateur gestion moteur) et le second met l'accent sur la sécurité des logiciels embarqués (vérification rapide des performances et des propriétés de synchronisation des systèmes logiciels automobiles).

«Nous sommes heureux de collaborer avec l'Université du Luxembourg dans ces projets de recherche qui nous permettront d'améliorer la fiabilité des véhicules à l'avenir,» a déclaré Steve Kiefer, Président Delphi Powertrain Systems. «Ce programme conjoint vise à accélérer le développement de systèmes logiciels du calculateur gestion moteur plus fiables pour l'industrie automobile,» a-t-il ajouté.

«Les calculateurs (ECU) sont parmi les systèmes embarqués les plus complexes actuellement en cours développement. Assurer la sécurité et la bonne performance des calculateurs est une science d'ingénierie majeure. Delphi est un groupe de dimension mondiale qui développe des systèmes extrêmement fiables, et je suis impatient de partager de nombreuses années de collaboration et de progrès technique,» a déclaré le Professeur Lionel Briand, directeur du programme, SnT.

Projet destiné à développer des technologies de vérification automatisée et de validation efficace des systèmes logiciels de calculateurs de gestion moteur.

Les véhicules modernes sont de plus en plus caractérisés par des systèmes de contrôle électronique. La quantité et la complexité des logiciels utilisés dans les calculateurs (ECU) des véhicules d'aujourd'hui augmentent rapidement. A titre d'exemple, les voitures haut de gamme de nos jours disposent d'au moins 70 calculateurs reliés par plus de cinq systèmes différents de bus. Les éléments moteurs de cette croissance sont les nouvelles législations sur les émissions de gaz d'échappement, la demande de réduction de la consommation de carburant et une mise sur le marché plus rapide, ainsi que les attentes croissantes des clients en termes de confort, de fiabilité et de variété. Pour surmonter ces défis, les constructeurs automobiles et les fabricants de calculateurs doivent compter sur des techniques rentables



pour la vérification et la validation de leurs logiciels. Le programme de recherche dirigé par Delphi et le SnT vise à développer des technologies de vérification automatisée et de validation efficace et efficiente pour les systèmes logiciels des calculateurs.

Avec la signature de cet accord, Delphi devient le 15^e membre à rejoindre le programme de partenariat SnT. Ce programme permet au Centre Interdisciplinaire pour la Sécurité, la Fiabilité et la Confiance et à ses partenaires de développer ensemble des projets de recherche et de nouvelles technologies. Les recherches sont menées conjointement; SnT et ses collaborateurs mettent en commun leur savoir-faire et leurs ressources pour atteindre des objectifs communs. La contribution des partenaires de SnT se fait à tous les niveaux : depuis une représentation au sein du Conseil d'administration jusqu'au soutien opérationnel par le biais Conseil consultatif industriel en passant par la contribution aux ressources des projets.

www.delphi.com
www.uni.lu

Delphi, leader parmi les équipementiers automobiles mondiaux, et le Centre Interdisciplinaire pour la Sécurité, la Fiabilité et la Confiance (SnT) de l'Université du Luxembourg ont signé un accord de coopération de quatre ans sur un programme de recherche conjoint impliquant des systèmes de contrôle électroniques pour les applications automobiles.

This research is motivated by both industry needs for efficient and predictive numerical solutions for damage and failure and scientific advances beyond the current state-of-the-art as tackled by this research performed at the CRP Henri Tudor in the context of SIMUCOMP project. Such research could allow design and stress engineers assess the structural integrity and the damage tolerance of lightweight composite structures through provision of new accurate and predictive multi-scale failure models combined with original and computationally efficient novel numerical methods. Such drastic innovation, implemented in the Manufacturing Industry Corporate Innovation Programme (CIP Industry) of Tudor, will ultimately participate in designing lighter and stronger composites for the construction and transportation industry which could lead to reduced carbon emissions but also improved efficiency and recyclability. This short contribution is concerned with crack nucleation and growth in long fibre reinforced composites (FRC) using the eXtended Finite Element Method (XFEM) and the cohesive zone model.

CRACK GROWTH IN FIBRE-REINFORCED COMPOSITES: EXPERIMENTAL ANALYSIS, MODELLING AND SIMULATION

Dr. Ahmed Makradi , Dr. Lyazid Bouhala, Dr. Salim Belouettar



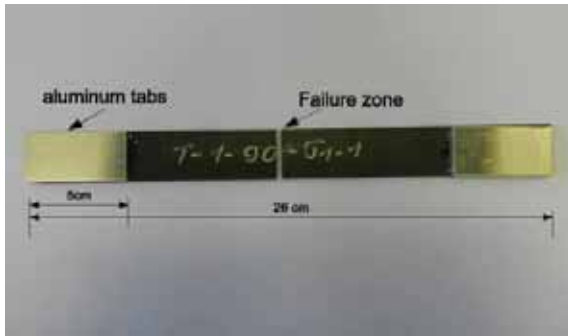
XFEM allows to model cracks within a finite element without the requirement of remeshing. The level-set concept is used to localize the fibre/matrix interfaces and to perform the enrichment. The problem is discretized by means of two-dimensional finite elements in the plane strain framework and the fibres are considered as perfectly bonded to the matrix. The transition between perfectly bonded interface and debonded interface is governed by a cohesive zone model. The obtained results were compared to the existing analytical results and then extended to more complex FRC configurations. Abstract This research is motivated by both industry needs for efficient and predictive numerical solutions for damage and failure and scientific advances beyond the current state-of-the-art as tackled by this research performed at the CRP Henri Tudor in the context of SIMUCOMP project. Such research could allow design and stress engineers assess the structural integrity and the damage tolerance of lightweight composite structures through provision of new accurate and predictive multi-scale failure models combined with original and computationally efficient novel numerical methods. Such drastic innovation, implemented in the Manufacturing Industry Corporate Innovation Programme (CIP Industry) of Tudor, will ultimately participate in designing lighter and stronger composites for the construction and transportation industry which could lead to reduced carbon emissions but also improved efficiency and recyclability. This short contribution is concerned with crack nucleation and growth in long fibre reinforced composites (FRC) using the eXtended Finite Element Method (XFEM) and the cohesive zone model. XFEM allows to model cracks within a finite element without the requirement of remeshing. The level-set concept is used to localize the fibre/matrix interfaces and to perform the enrichment. The problem is discretized by means of two-dimensional finite elements in the plane strain framework and the fibres are considered as perfectly bonded to the matrix. The transition between perfectly bonded interface and debonded interface is governed by a cohesive zone model. The obtained results were compared to the existing analytical results and then extended to more complex FRC configurations.

Keywords: Damage tolerant composite, modelling, XFEM, CIP Industry

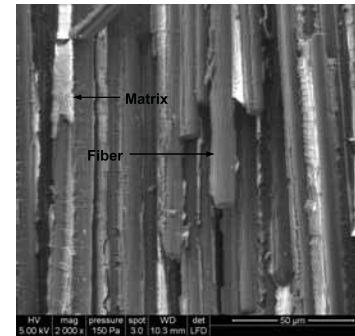
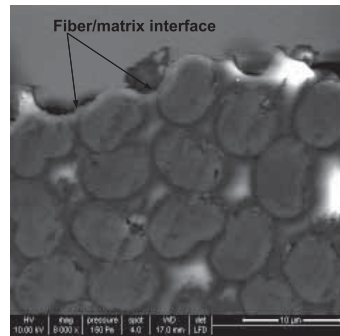
Introduction

Although commonly used in several industrial sectors (e.g. aeronautics and space, automotive, ship-building, sports goods), the simulation and prediction of composite damage up to complete failure, is still subject to serious challenges. Frequently used conservative or empirical approaches often lead to heavy, oversized, and less competitive products, while models such as Continuum Damage Mechanics (CDM) or softening plasticity that seek for solutions averaging crack effects throughout the volume elements suffer from severe limitations (mesh dependency, inability to match crack propagation angle with experiments, etc.) impeding multi-scale analyses. The opportunity tackled SIMUCOMP project, funded by Metara+ ERA net and the FP7 EU research programmes, is to involve the novel development of state-of-the-art damage and failure modelling techniques at different scales (micro, meso, macro) coupled to appropriate scale and damage-to-fracture transition techniques. Composites in general and fibre Reinforced

Composites (FRC) more specifically show very complex failure mechanisms resulting on the one hand from the material brittleness of both constituents, fibres (inclusion) and matrix, and on the other hand from their interface behaviour. An overview of the different aspects, including fibre-matrix debonding delamination, is given in [1]. This makes very difficult to reveal damage mechanisms from mechanical tests (see the experimental section). Therefore, there is always a big need to conduct reliable simulations to understand these complex phenomena in order to improve the material properties. This contribution concerns the matrix/fibre debond growth in long fibre reinforced composites [2]. This typical damage can be numerically analysed using smeared crack models, where the crack opening is represented by strain concentrations [3]. A second alternative is explicitly to consider the crack in the numerical model [4]. The crack growth in FRC has traditionally been simulated through pre-computed solutions which commonly simplify the complex stress state present around the crack fronts, almost leading to over-conservatism. These shortened techniques are progressively being superseded by a range of numerical approaches and methods with various degrees of



1_ Failure of [90x] composite specimen submitted to a tensile test



(a) Fibre/matrix debonding: cross-section view (b) Fibre/matrix debonding: longitudinal view
2_ SEM images of a [90x] composite specimen after failure

simplification most commonly based on the popular finite element method (FEM). In [5], the FEM is associated with the technique of the unit cell to develop a micromechanical in order to model the local damage evolution and the global stiffness reduction of composites randomly distributed fibres. Another alternative method to model interface damage consists of incorporating the interface law into a Finite Element formulation is to use zero-thickness interface elements. These embedded finite elements have a constitutive equation linking the relative displacement to the traction across the interface but this causes mesh dependence of the results. Yet, these are cumbersome to set-up, computationally intensive and notoriously lack robustness, leading to costly user intervention and lack of confidence in attempting realistic simulations. This is because traditional simulation methods, such as the FEM are not well adapted to modelling crack growth because the rapid spatial variation of stress ahead of the crack front, and because the requirement for the mesh to conform to the crack faces. The combination of these two limitations requires the FEM to regenerate fine meshes (re-meshing) at each crack growth step. Thus, most algorithms rely on a remeshing approach. Even when a mesh can be generated, the elements are often inadmissibly distorted which can cause the next crack advance step to abort. Moreover, the very large number of elements required around the crack front increases the computational time prohibitively.

The extended finite element method (XFEM) [6, 7] answers these drawbacks, enhances accuracy and offers a more elegant approach to model cracks within a finite element framework without the requirement of remeshing. Indeed, XFEM is a versatile tool for the analysis of problems characterized by discontinuities and complex geometries [8], without requiring the mesh to conform to these boundaries. XFEM uses the concept of partition of unity [9] and the standard Galerkin procedure. The method was originally presented by Belytschko and Black [10] for enriching FEM approximations to solve growth problems with minimal remeshing. Moes et al. [11] introduced a more elegant approach by adapting an enrichment that includes the asymptotic near tip field and a Heaviside function $H(x)$. Sukumar

et al. [12] extended the concepts to the three-dimensional static crack modeling. Since these pioneering works, X-FEM has been applied to many kinds of problems such as crack and crack nucleation [13]; modelling of inclusions, holes and material interfaces [14]; failure analysis of microstructured materials like functionally graded materials [15]; modelling of material interfaces such as elastic bi-material interface cracks problem [14]; simulation of crack growth in layered composite structures, with particular emphasis on the X-FEM's capability in predicting the crack path in near-interfacial fracture [12]. Later on, X-FEM has been extended [16] to the case of crack growth involving a cohesive law on the crack faces and sophisticated numerical methodologies has been to simulate cohesive crack propagation [13]. The inclusion of cohesive forces transmitted through the cracks is straightforward and does not require the incorporation of interface finite elements [17, 18]. The cohesive zone model describes the material intrinsic forces that act against the growth of an existing crack. These intrinsic forces are represented by a relation between the stress vector and the displacement jump along the crack surfaces. If a cohesive crack is present, the total potential of the body has to be modified to account for the additional cohesive forces transferred through the crack. Details could be found in the in [19]. This contribution illustrates the application of the XFEM and the cohesive model to simulate the fibres/matrix debonds growth. The XFEM approach is reviewed and adapted to the context of FRCs. The experimental tests on [90x] composites are described and some numerical results are presented.

Experimental characterisation and analysis

The unidirectional carbon fibres (prepreg Hexply M10.1/38%/UD300/HS) were supplied by Composites Distribution, France. The prepreg is made of M10.1 epoxy resin reinforced high strength carbon fibres UD300/CHS with a volume fraction of about 52.2%. The test specimens [90x], shaped into rectangular parallelepipeds, were cut using a diamond blade. The tensile tests were conducted according to the specifications of the ISO-527-4 standard at a constant cross-head speed of 2 mm/min. To prevent gripping damage, Aluminum tabs were glued to both ends of the

l (mm)	e (mm)	E (MPa)	ν	σ_r (MPa)	ϵ_r (%)
25.24	2.15	8516	0.03328	34.05	0.406

Table 1_ Geometrical and Mechanical properties of the composite material

tested specimen. Table 1 summarizes the average dimensions of the five tested specimens (thickness e , mm and width l , mm). The mechanical properties are reported in Table (1). Figure 1 shows the specimen failure after testing and Figure 2 shows two scanning electron microscopy (SEM) images taken at the fracture zone (see Figure 1). These images show that the composite crack is rather governed by fibre/matrix debonding than matrix cracking.

Extended finite element method (XFEM)

The essential idea in XFEM is to add discontinuous enrichment functions to the finite element approximation using the partition of unity. With regard to the problem analysed in this paper, the displacement approximation can be composed by three parts: the continuous contribution, the displacement jump through the crack and the displacement gradient jump at the fibre/matrix interface.

$$\mathbf{u}^h(\mathbf{x}) = \sum_{i \in N_u} N_i \mathbf{u}_i + \sum_{i \in N_a} N_i H_i(\mathbf{x}) \mathbf{a}_i + \sum_{i \in N_b} N_i G(\mathbf{x}) \mathbf{b}_i \quad (1)$$

\mathbf{x} is the coordinates vector, \mathbf{u}^h is the approximated displacement and N_i stand for the standard shape functions. N_a and N_b are the sets of enriched nodes and N_u represents the total number of nodes within the domain Ω . \mathbf{u}_i represents the nodal displacement, H_i is the displacement enrichment function in the vicinity of cracks and G is the displacement enrichment function in the vicinity of interfaces. \mathbf{a}_i , \mathbf{b}_i are two additional degrees of freedom that describe, respectively, the displacement jump through the crack and the displacement gradient at the fibre/matrix interface. The displacement enrichment function H_i is represented by the sign of the level-set function. The absolute function of the level-set function [20] is used as enrichment function G at the interface. Bearing in mind that the branch enrichment function at the crack tip is not considered since the crack tip singularity vanishes in the presence of the cohesive model. Cracks are characterized by a discontinuous displacement field. Thus, the modified Heaviside function is given as:

$$\text{sign}(\mathbf{x}) = \begin{cases} +1 & \text{if } \mathbf{n} \cdot (\mathbf{x} - \mathbf{x}_{\Gamma_c}) > 0 \\ -1 & \text{if } \mathbf{n} \cdot (\mathbf{x} - \mathbf{x}_{\Gamma_c}) < 0 \end{cases} \quad (2)$$

where \mathbf{x}_{Γ_c} are the coordinates of a node at interface and \mathbf{n} is the outward normal vector on this node. Using Heaviside function, as an enrichment function, requires the crack tips to be located on element edges. Since a cohesive model is used for the tractions across the crack, the stress field in the vicinity of the crack tip does not have singularity. This further enables the interpolation to represent singular stress fields as assumed in linear elastic fracture mechanics. The zero-level ($\phi(\mathbf{x}) = 0$) is used to represent the fibre/matrix interfaces and $\phi(\mathbf{x})$ is given as:

$$\phi(\mathbf{x}) = \text{sign}(\mathbf{x}) \cdot \text{dist}(\mathbf{x}) \quad (3)$$

$\text{dist}(\mathbf{x})$ is defined as the closest distance from a given point to the interface such as $\text{dist}(\mathbf{x}) = \min ||\mathbf{x} - \mathbf{x}_{\Gamma_c}||$. In order to avoid getting blending element region near the enriched elements, the enrichment function H_i in equation (1) is introduced as the sign of the shifted level-set as:

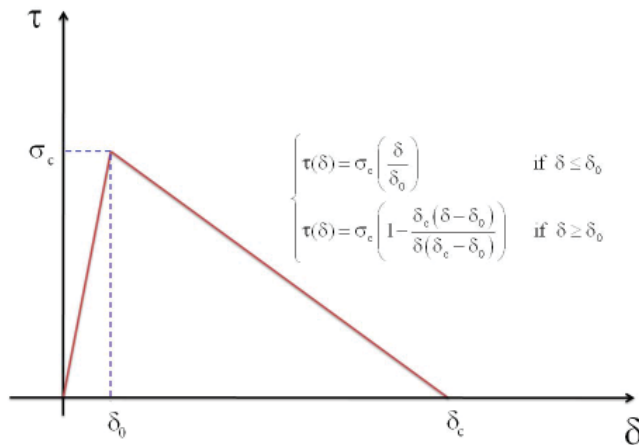
$$H_i(\mathbf{x}) = \text{sign}(\phi(\mathbf{x})) - \text{sign}(\phi(\mathbf{x}_i)) \quad (4)$$

Near the fibre/matrix interfaces, the modified enrichment function as in [20] is used

$$G(\mathbf{x}) = \sum_j N_j(\mathbf{x}) |\phi_j(\mathbf{x})| - \left| \sum_j N_j(\mathbf{x}) \phi_j(\mathbf{x}) \right| \quad (5)$$

Modelling Crack initiation and growth

Commonly, fracture along an interface between two dissimilar materials is of mixed mode [21]. A linear holonomic cohesive traction-separation law is used (see Figure 3). The cohesive model is represented by three distinct zones: a crack free surface zone where the cohesive forces are null, a process zone where the crack opening is governed by the cohesive law and a blank (safe) zone. Crack initiation is assumed to occur at the fibre/matrix interface, which usually acts as a stress concentrator in bi-material systems. The crack onset point is detected by adopting Ye [21] quadratic failure criterion, which accounts for the interaction be-



3_ The used cohesive law

tween normal and tangential interfacial stresses, assuming an infinite strength in compression [21]:

$$\sqrt{\left(\frac{\sigma_n}{\sigma_{nc}}\right)^2 + \left(\frac{\sigma_t}{\sigma_{tc}}\right)^2} \geq 1 \quad (6)$$

σ_{nc} and σ_{tc} are respectively the strength of the interface in the normal and tangential directions. Equation 6 is reduced to $\sigma_n \geq \sigma_{nc}$ when the failure in the tangential direction is neglected.

The initiation of cracks is determined by the interfacial strength and the progression of the crack is determined by the critical energy release rate. Indeed, stress based and an energy-based criteria are used one simultaneously ([21]), since either of them represent a necessary but not sufficient condition for crack onset. On one hand, the only use of the stress criterion is able to find the minimum value of the applied load leading to failure, but it cannot lead to an explicit determination of the size of the originated crack. On the other hand, the application of the energy-based criterion requires an a priori existing crack. The area under the (σ_n, δ_n) curve represents the energy release rate G_c and $\delta_c = 2G_c/\sigma_c$ is the critical opening. In the absence of cracks the (σ_n, δ_n) curve increases until a maximum stress σ_c (see Figure 3). If the stress after each equilibrium step exceeds the tensile strength of the material at any integration point, an additional crack is then introduced.

The defined zero level-set function (see Figure 6) describes accurately the position of the fibre/matrix interface and the elements crossed by the interface as well. The interface enrichment function (Eq.(5)) is validated, in the case of a perfectly bonded fibre embedded in an infinite matrix, by comparing the calculated stresses at the fibre/matrix interface to those obtained analytically, on the same configuration, by Gorbarikh et al. ([22]).

Numerical Simulations

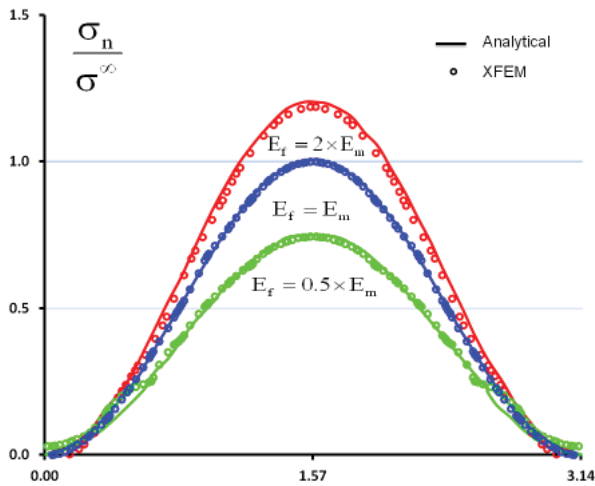
In what follow, the mechanical properties of the fibre and the matrix are considered as isotropic and the composite is subjected to a uni-axial remote load. The XFEM simulation is calibrated using the experimental data. The energy release rate is considered equal to ($G_c = 0.01 \text{ N/mm}$) and

the ultimate uni-axial strength value is taken as ($\sigma_c = 1 \text{ MPa}$). Linear material properties were assigned to the elements since the fibre and the matrix are considered as isotropic (see Table 1).

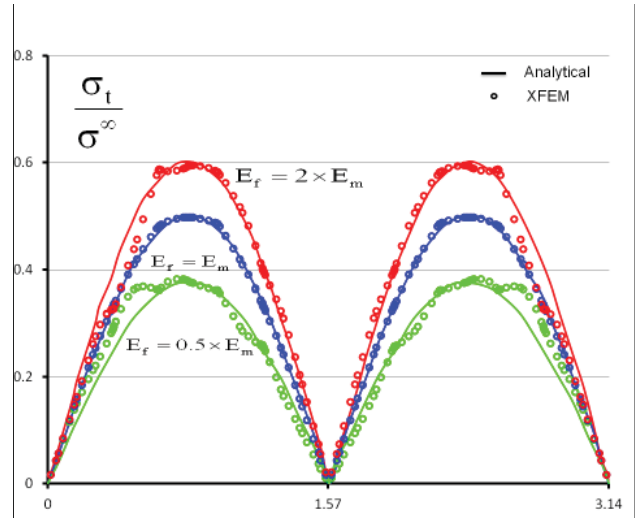
Numerical computations are performed for both crack initiation and propagation, with reference to a 2D composite structure model (see Figure 5) composed of one, two and multiple arrangements of fibres assumed perfectly bonded to the matrix. The proposed problem is discretized by means of two-dimensional finite elements in the plane strain framework. Due to the symmetry only half of the fibre/matrix interface $[0, \pi]$ will be presented. In Figure 4 are illustrated the normal and the tangential stresses along the fibre/matrix interface for different fibre to matrix stiffness ratio. From this figure, one can see that the maximum normal stress for the different fibre/matrix stiffness ratios is obtained at $\theta = \pi/2$. This corresponds likely to the debonding onset in the case of uniaxially loaded single fibre/matrix composite. However, the maximum of the tangential stress is obtained at $\pi/4, 3\pi/4$.

A set of 2809 quadrilateral elements and 2916 nodes were used, for the modelling of case of one fibre, of which 144 nodes were enriched. The ratio of the matrix edge length to fibre radius is taken as equal to six, in order to avoid boundary effects. The radius of the fibre is considered as $R = 1 \text{ mm}$. The composite is subject to a remote tension of $\sigma^\infty = 0.85 \text{ MPa}$ along the horizontal direction (Figure 5). The crack onset and growth at the inclusion/matrix interface are illustrated in Figures 6d-f. From these figures, one can notice that the crack onset takes place at the intersections of the inclusion/matrix interface and at the symmetry axis along the loading direction where the concentration of stresses is maximal. Further, on both sides of the inclusion, the debonding arcs are symmetrical relative to the axis perpendicular to the loading direction. This is mainly due to uniform distribution of the stress field on both sides of the inclusion. The maximum fibre/matrix debonding semi-angle, which depends on the remote applied load, is about $\pi/3$.

Two fibres (inclusions) embedded in an infinite plate is also considered. The objective is to investigate the fibre-track



(a) Normal stress along the interface bonding



(b) Tangential stress along the interface

4_ Comparison between analytical and numerical solutions : case of perfect bonding

ing onset in the case of uniaxially loaded single fibre/matrix composite. However, the maximum of the tangential stress is obtained at $\pi/4, 3\pi/4$.

A set of 2809 quadrilateral elements and 2916 nodes were used, for the modelling of case of one fibre, of which 144 nodes were enriched. The ratio of the matrix edge length to fibre radius is taken as equal to six, in order to avoid boundary effects. The radius of the fibre is considered as $R = 1 \text{ mm}$. The composite is subject to a remote tension of $\sigma^\infty = 0.85 \text{ MPa}$ along the horizontal direction (Figure 5). The crack onset and growth at the inclusion/matrix interface are illustrated in Figures 6d-f. From these figures, one can notice that the crack onset takes place at the intersections of the inclusion/matrix interface and at the symmetry axis along the loading direction where the concentration of stresses is maximal. Further, on both sides of the inclusion, the debonding arcs are symmetrical relative to the axis perpendicular to the loading direction. This is mainly due to uniform distribution of the stress field on both sides of the inclusion. The maximum fibre/matrix debonding semi-angle, which depends on the remote applied load, is about $\pi/3$.

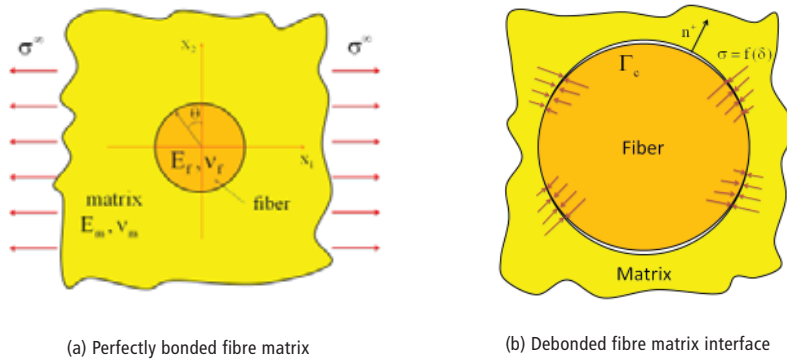
Two fibres (inclusions) embedded in an infinite plate is also considered. The objective is to investigate the fibre-fibre interaction and the influence of the positioning of the two fibres within the matrix on the debond cracks process as well. This simulation is performed using a set of 3025 quadrilateral elements and 3136 nodes of which 288 nodes were enriched. The mechanical and the geometrical properties are those reported in the previously. In order to cover the all debonding scenarios, a parameter α is introduced, which represents the angle between the line connecting the two centres of the inclusions and the direction of loading. Three typical situations (polar angles) are considered: $\alpha = \pi/2$, $\alpha = \pi/4$ and $\alpha = 0$ for the present analysis with a Level-set function defined as Figure 8-a. The initial positions of the fibres are defined by the level-set function as described in Figure 7-a. Note that the maximum value of the interface stresses are attained at different values of the polar angle α (measured counter-clockwise from the positive x-axis). As a consequence, each analysis leads to a different

location of the onset point. In the case of $\alpha = \pi/2$, the stress along the loading direction, before debonding, is depicted in Figure 8-b. The deformed mesh at the end of the simulation is plotted in Figure 8-c. The progressive debonding is shown in Figure 8d-f, where the debonding behaviour and the maximum length of the debonded arcs are not sensitive to the interactions between the two fibres. Good agreement was found with the results reported in [23]. In case of $\alpha = \pi/4$, (see Figures 9a-f) Interface debonding occurs only in the two external arcs when the interface debonding occurs along the two internal fibre/matrix interfaces (see Figure 7) for $\alpha = 0$.

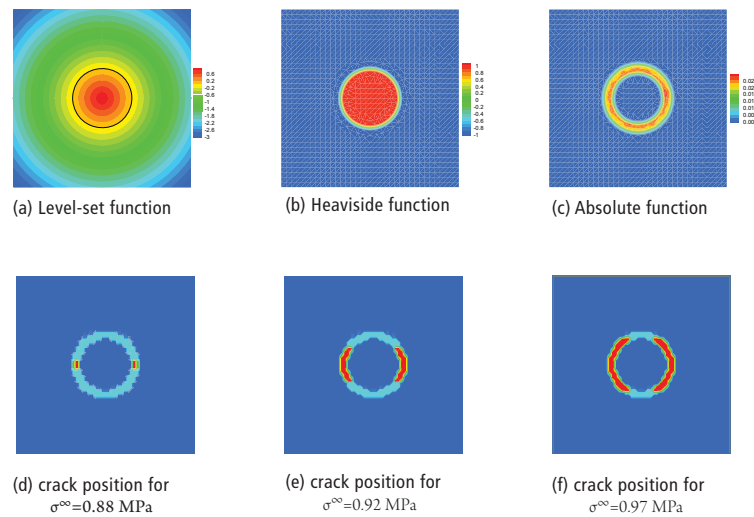
To demonstrate the effectiveness of the proposed approach in modelling crack nucleation and propagation in multi-fibrous composites, finite matrices containing a large number of fibres regularly and randomly distributed are considered. Figure 10 visualizes the set of the inclusions distribution within the matrix. This illustration uses the sign and the level-set functions. This implicit representation of the inclusions and the interfaces is used in this context [8]. The numerical simulation is performed using a set of 19600 quadrilateral elements with 2156 enriched nodes. The distribution effects is analysed in the case regularly and randomly distributed fibres. This analysis is performed for two typical fibre size ($R = 0.4 \text{ mm}$ and $R = 0.488 \text{ mm}$) are considered subjected to two different loading situations ($\sigma^\infty = 0.15 \text{ MPa}$) and ($\sigma^\infty = 0.25 \text{ MPa}$). The resulting debonding growth is depicted in Figure (11). It worth noticing that for the same loading condition, the resulting crack scenario depends on the considered RFC configuration and the induced interaction between the fibres. Indeed, the debonding is symmetrical in the case of well-organized microstructure and irregular when some fibres are overstressed. In both situations, of regular and arbitrary distributed fibres, the same applied load leads to less stressed inner fibres for large size fibres and the debonding increases with the increase of the applied load.

Conclusion

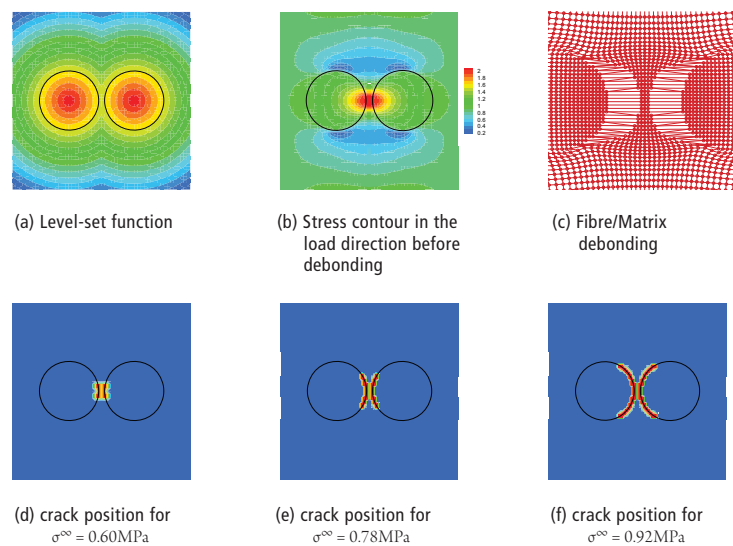
The XFEM and a cohesive zone model are used to investigate the crack initiation and growth in fibre reinforced composite. This accounts for an efficient methodology to



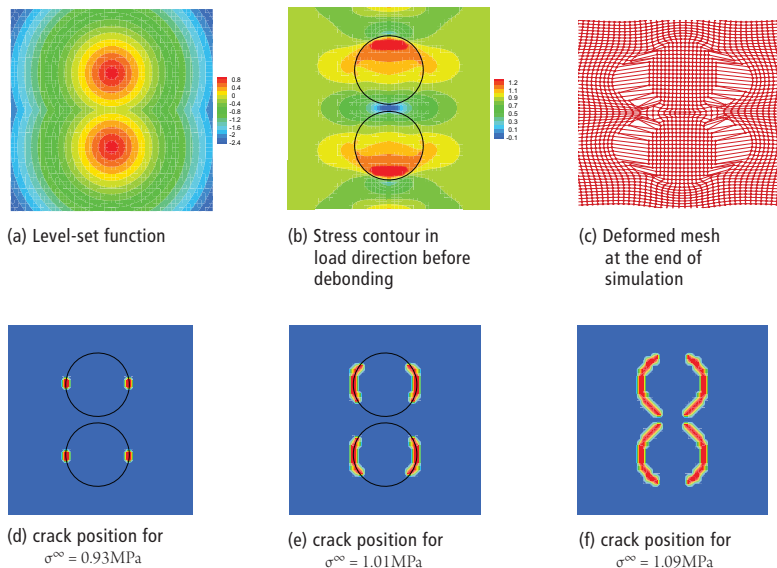
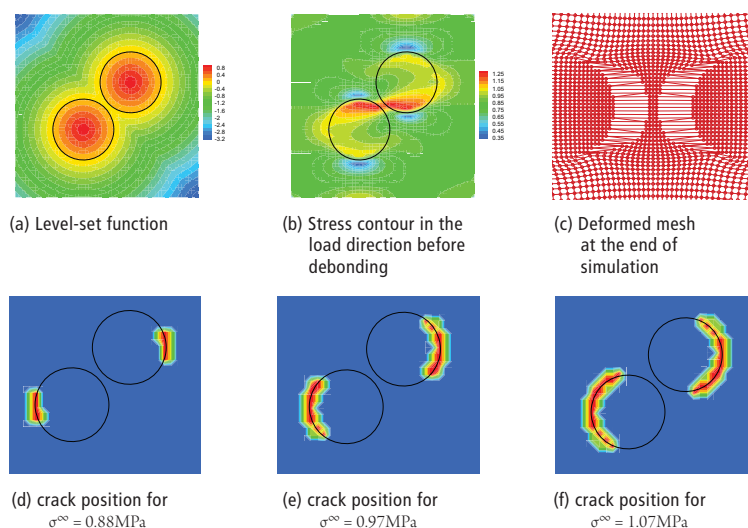
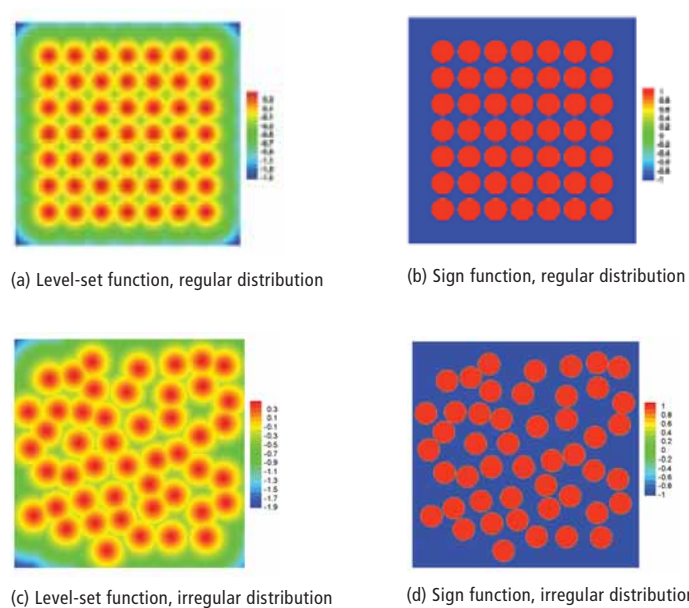
5_ Loading conditions and Cohesive forces



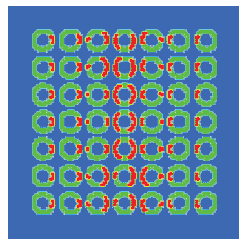
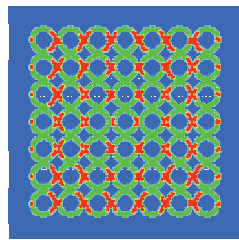
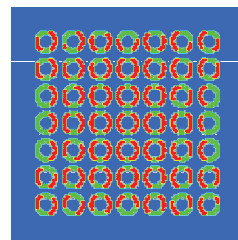
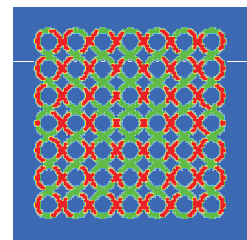
6_ Progressive debonding in single fibre model



7_ Progressive debonding in double inclusion model $\alpha = 0$


8_ Progressive debonding in double inclusion model $\alpha = \pi/2$

9_ Progressive debonding in double inclusion model $\alpha = \pi/4$


10_ 49 regularly distributed inclusions and 48 randomly distributed ones in a finite matrix

(a) $R = 0.4 \text{ mm}$, $\sigma^\infty = 0.15 \text{ MPa}$ (b) $R = 0.488 \text{ mm}$, $\sigma^\infty = 0.15 \text{ MPa}$ (c) $R = 0.4 \text{ mm}$, $\sigma^\infty = 0.25 \text{ MPa}$ (d) $R = 0.488 \text{ mm}$, $\sigma^\infty = 0.25 \text{ MPa}$

11_ Debonding growth in regularly distributed inclusions at iteration 3

the fibre-matrix debonding without any additional numerical artefact. The implemented method was successfully used to investigate the crack initiation and growth in the case of multi-fibres reinforced matrix where the interaction between fibres according to their position their sizes is emphasised.

Perspectives

The method presented herein complements the competences of the Modelling and Simulation Unit of CRP Henri Tudor. Together with the know-how of its Materials Unit and the departments of Environmental Technologies and Technology Watch, the CRP Henri Tudor through its Manufacturing Industry Programme not only can propose a comprehensive offer for the composite materials domain but also actively works to remain at the cutting edge of technologies needed for this high-end sector.

Acknowledgments

The authors acknowledge the financial support of Matera+ and the FP7 EU programme. The financial support of the FNR (INTER programme) is also acknowledged.

www.tudor.lu

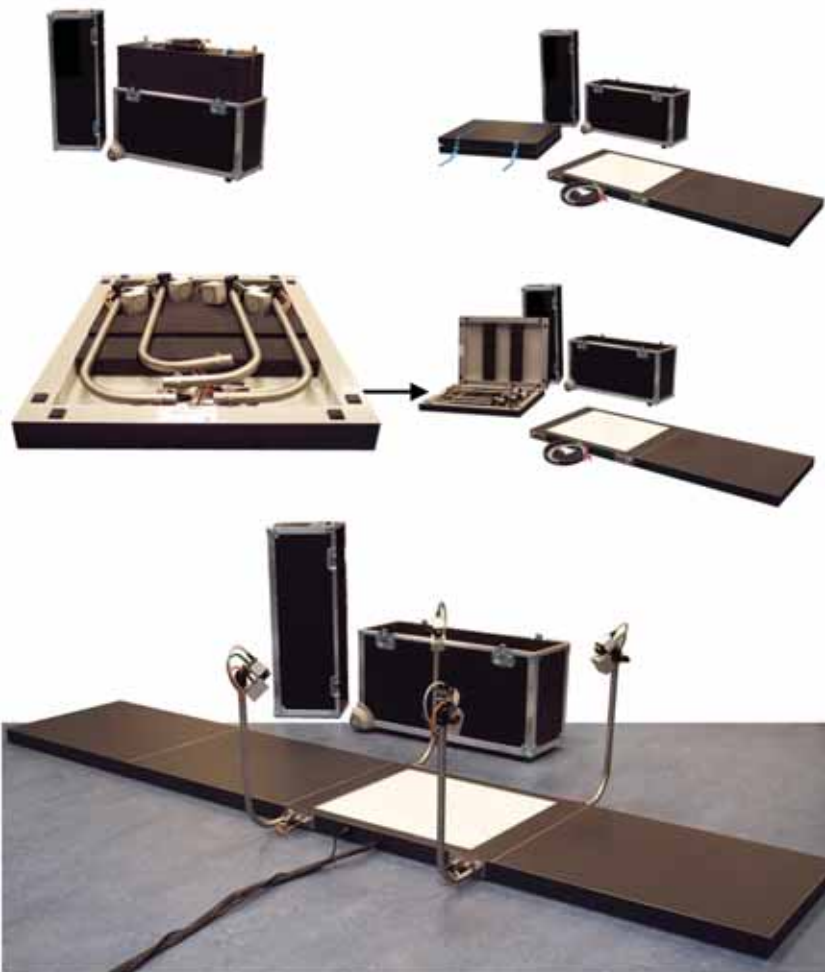
- 1_ J Andersons and M Knig. Dependence of fracture toughness of composite laminates on interface ply orientations and delamination growth direction. *Composites Science and Technology*, 64(13-14) :2139 – 2152, 2004.
- 2_ John W. Hutchinson and Henrik M. Jensen. Models of fiber debonding and pullout in brittle composites with friction. *Mechanics of Materials*, 9(2) :139 – 163, 1990.
- 3_ Y. Huang, W. Wang, C. Liu, and A.J. Rosakis. Analysis of intersonic crack growth in unidirectional fiber-reinforced composites. *Journal of the Mechanics and Physics of Solids*, 47(9) :1893 – 1916, 1999.
- 4_ Javier Gonzalez and W.G. Knauss. Strain inhomogeneity and discontinuous crack growth in a particulate composite. *Journal of the Mechanics and Physics of Solids*, 46(10) :1981 – 1995, 1998.
- 5_ Marek Romanowicz. Progressive failure analysis of unidirectional fiber-reinforced polymers with inhomogeneous interphase and randomly distributed fibers under transverse tensile loading. *Composites Part A : Applied Science and Manufacturing*, 41(12) :1829 – 1838, 2010.
- 6_ T. Belytschko, N. Moes, S. Usui, and C. Parimi. Arbitrary discontinuities in finite elements. *International Journal for Numerical Methods in Engineering*, 50 :993– 1013, 2001.
- 7_ T. Belytschko N. Moes, J. Dolbow. A finite element method for crack growth without re-meshing. *International Journal for Numerical Methods in Engineering*, 46 :131–150, 1999.
- 8_ Mohammed Mounnassi, Salim Belouettar, Eric Bechet, Stephane P.A. Bordas, Didier Quoirin, and Michel Potier-Ferry. Finite element analysis on implicitly defined domains : An accurate representation based on arbitrary parametric surfaces. *Computer Methods in Applied Mechanics and Engineering*, 200(5-8) :774 – 796, 2011.
- 9_ J. M. Melenk and I. Babuska. The partition of unity method : Basic theory and applications. *Computer Methods in Applied Mechanics and Engineering*, 139 :289– 314, 1996.
- 10_ T. Belytschko and T. Black. Elastic crack growth in finite elements with minimal remeshing. *International Journal for Numerical Methods in Engineering*, 45 :601– 620, 1999.
- 11_ T. Belytschko N. Moes, J. Dolbow. A finite element method for crack growth without remeshing. *International Journal for Numerical Methods in Engineering*, 46 :131–150, 1999.
- 12_ N. Sukumar, N. Moes, T. Belytschko, and B. Moran. Extended finite element method for three dimensional crack modelling. *International Journal for Numerical Methods in Engineering*, 48 :1549–1570, 2000.
- 13_ U. Perego S. Mariani. Extended finite element method for quasi-brittle fracture. *Int. J. Num. Meth. in Eng.*, 58 :103126, 2003.
- 14_ N. Moes T. Belytschko N. Sukumar, D.L. Chopp. Modeling holes and inclusions by level sets in the extended finite-element method. *Comput Meth Appl Mech Eng*, 190 :61836200, 2001.
- 15_ M. Gosz J. Dolbow. On the computation of mixed-mode stress intensity factors in functionally graded materials. *Int J Solids Struct*, 39 :25572574, 2002.
- 16_ T. Belytschko G. Zi. New crack-tip elements for xfm and applications to cohesive cracks. *Int J Numer Meth Eng*, 39 :22212240, 2003.
- 17_ T.-P. Fries and T. Belytschko. The extended/generalized finite element method : An overview of the method and its applications. *International Journal for Numerical Methods in Engineering*, 84(26) :253–304, 2010.
- 18_ B. Moran N. Sukumar, D.L. Chopp. Extended finite element method and fast marching method for three-dimensional fatigue crack propagation. *Engineering Fracture Mechanics*, 70(1) :29 – 48, 2003.
- 19_ J. Hogberg. Cohesive zone modeling of crack nucleation at bimaterial corners. *International Journal of Fracture*, 141(3) :549–559, 2006.
- 20_ N. Moes, M. Cloirec, P. Cartraud, and J.-F. Remacle. A computational approach to handle complex microstructure geometries. *Computer Methods in Applied Mechanics and Engineering*, 192(28-30) :3163 – 3177, 2003.
- 21_ L. Ye. Role of matrix resin in delamination onset and growth in composite laminates. *Compos Sci Technol.*, 33 :257–277, 1988.
- 22_ I. Verpoest L. Gorbatikh, S. Lomov. Elastic compliance of a partially debonded circular inhomogeneity. *International Journal of Fracture*, 131 :211–229, 2005.
- 23_ V.I. Kushch, S.V. Shmegeva, and L. Mishnaevsky Jr. Elastic interaction of partially debonded circular inclusions. ii. application to fibrous composite. *International Journal of Solids and Structures*, 48(16-17) :2413– 2421, 2011.

Spiderman, Tintin, Le Seigneur des Anneaux, Hulk, Avatar, Tron, Star Wars... Le point commun à l'ensemble de ces films est la motion capture pour la réalisation d'animations virtuelles. Des marqueurs réfléchissants sont collés sur différentes parties du corps d'une personne pour enregistrer ses mouvements dans un studio. Des caméras (optoélectroniques) sont positionnées autour de la scène et enregistrent la position 3D de chaque marqueur au cours du mouvement. Ces derniers servent ensuite à reconstruire virtuellement la personne. Différents procédés informatiques sont ensuite menés de manière à changer la visualisation du personnage et de l'environnement dans lequel il se trouve. Plusieurs jeux vidéo utilisent également cette procédure pour réaliser des scènes d'action les plus réalistes possibles.



DÉVELOPPEMENT D'UN SYSTÈME POUR L'ANALYSE BIOMÉCANIQUE DU PIED_

Guido Becker, Marc Schmiz



rer l'amplitude articulaire de la hanche (i.e. l'angle entre la cuisse et le tronc) avant l'opération, quelques semaines après l'opération, puis quelques mois après une période de rééducation fonctionnelle, vérifiant ainsi que la mobilité articulaire de la hanche est correcte. Cette procédure est communément employée, notamment pour l'analyse du membre inférieur (pied, jambe et cuisse) pendant la marche, la course, le saut, en position statique, etc. Parmi les trois segments que composent le membre inférieur, le pied demeure le plus complexe à analyser: nombre important d'os, de ligaments et de muscles (vingt-six os dans un pied, soit un quart des os du corps humain avec les deux pieds). De nos jours, l'analyse biomécanique du pied est principalement utilisée pour des évaluations cliniques en réadaptation chez l'enfant et l'adulte. Un grand nombre de systèmes d'analyse du mouvement est disponible sur le marché pour de telles applications. Généralement, un laboratoire d'analyse de la marche est spécifiquement dédié à ces systèmes. Associés à l'analyse du mouvement, des plateformes de force sont intégrées dans le sol afin de mesurer en parallèle l'impact du pied (force de réaction au sol) lors du pas. Pour être attractif pour les cliniciens, ces systèmes doivent idéalement être:

- _précis, pour mesurer des angles articulaires de faibles amplitudes
 - _portable et peu encombrant, évitant ainsi l'utilisation d'un local spécifique pour les mesures
 - _relativement peu coûteux, de manière à être accessible par la plupart des cliniciens
 - _facile à utiliser, pour ne pas avoir à recourir à un personnel technique pour son fonctionnement
 - _rapide, en vue d'établir un diagnostic juste après l'analyse.
- Un tel système n'existe malheureusement pas, pour des raisons techniques (e.g. plateformes de force et système portable). Néanmoins, un compromis entre ces différents critères peut être fait

Ces technologies sont également employées pour des applications cliniques et sportives. Cette fois, on parle d'analyse (biomécanique) du mouvement: la trajectoire des marqueurs permet de quantifier un mouvement donné (angle, distance). Pour illustrer ce point, imaginons par exemple une personne subissant une intervention chirurgicale pour la pose d'une prothèse de hanche, suite à une arthrose sévère. L'analyse du mouvement est alors utilisée pour mesu-

Dans cette optique, la société Lion Systems a récemment développé le Minilab afin de proposer le premier système répondant à l'ensemble des critères précédemment cités. Ce système est disposé dans une valise de transport. Il est composé de quatre blocs qui définissent un couloir de

Ankle Joint Report

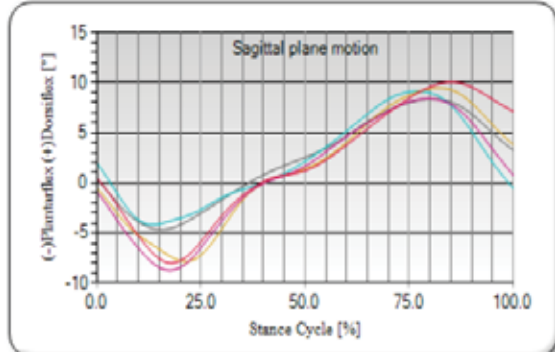
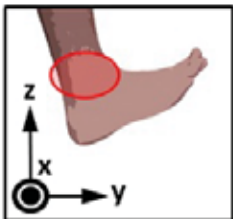


Date of Exam : 11/23/2012
Examiner : William
Patient Number : 9
First Name : William
Last Name : Samson
Remarks : Healthy patient test

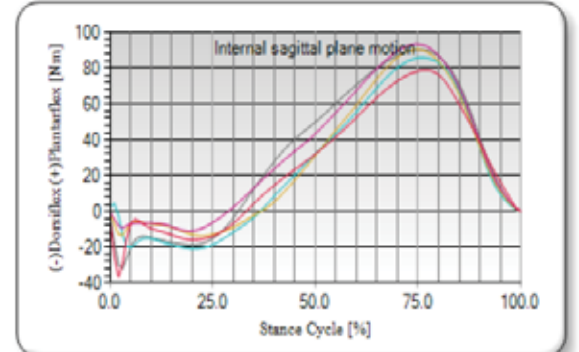
Date of Birth : 8/6/1981
Body Mass : 66
Size : 169

Kinematic

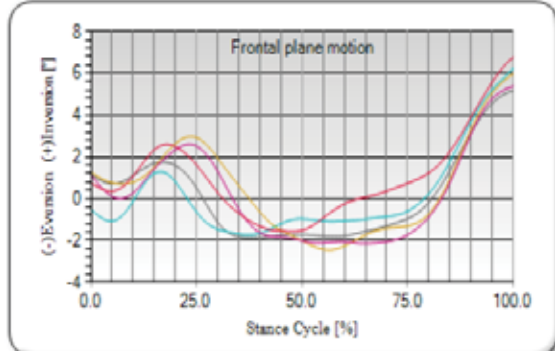
Dynamic



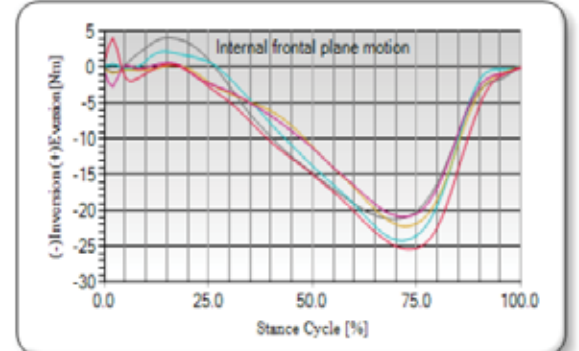
Max Angle[°]	8.3	9.1	9.4	8.3	10.0
Min Angle[°]	-4.6	-4.1	-7.8	-6.7	-7.9
Range Angle[°]	12.9	13.2	17.3	17.0	18.0



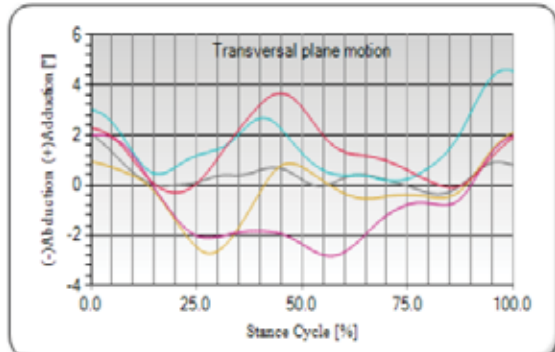
Max Moment[Nm]	90.42	85.78	90.54	93.53	78.87
Min Moment[Nm]	-31.73	-20.76	-13.52	-10.87	-36.59



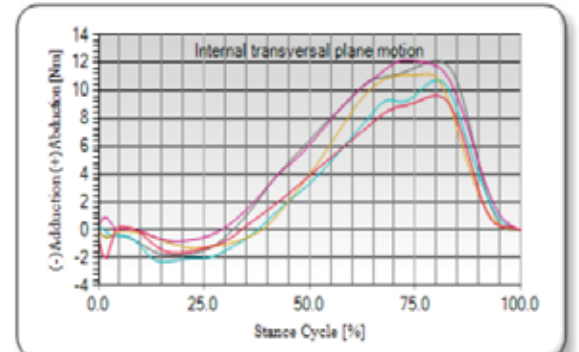
Max Angle[°]	5.1	6.2	5.9	5.3	6.7
Min Angle[°]	-1.8	-1.7	-2.4	-2.1	-1.5
Range Angle[°]	7.0	7.9	8.4	7.5	8.3



Max Moment[Nm]	4.15	2.19	0.24	0.62	4.11
Min Moment[Nm]	-21.14	-24.18	-22.17	-20.83	-25.42

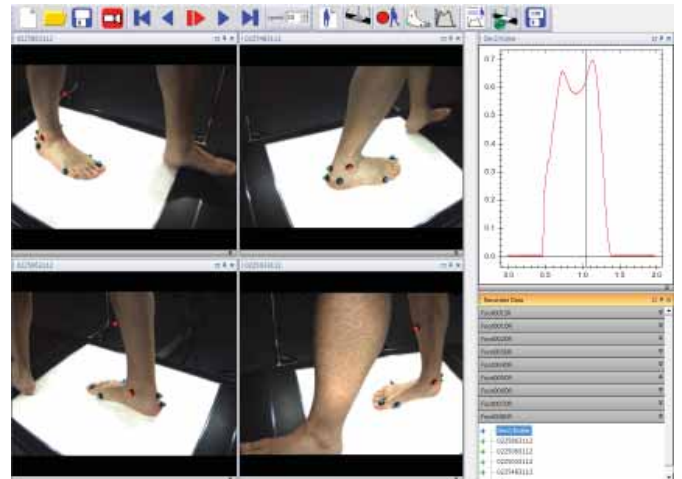
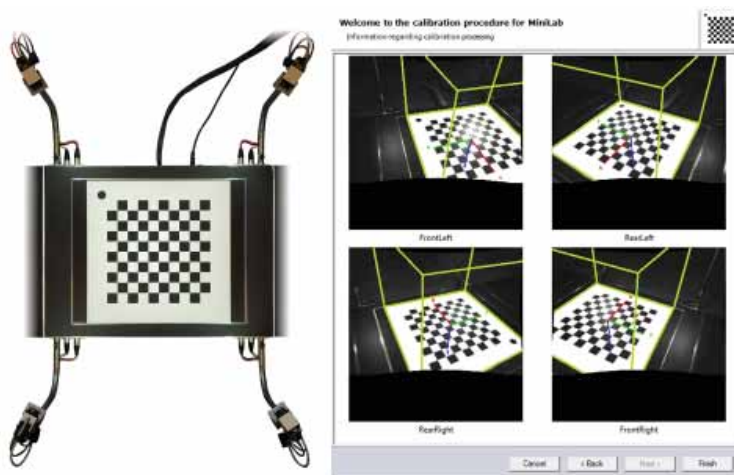


Max Angle[°]	2.0	4.6	2.0	1.9	3.6
Min Angle[°]	-0.3	0.1	-2.7	-2.8	-0.2
Range Angle[°]	2.4	4.4	4.8	4.8	3.9



Max Moment[Nm]	12.10	10.73	11.19	12.17	9.64
Min Moment[Nm]	-1.83	-2.29	-1.32	-0.82	-2.03





marche de 3.2m. Ces blocs sont conçus en structure alvéolaire afin d'optimiser le poids du système. Une plateforme de force (1000Hz) est intégrée dans le bloc principal (au milieu du couloir de marche). Quatre bras métalliques sont fixés de part et d'autre de ce bloc. Un éclairage (LED) et une caméra couleur (140Hz, 656×490 pixels) sont disposés à l'extrémité de chacun de ces bras afin d'illuminer et d'enregistrer le déroulé du pas lors de la marche ou de la course. Les connexions (alimentations, Ethernet) sont également intégrées dans le bloc principal. L'enregistrement de l'ensemble de ces capteurs (caméras et plateforme de force) est réalisé avec le logiciel de synchronisation Multi Sensor-Control (MSC). Une calibration du système est nécessaire pour convertir l'information 2D de chaque caméra (image) en une seule information 3D. Un damier (disposition et taille des cases connues par MSC) est placé sur le bloc principal du couloir de marche et est enregistré. Une fois cette opération réalisée, le système est calibré et est opérationnel pour des mesures avec des *précisions* linéaire et angulaire de 0.5mm et de 0.6°, respectivement. Contrairement aux systèmes de mesure traditionnels, des marqueurs de couleur (et pas réfléchissants) sont utilisés. Ces derniers sont positionnés sur des points anatomiques précis du pied. La personne réalise alors plusieurs essais dans le couloir de marche. MSC détecte alors automatiquement la position et le nom de chaque marqueur au cours du temps. Les paramètres décrivant la biomécanique articulaire du pied sont calculés à partir des trajectoires des marqueurs et des données de la plateforme de force : les angles et les moments articulaires 3D (flexions dorsale et plantaire, éversion et inversion, adduction et abduction) de la cheville et de l'articulation métatarso-phalangienne (« articulation des orteils »), la force de réaction au sol 3D (antéropostérieure, médio-latérale et verticale) et le déplacement de centre de pression. Ces paramètres sont définis pour chaque essai de marche ou de course. Enfin, un rapport personnalisé de la personne mesurée synthétise l'ensemble des essais et servira de support d'analyse pour : l'aide au diagnostic clinique, l'aide au choix de chaussure adaptée à sa foulée, l'évaluation pré/post opération ou rééducation, la comparaison de différentes populations (enfants ou adultes, amateur ou professionnel).

Le Minilab permet donc de répondre aux attentes de l'analyse du mouvement tout en établissant un compromis entre les cinq critères attendus pour ce type de système. Bien que le Minilab n'utilise pas des caméras optoélectroniques de la motion capture traditionnelle, la précision obtenue est suffisante pour les mesures actuelles. L'un des points forts du Minilab est l'intégration de la plateforme de force dans le couloir de marche. De plus, les caméras se démontent et se rangent dans l'un des blocs du couloir de marche. Ainsi, le Minilab est *portable et compact*. En utilisant un nombre réduit de caméras couleurs plutôt qu'optoélectroniques, le coût du système peut être réduit, rendant le Minilab *abordable*, en comparaison aux systèmes traditionnels. Un autre point du Minilab concerne le logiciel spécialement conçu pour une prise en main rapide. L'utilisation de l'interface graphique peut se résumer en six icônes pour les six étapes nécessaires au fonctionnement du système (calibration, création d'un nouveau sujet, enregistrement, traitement automatique des essais, analyse des essais, rapport), facilitant ainsi une éventuelle utilisation avec un écran tactile. Plusieurs options permettent de personnaliser les paramètres d'enregistrement (e.g. durée et fréquence d'acquisition) et de traitement (e.g. détection des couleurs, filtrage des données). Une configuration par défaut permet toutefois une *utilisation simple*, convenant au plus grand nombre d'utilisateurs. Enfin, le Minilab est optimisé pour un *processus rapide* : opérationnel en 20 min (montage du système et calibration), il faut en moyenne 15 minutes de la pose des marqueurs au rapport de mesure pour cinq essais. Des investigations sont en cours pour proposer des déclinaisons du système à d'autres applications : caméras plus performantes (400Hz) pour la mesure de déplacements très rapides, système sans plateforme de force pour réduire le coût du système, augmentation du nombre de marqueurs sur le pied pour des analyses cliniques ou sportives plus complètes dans la recherche.

www.lionsystems.lu



EVA

ENVIRONNEMENT ET
AGRO-BIOTECHNOLOGIES



ISC

INFORMATIQUE, SYSTEMES
ET COLLABORATION



SAM

SCIENCE ET ANALYSE
DES MATERIAUX



CRP - GABRIEL LIPPMANN

TROIS DÉPARTEMENTS AU SERVICE DE VOTRE INNOVATION

Acteur majeur de la recherche scientifique et du transfert de technologie au Luxembourg, le CRP - Gabriel Lippmann met à votre service ses compétences de haut niveau et ses technologies de pointe.



RETHINK INNOVATION THINK TUDOR

As a leader in applied research in Luxembourg, Tudor responds to your needs by mobilising its scientific and technological competences in nine innovation programmes, each targeting specific challenges.

MANUFACTURING INDUSTRY

CONSTRUCTION

ECOTECHNOLOGY

MOBILITY

TRANSPORT & LOGISTICS

HEALTH

PUBLIC SERVICES

INNOFINANCE

HUMAN CAPITAL

tudor
PUBLIC RESEARCH CENTRE HENRI TUDOR

Innovating together

For further information: www.tudor.lu/innovation-programmes



Do you want to exploit your research results?

Find collaboration partners on the Luxembourg Portal for Innovation and Research.

The portal is an invaluable source of information on R&D and innovation in Luxembourg – an essential tool for identifying potential partners, increasing the visibility of your knowledge, learning more about innovative companies and research institutes in Luxembourg, browsing national and European calls for proposals and keeping up to date with the latest news.

www.innovation.public.lu

Innovation and research start here.



Supported by:



European Union
European Regional Development Fund
Investing in your future

Interested in an AFR grant? Check eligibility conditions and deadlines for forthcoming calls. Go and see what's behind on www.fnr.lu/afr



PhD and Postdoc Grants for Public-Private Partnerships See what's behind.

Through its **AFR Grant Scheme**, the National Research Fund Luxembourg (FNR) supports **PhD and Postdoc researchers** in Luxembourg and abroad. Next to offering grants for research projects carried out in public research institutions, AFR strongly encourages research projects performed **as public-private partnerships (PPP) with Luxembourg-based companies**. The salary of the PhD or Postdoc researcher who will work on a research project as a member of the company's staff will be paid through the AFR-PPP grant scheme, whereas the full costs of the research will be borne by the company. In order to benefit of the **financial support** for PPP under AFR, an innovative research project needs to be developed jointly by the PhD/Postdoc candidate, the private company and a public research institution in Luxembourg or abroad.

AFR contributes to the development of human resources in Luxembourg research, translated in the long term by an increased number of qualified researchers pursuing a research career beyond their period of AFR funding.

Interested in hosting an AFR fellow during his or her PhD or Postdoc training? Go and see what's behind on www.fnr.lu/afr or send an email to afr@fnr.lu

AFR
FUNDING SCHEME
FOR PHDS AND POSTDOCS
(AIDES À LA FORMATION-RECHERCHE)



 Fonds National de la
Recherche Luxembourg
INVESTIGATING FUTURE CHALLENGES